Scuola Internazionale Superiore di Studi Avanzati - Trieste

Expression and physiological role of stomatin-domain proteins in the olfactory epithelium

Thesis submitted for the degree of "Doctor Philosophiae"
Academic Year 2018/2019

CANDIDATE
Kevin Yarib Gonzalez Velandia

SUPERVISOR
Prof. Anna Menini

CO-SUPERVISOR
Dr. Simone Pifferi

SISSA - Via Bonomea 265 - 34136 TRIESTE - ITALY

Scuola Internazionale Superiore di Studi Avanzati

Trieste

Expression and physiological role of stomatin-domain proteins in the olfactory epithelium

Thesis submitted for the degree of "Doctor Philosophiae"

Academic Year 2018/2019

CANDIDATE

Kevin Yarib Gonzalez Velandia

SUPERVISOR

Prof. Anna Menini

CO-SUPERVISOR

Dr. Simone Pifferi

DECLARATION

The original work presented in this Thesis was carried out at the International School for Advances Studies, SISSA, Trieste, between November 2015 and October 2019 under the supervision of Dr. Simone Pifferi and Prof. Anna Menini.

Abstract

The olfactory system is a chemosensory system that detects volatile molecules, called odorants, responsible for valuable information from the environment such as sources of food, predators or hazardous substances. The detection of odorants is carried out by the olfactory sensory neurons, the primary cellular sensors. The vast variety of molecules that the olfactory system can detect is due to the expression of a huge repertoire of molecular receptors that directly bind the odorants, called olfactory receptors. These are the primary molecular sensors which are expressed mainly in the ciliary membrane of the olfactory sensory neurons. Each olfactory sensory neuron expresses only one type of olfactory receptor, and all neurons transduce the odorant signals by a common signaling pathway. The core elements of this signaling pathway are well established: the binding of odorants by an olfactory receptor leads to the sequential activation of $G\alpha_{olf}$ and adenylyl cyclase III. The increase of ciliary cAMP opens CNG channels, and the entry of calcium through these channels leads to the opening of the calcium-activated chloride channel TMEM16B allowing an efflux of chloride ions from the cell. The opening of CNG and TMEM16B channels underlies the depolarizing receptor potential induced by the detection of odorants in olfactory sensory neurons.

In addition to the core elements of the odorant transduction machinery, other proteins could play a role in the detection of odorants, especially as potential regulators of the transduction machinery. For example, some members of the stomatin family are highly expressed in the olfactory epithelium. Stomatin-domain proteins have emerged as general regulators of ion channels and transporters and have been shown to be involved in transduction mechanisms in other sensory systems. Stomatin-domain proteins are highly conserved and anciently evolved membrane proteins. In the mammalian genome, five members have been identified: *Stomatin*, stomatin-like protein-1 (*STOML-1*), stomatin-like protein-2 (*STOML-2*) stomatin-like protein-3 (*STOML -3*) and *Podocin*. Some members of this family have been shown to be expressed in the olfactory epithelium and *Stomatin* and *STOML-3* mRNAs are present at very high levels. Stomatin and STOML-3 proteins have been isolated in calcium-dependent signaling complexes in cilia extracts from the olfactory epithelium and STOML-3 proteins have been shown to localize mainly in the cilia of the neurons, where transduction of odorants takes place, and to interact with ACIII.

The main aim of this thesis was to confirm and extend our understanding about the expression and localization of the stomatin family in the olfactory epithelium. I confirmed the localization of STOML-3 in the cilia of the olfactory sensory neurons. Moreover, we found that Stomatin is present also in these structures. In contrast, I revealed that STOML-1 and STOML-2 localizes in the central layer of the olfactory epithelium, in the soma of the neurons.

To study the role of these proteins in the function of the olfactory epithelium I used a loss of expression approach. I used two KO mice models: a STOML-3 KO and a

Stomatin/STOML-1/STOML-3 triple KO. First, I studied in detail the development in these KO animals. I did not find differences in the number of olfactory neurons, apoptotic, globose or horizontal basal cells and in the morphology of the cilia of the neurons. I did not observe changes in the expression and the localization of several members of the transduction machinery and potential targets of stomatin-domain proteins.

Then, I measured the physiological response to odorants in KO animals by performing electro-olfactogram recordings. I found a reduction in the amplitude of the response in both KO animals, especially in older mice. The magnitude of the reduction was similar in both KO mice, suggesting that STOML-3 is the main responsible for this effect.

The results in this thesis establish the first evidences that stomatin-domain proteins modulate the odorant response in mice and provide the foundation for future work aimed at clarifying the physiological role of the stomatin family in the olfactory system.

Table of Contents

List of abbreviations

aa	amino acid
ASIC	Acid sensing ion channels
ATP	Adenosine triphosphate
ACIII	Adenylyl cyclase type III
AOB	Accessory olfactory bulb
cAMP	Cyclic adenosine monophosphate
CNG	cyclic nucleotide-gated cation channel
DAPI	4 ',6-diamidino-2-fenilindol
DRG	dorsal root ganglion
GPCR	G protein coupled receptor
GFP	Green fluorescent protein
GG	Grueneberg's ganglion
Gαolf	Olfactory-specific guanosine triphosphate (GTP)-binding protein alpha subunit
HBC	Horizontal basal cells
IAA	Isoamyl acetate
kDa	kilo-Dalton
MOB	Main olfactory bulb
OAG	oleoyl-2-acetyl-sn-glycerol
OB	Olfactory bulb
OE	Olfactory epithelium
OMP	Olfactory marker protein
OR	Odorant/olfactory receptor
OSN	Olfactory sensory neuron
PDE	Phosphodiesterase
SLC4A1	Anion exchanger 1
SO	Septal organ of Masera
STOML-1	Stomatin-like protein 1
STOML-2	Stomatin-like protein 2
STOML-3	Stomatin-like protein 2
TRPC6	Transient receptor potential canonical 6
VNO	Vomeronasal organ
VSN	Vomeronasal sensory neuron

1. Introduction

1.1 The sense of smell

The sensory systems such as the visual, auditory, somatosensory, gustatory and olfactory system provide the animals with the ability to detect and perceive changes in the environment. Among all of them, the gustatory and the olfactory systems are grouped in the sensory category called chemosensation, that is the ability to detect molecules present in the environment: airborne molecules in the case of the olfactory system and fluid-phase molecules in the case of the gustatory system. A hallmark feature of the chemosensory systems is the huge range of diversity of molecules they can detect. The olfactory system allows organisms to discriminate thousands of low molecular mass compounds, mainly aliphatic and aromatic carbon-based molecules with diverse functional groups, for example: aldehydes, esters, ketones, alcohols, alkenes, carboxylic acids, amines, imines, thiols, halides, nitriles, sulphides and ethers (Bozza et al., 2002; Dulac and Torello, 2003; Firestein, 2001; Mombaerts, 2004).

The olfactory system detects volatile molecules, which can provide valuable information from the environment, for example sources of food, spoiled food, detection of prey or predators approaching, and also nonvolatile molecules which can regulate social interaction among conspecific individuals. Olfaction is critical for animal survival and reproduction and not surprisingly the systems of chemical detection are the most ancient evolved (Ache and Young, 2005; Firestein, 2001; Tirindelli et al., 2009). One more remarkable feature of the olfactory system is the ability to detect a wide range of intensities of stimuli. Indeed, activity-dependent feedback mechanisms during the transduction signaling induce the adaptation of the sensory neurons contributing to the increase of the dynamic range of the response (De Palo et al., 2012; Kurahashi and Menini, 1997; Zufall and Leinders-Zufall, 2000). Finally, the olfactory system can be also extremely selective, for example the mouse is even able to distinguish between enantiomer molecules (Laska and Shepherd, 2007).

1.2 The olfactory system

The olfactory system can be divided in two parts: the peripheral olfactory system, which is in contact with the external environment and where the detection of external stimuli takes place; and the central olfactory system, in the forebrain, which is involved in processing of the sensory information generating the odor perception and motor and emotional responses (Firestein, 2001; Imai, 2014; Su et al., 2009).

The peripheral olfactory system is located in the nasal cavity of the mouse head. The nasal cavity is a large, air-filled space above and behind the nose. The nasal septum divides the

nasal cavity in two *fossae* and each *fossa* is the continuation of one of the two nostrils. The nasal cavity is the uppermost part of the respiratory system and provides the nasal passage for inhaled air from the nostrils to the respiratory tract (Barrios et al., 2014). The airborne molecules enter into the nasal cavity during the breathing cycle and can be detected by the diverse organs that compose the olfactory system. Concentration of the odorants together with other factors such as the oscillatory entrance into the nasal cavity of these molecules during sniffing determine the neural activity generated by their detection in the primary sensory neurons (Mainland et al., 2014; Wachowiak, 2011).

The peripheral olfactory system comprises several organs: the Grueneberg's ganglion (GG), the septal organ of Masera (SO), the vomeronasal organ (VNO) and the olfactory epithelium (OE). These structures differ in terms of location in the nasal cavity (Figure 1), size, type and number of sensory neurons, complexity of the receptors they express, and the projection of their sensory neurons to the central nervous system (Barrios et al., 2014; Chamero et al., 2012; Kaupp, 2010; Munger et al., 2009; Su et al., 2009; Tirindelli et al., 2009).

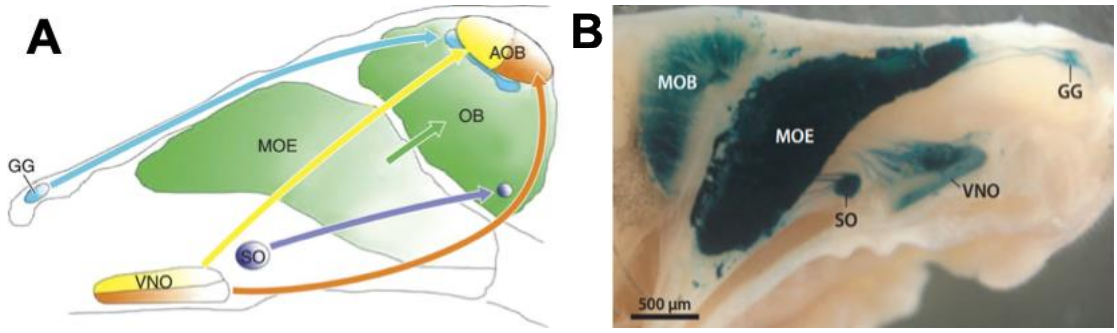

Figure 1: Anatomical localization of different olfactory subsystems in the mouse nasal cavity. A, schematic sagittal view of the olfactory cavity showing the spatial location of the four olfactory subsystems with their projections to the olfactory bulb (OB). In green the olfactory epithelium OE (also called main olfactory epithelium MOE), which projects the axons of the OSNs to the main olfactory bulb (MOB). The MOB contains the largest portion of the OB. The vomeronasal organ (VNO) in yellow and orange sends the axons of the vomeronasal sensory neurons to the accessory olfactory bulb (AOB). In purple the septal organ of Masera (SO), which make projections into a specific location in the ventral MOB. Finally, the Grueneberg's ganglion (GG) in blue, which projects to the dorso-caudal region of the MOB close to the AOB. Sensory neurons from the olfactory system express the protein called olfactory marker protein (OMP). B, sagittal whole-mount view of the nasal cavity and forebrain using an OMP-IRES-tau:LacZ mouse stained blue with X-gal (images modified from Munger et al., 2009; Tirindelli et al., 2009).

1.3 The olfactory epithelium

The general features of the olfactory system are conserved across vertebrates. The OE is a pseudostratified sensory epithelium located in the nasal cavity. The OE is the biggest of the four olfactory subsystems and it extends over a big portion of the nasal cavity from anterior to posterior and from dorsal to ventral regions of the cavity (Figure 1). In addition to the wide

distribution, the OE is arranged in cartilage-supported folds called turbinates, which increase dramatically its surface (Figure 2A). The OE is composed mainly by three cell types: the supporting or sustentacular cells (SC), the basal cells (BS) and the olfactory sensory neurons (OSN) which are the primary sensory cells detecting the odorants entering into the nasal cavity (Figure 2B).

The three cellular components are arranged in separate layers. The cell bodies of the supporting cells are aligned almost in a single layer in the apical part of the epithelium. Supporting cells are columnar epithelial cells with broad apical cell bodies, which make thinner projection towards the *lamina propria*. Their apical membranes present microvilli, which protrude into the nasal cavity and are intermingled with the cilia of the OSNs. The physiological role of supporting cells is still not well understood and several functions have been proposed. Data suggested that supporting cells provide electrical isolation of the dendrites of the OSNs (Breipohl et al., 1974) and regulate the ionic composition of the mucus (Menco et al., 1998). Supporting cells express several types of cytochrome P450 isoforms providing a possible mechanism to detoxification of the inhaled xenobiotic molecules (Dahl and Hadley, 1991; Ling et al., 2004). Finally, supporting cells are responsible for phagocytosis of dead cells (Suzuki et al., 1996).

The OE maintains a steady-state population of OSNs because undergoes constitutive neurogenesis throughout the animal lifespan (Graziadei and Graziadei, 1979; Mackay-Sim and Kittel, 1991). The neurogenesis relies on the basal cells, which as the name indicates have basal location in the OE (Figure 2B). The basal cells are composed by two subpopulation of stem cells: the globose basal cells (GBCs) and the horizontal basal cells (HBCs). Olfactory neurogenesis is normally sustained through differentiation of globose basal cells, which are proliferatively active neurogenic progenitor cells (Carter et al., 2004; Fletcher et al., 2017; Iwai et al., 2008). However, the OE can be regenerated also after the targeted destruction of the sensory neurons or sustentacular cells, or more severe injury to the entire tissue (Graziadei et al., 1979; Herrick et al., 2017; Iwai et al., 2008). Indeed, following such type of injury, the quiescent HBCs become activated to differentiate and reconstitute all major cell types in the epithelium (Fletcher et al., 2017; Iwai et al., 2008; Leung et al., 2007).

The epithelial surface is covered by a layer of mucus that is produced by Bowman's glands. The secretory portion of the glands resides in the *lamina propria*, and the duct of each gland crosses the OE until it reaches the lumen of the olfactory cavity (Figure 2B-3C; Nomura et al., 2004).

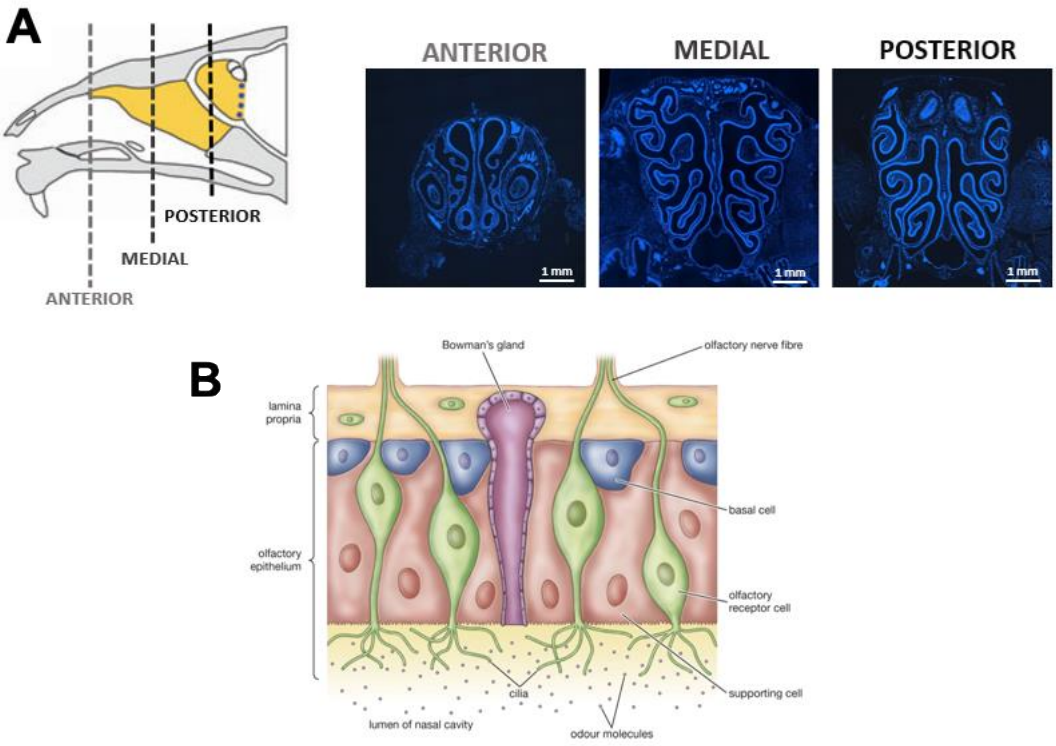

Figure 2: Anatomical organization of the olfactory epithelium. A, left, schematic sagittal view of the olfactory cavity with the spatial location of the OE in yellow (image modified from Munger et al., 2009). The dotted lines represent the planes of the coronal sections of the nasal cavity stained with DAPI which are shown on the right, in blue (Data unpublished from Gonzalez & Menini). The OE is arranged in folds called turbinates which increase in complexity towards the posterior region of the nasal cavity. The turbinates fill the space of the cavity increasing the sensitive surface. B, scheme of a magnified section of the OE showing the main different cell types in color code (image modified from Encyclopaedia Britannica, 2012).

1.3.1. The olfactory sensory neurons

The OSNs are responsible for the detection of the odorants that arrive to the OE during breathing or sniffing. The cell bodies of the OSNs locate in the central layer of the OE, above the basal cells and below the supporting cells (Figure 2B). The OSNs are the most abundant cell type in the OE and express the olfactory marker protein (OMP), a protein that has been widely used as molecular marker of mature olfactory neurons, and recently it has been found play key role in the physiology of the neurons controlling the basal levels of cAMP (Figure 3A; Dibattista and Reisert, 2016). OMP also expresses in the sensory neurons from the other organs of the olfactory system (Figure 1B). The OSNs are bipolar cells with a single dendrite and a single axon (Figure 3B). Each OSN extends the dendrite to the luminal surface of the OE, among the bodies of the supporting cells (Figure 3C). Each dendritic ending terminates with an enlargement called “knob” from which several immotile cilia irradiate (Figure 3 B-D; Morrison and Costanzo, 1990). The cilia are very important structures because they contain all the molecular machinery that detects the odorants and transduce their binding with the

receptors into an electrical signal. Moreover, the geometry of the cilia ensures a very high surface/volume ratio that optimizes the detection capability of the OSNs. The cilia are embedded in a layer of mucus mainly produced by the Bowman's glands. Therefore, the odorants entering during the breathing cycle must be solubilized by the mucus to come in contact with the cilia of the sensory neurons. Moreover, the ionic composition of the mucus plays a fundamental role to ensure the ionic gradients necessary to sustain the transduction currents (Kleene, 2008).

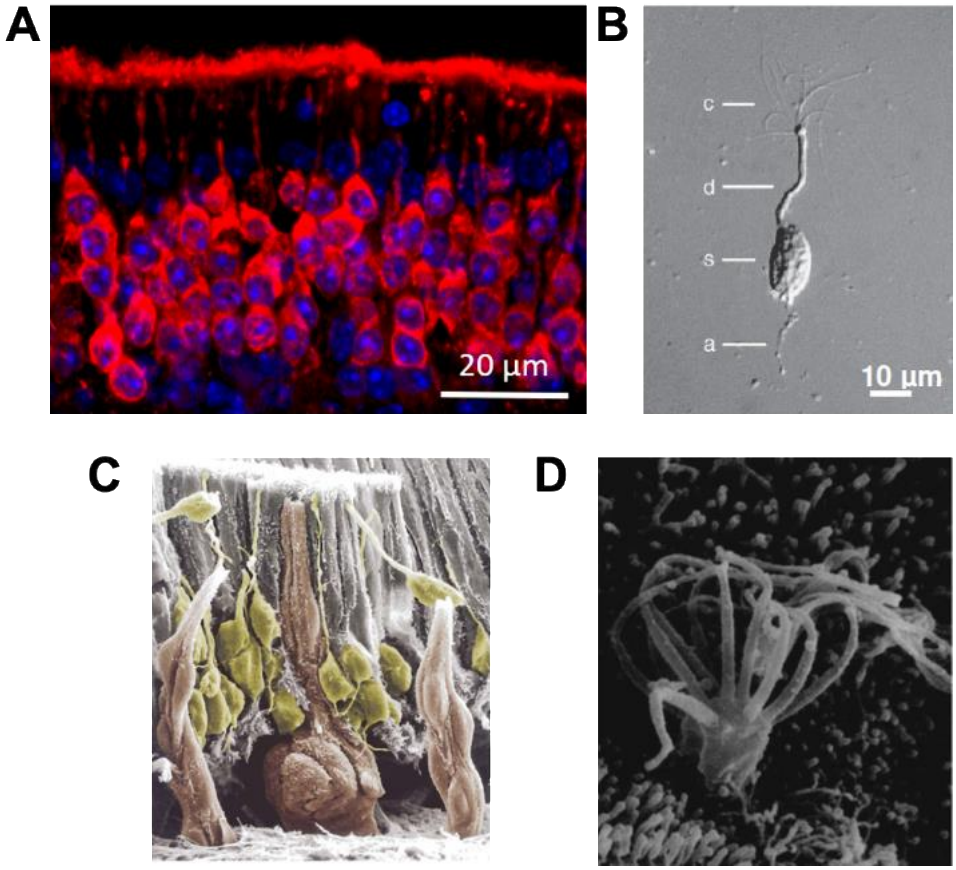

Figure 3: Anatomical organization of the olfactory sensory neurons. A, confocal image of a coronal section from mouse OE immuno-stained for the olfactory marker protein in red. OMP is broadly localized in each neuron including soma, dendrite, cilia and axon. Nuclei are stained in blue with DAPI (Data unpublished from Gonzalez & Menini). B, differential interference optic image from an isolated frog OSN where is possible to distinguish the bipolar morphology of this type of neurons: c, cilia; d, dendrite; s, soma; a, axon (modified from Kleene and Gesteland, 1981). C, scanning electron image of rat OE. Different structures are highlighted in color code: in yellow the OSNs, in pink the Bowman's glands, in gray mainly supporting cells in the upper part of the OE (no scale bar available) (modified from Nomura et al., 2004). D, image of human OSN knob with its cilia obtained with scanning electron microscope (factor of magnification x18525, no scale bar available; modified from Morrison and Costanzo, 1990).

The primary chemo-electrical signal is generated in the cilia and distal dendrite of each OSN. The transduction process produces a graded receptor potential in response to odorant detection. These graded electrical signals are subsequently transformed into action potentials that travel along the single axons of the OSNs, conveying the information about odorant detection. The axons of the OSNs contain voltage dependent channels that are involved in the electrical conduction of the action potentials (Bolz et al., 2017; Schild and Restrepo, 1998; Weiss et al., 2011). From a functional point of view, we could divide the OSNs in two parts: the cilia, where the detection of the odorants occurs, and the axon, which transmits the action potentials working as conduction cable.

The olfactory system can recognize and discriminate a large number of molecules and this capability is based on the expression of more than 1000 olfactory G coupled protein receptors (GPCR) in mouse and rat (Buck and Axel, 1991). These proteins are named olfactory or odorant receptors (OR) as they are the primary molecular sensors of odorants. The ORs are located on the surface of the OSNs, mainly in the cilia. Although the general organization of the OE is very similar among vertebrates, large differences in terms of the number of OR genes are present, for example: human, 388 genes; mouse, 1037 genes; rat, 1201 genes; dog, 871 genes; chicken, 82 genes; frog, 410 genes (Tirindelli et al., 2009). Each OSN expresses only one type of OR. The hundreds or thousands OSNs expressing a given type of receptor are dispersed randomly in only one of four zones present in the olfactory cavity through the dorsoventral axis (Ressler et al., 1993, 1994; Sullivan et al., 1995).

The MOB is the first relay center of the olfactory information carried by the OSNs. In mice, the MOB is the most anterior brain structure, dorso-posterior with respect to the nasal cavity and immediately above the cribriform plate. The precise specificity in the connectivity is essential to translate electrical activity into meaningful neuronal code, and the olfactory system follows a particular organizational principle to achieve this. Molecular-genetic studies using transgenic mice have shown that neurons expressing a particular receptor, no matter where they are found in the OE, converge to 2 or few single spots on each of the two hemi bulbs of the MOB (Feinstein and Mombaerts, 2004; Mombaerts et al., 1996; Vassalli et al., 2002). These spots are called glomeruli, which are spherical neurophil-like structures of 50–100 μm in diameter and are located in the external layer of the OB. The axons of OSNs and the dendrites of the main projection cells in the bulb, the mitral cells, converge in the glomeruli. Each glomerulus receives afferences only from OSNs expressing the same type of OR. This sets a sensory map, with the glomerulus as a functional unit where the information coming from a single type of OR is integrated and maintained in a separated channel. In addition, other neurons are involved in the connection among different glomeruli and among the mitral cells (periglomerular cells and granule cells respectively) integrating the information. Eventually, the information is sent to other centers in the brain such as the anterior olfactory nucleus, the piriform cortex, the cortical amygdala or the lateral entorhinal cortex (Courtiol and Wilson, 2017; Nagayama et al., 2014).

1.3.2. Olfactory transduction

The sensory cilia are enriched in the ORs and other signaling components that mediate the transduction cascade. The olfactory transduction is a chain of molecular events, which occurs in the cilia of the OSNs after the binding of an odorant to a specific OR (Figure 4). This process translates a discrete chemical signal, the odorant, into a graded electrical one, the depolarizing receptor potential. The odorant receptors are the variable component in transduction, and a given OSN expresses only one type of OR, but the other components are constant and common to all OSNs.

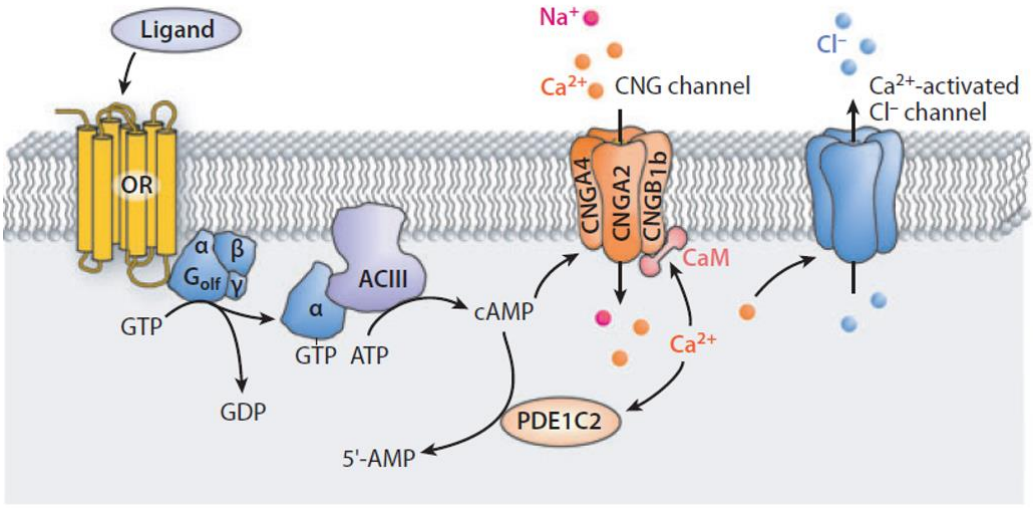

Figure 4: Core elements of the odorant transduction machinery. The odorant transduction is mediated by a signaling pathway composed by multiple steps. The ORs in the membrane of the cilia of the OSNs bind to the odorants arriving into the nasal cavity. This binding leads the activation of the Gαolf-containing heterotrimeric G-protein. Then $G\alpha_{olf}$ subunit activates the adenylyl cyclase type III (ACIII) which produces cAMP. cAMP gates a cyclic nucleotide-gated (CNG) cation channels composed by three types of subunits: CNGA2, CNGA4 and CNGB1b. This allows the depolarizing influx of Na^+ and Ca^{2+}.The increase of cytosolic calcium opens the calcium activated chloride channel named TMEM16B, which allows the efflux of chloride outside the cell contributing to further depolarize the OSN. Other proteins such a phosphodiesterase (PDE) and calmodulin are involved in the negative feedback of this process. PDE decrease the levels of cAMP and calmodulin reduces the sensitivity of the CNG channel to cAMP (modified from Munger et al., 2009).

The binding of an odorant molecule to an OR induces a conformational change in the receptor that activates a Gαolf-containing heterotrimeric G-protein (Belluscio et al., 1998; Jones and Reed, 1989). The activated $G\alpha_{olf}$ subunit activates the adenylyl cyclase type III (ACIII), the key enzyme of this process (Bakalyar and Reed, 1990; Pace et al., 1985; Wong et al., 2000). ACIII is a membrane protein that converts adenosine triphosphate (ATP) into cyclic adenosine monophosphate (cAMP). The increasing of cAMP concentration in the ciliary lumen results in the opening of cyclic nucleotide-gated (CNG) cation channels that are permeable to cations like Ca^{2+}, Na^+ and K^+ (Boccaccio and Menini, 2007; Firestein, 2001; Nakamura and

Gold, 1987; Pifferi et al., 2006). This channel is composed by different subunits: CNGA2, CNGA4 and CNGB1b (Bönigk et al., 1999; Brunet et al., 1996; Liman and Buck, 1994; Michalakis et al., 2006; Zheng and Zagotta, 2004). The opening of CNG channels produces a net depolarizing current, essential for the generation of action potentials in the OSNs. The entry of calcium has several consequences. Calcium gates calcium-activated chloride channels in the OSNs (Boccaccio and Menini, 2007; Kurahashi and Yau, 1993; Lowe and Gold, 1993; Reisert and Reingruber, 2019). This current is mediated by the channel TMEM16B (Billig et al., 2011; Dibattista et al., 2017; Pifferi et al., 2012; Stephan et al., 2009). The OSNs have high chloride concentration inside the cilia (Kaneko et al., 2001, 2004; Nakamura et al., 1997; Reuter et al., 1998) so the opening of this calcium-activated chloride currents produces a further depolarizing efflux of Cl^- which is important in the response amplification (Kurahashi and Yau, 1993; Li et al., 2018; Lowe and Gold, 1993; Pietra et al., 2016; Reisert and Reingruber, 2019)

The use of signaling pathway during transduction of odorants represents an advantage because it allows amplification in each step of this process, but additionally it gives the possibility to introduce negative feedback. To ensure faithful temporal representation of odor stimuli and extension of the dynamic range of detection, the OSNs uses mechanisms of termination and adaptation of the response to odorants and Ca^{2+} is a key player in this process. Calcium binds to calmodulin which in turn decreases the sensitivity of the CNG channel to cAMP and therefore closes the channel (Bradley et al., 2004; Pifferi et al., 2006). In fact, OSNs expressing CNG mutant channels unable to bind calmodulin have a defected in the termination of the response to stimulation with odorants (Song et al., 2008). Additionally, odor-induced elevated cAMP is degraded by phosphodiesterases (PDEs). Two members of the calmodulin-dependent PDE family are expressed in the OSNs; PDE1C in the cilia and PDE4A in the dendrite, cell body and axon terminals but not in the cilia (Borisy et al., 1992; Cygnar and Zhao, 2009; Yan et al., 1995). Though PDE1C is expressed in the cilia, only double knockout mice for PDE1C and PDE4 present an impairment in the odorant response. These mutant mice have a slower termination of the response to short odorant stimuli and a decrease in the adaptation to long odorant stimulation (Cygnar and Zhao, 2009).

The previous elements constitute the canonical members of the odorant transduction machinery in mouse and most of vertebrates, however there are some other identified proteins that contribute to this process. As mentioned before the cytosolic chloride concentration in the cilia of the OSNs is high and important for the signal amplification during transduction. This high concentration of chloride possibly is in part maintained by the $Na^+/K^+/2Cl^-$ co-transporter NKCC1 (Hengl et al., 2010; Nickell et al., 2006, 2007; Reisert et al., 2005). In addition, it has been found that Nckx4, a potassium-dependent Na^+/Ca^{2+} exchanger which contributes to remove intracellular Ca^{2+} after the stimulation, is necessary for rapid response termination and proper adaptation of the OSNs. Indeed, *Nckx4*$^{-/-}$ mutant mice displayed prolonged odor evoked responses and stronger adaptation due to a prolonged increase of intracellular Ca^{2+} (Stephan et al., 2011). Finally, it has been found that also calcium-ATPases can participate in the ionic homeostasis in mice (Saidu et al., 2009) and other vertebrate species (Antolin et al., 2010; Castillo et al., 2007).

Several members of the odorant transduction machinery have high expression levels in the OE, as expected for an organ specialized in odorant detection, but additionally, members

of this machinery can express specifically in the OSNs and not in other cell types in the OE or other tissues. These conditions have been exploited in order to identify molecules that can participate in olfactory detection. In fact, in the past, differential expression screenings allowed the molecular identification of what we know today are the core elements of the odorant transduction machinery, for example the $G\alpha_{olf}$ and ACIII (Bakalyar and Reed, 1990; Jones and Reed, 1989). This differential expression of the elements of odorant transduction could be explained by regulation of olfactory-specific gene promotors and transcription factors. In fact, Wang et al. (1993) reported the characterization of the promotor sequences of various differentially expressed genes in the rat OE, including members of the odorant transduction machinery like Gαolf, ACIII and one of the subunits in the CNG channel (Wang et al., 1993). They found a particular consensus DNA-binding regulatory site for the binding of transcription factor Olf-1. Moreover, they found two additional gene, named *50.06* and *50.11*, which also contain this olfactory specific regulatory sequence. Later, the mouse homologue of gene *50.11* was identified as the member of stomatin family, *STOML-3* (see paragraph 1.4.4.; Goldstein et al., 2003).

1.4 Stomatin-domain protein family

1.4.1 Identification of stomatin proteins

The stomatin family is composed by small and highly conserved proteins present in all domains of life. The members of this family are defined by the presence of a core domain called stomatin domain. Stomatin-domain proteins have broad expression in cells and tissues, and they mainly associate to the cytosolic side of the cell membrane. The first mammalian stomatin-domain protein was originally identified in the search of the causes of a particular type of anemia called stomatocytosis. One of the main causes of anemia is the breaking of the red blood cells, called hemolytic anemia. The causes of hemolytic anemia are diverse, but a very common characteristic is the alteration of the shape of the red blood cells leading to their rupture. For example, in one of the first types of identified anemias, some of the red blood cells were sphere-shaped instead of the normal bi-concave disk shape, and therefore this type of anemia was named spherocytic anemia or spherocytosis (Dhaliwal et al., 2004). Some anemias are inherited diseases, due to mutations mainly in genes encoding proteins associated with the cytoskeleton (e.g. Spectrin) or cytoskeleton-membrane adaptor proteins (e.g. Ankyrin), which alter the shape of the cell. Another gene mutated in patients with hereditary spherocytosis is the anion exchanger 1 (also called Band 3 anion transport protein or *Slc4a1*) which exchanges HCO_3^- and Cl^-. This exchanger is critical for the function of the red blood cells because it allows bicarbonate to move out from the erythrocytes. SLC4A1 interacts with many proteins in the membrane of erythrocytes forming highly organized complexes which also interact with the cytoskeleton. The abnormal shape observed in these patients can be a consequence of changes in the osmotic balance or alterations in the interaction of proteins in the membrane of the erythrocytes (Dhaliwal et al., 2004; Lux, 2016; Reithmeier et al., 2016).

In 1961, Lock et al. identified a different type of hemolytic anemia. Using stained films of blood cells, they showed that many of the erythrocytes of some anemic patients contained a well demarcated, linear unstained area across their center, instead of the normal circular area of pallor. This mouth-like alteration is very similar to the stoma of plant leaves, so these researchers decided to choose the term 'stomatocytosis' to describe this condition which differed from hereditary spherocytosis (Figure 5; Lock et al., 1961).

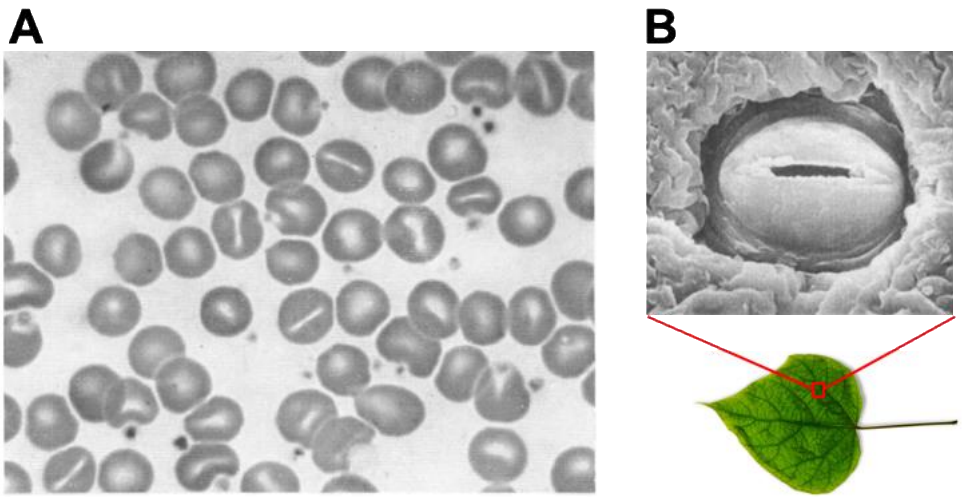

Figure 5: Morphology of red blood cells from a patient with stomacytosis. A, light microscope picture of red blood cells from first study reporting the characterization of stomacytosis (scale bar is not available from the original reference) (Lock et al., 1961). B, Scanning electron micrograph of a stoma in a leaf of *Hebe spp* (factor of magnification or scale bar are not available from the original reference; modified from Willmer and Fricker, 1996).

Some findings suggested that in stomacytosis is characterized by a defect in the ion permeability of the membrane in the red blood cells (Oski et al., 1969). For this reason, part of the effort to study the causes of this disease was directed to identify changes in the membrane of these cells. In 1982, by using one-dimensional sodium dodecyl sulfate (SDS) gel electrophoresis with protein extracts from red blood cell membranes, it was possible to identify a band that decreased in patients with stomacytosis. Indeed, by this type of electrophoresis it was possible to observe 8 strong bands numbered from 1 to 8, band number 1 with the highest molecular mass and band number 8 with the lowest molecular mass. Band 7 could be separated into three components with approximate molecular weights of 30,000, 28,000, and 26,000 Da. It was found that the 28,000-dalton component (called band 7.2b) decreased in some patients with stomacytosis (Figure 6A; Lande et al., 1982). Some years later, it was determined the molecular identity of this band. A first analysis revealed a high composition of hydrophobic amino acids in the N-terminal of the predicted protein sequence (Figure 6B; Hiebl-Dirschmied et al., 1991; Stewart et al., 1992). Over the years, this misregulated protein took the name Stomatin. Mutations causing stomacytosis have not been found in the *Stomatin* gene. However, in recent years, particular mutations on the previously mentioned anion exchanger 1 (*Slc4a1*),

different to those that causes spherocytic anemia, has been found in individuals with stomacytosis (Bruce et al., 2005, 2009). Finally, it has been found that stomatin interact with SLC4A1 and aquaporin-1 suggesting a possible role of stomatin in the regulation of ion transport and osmotic balance (Rungaldier et al., 2013).

In the late 90s the view about stomatin-domain proteins began to expand. Mutant screenings in *Caenorhabditis elegans* allowed to find different genes *Mec-2*, *Unc-1* and *Unc-24*, which showed high homology with human *Stomatin*. MEC-2 was found expressed predominantly in six touch-receptor neurons and to be essential in mechanotransduction (Huang et al., 1995). UNC-1 was found required for normal responsiveness to volatile anesthetics (Rajaram et al., 1998) and UNC-24 was found required for normal locomotion (Barnes et al., 1996). Altogether, these findings revealed some important information: stomatin-like genes and proteins could be present even in basal organisms, they have a high level of conservation, more than one stomatin-like gene could be present in the genome of one species and stomatin-like proteins can play diverse roles. With the development of massive sequencing technologies during 90's and next decade, these general features about the stomatin family were further confirmed.

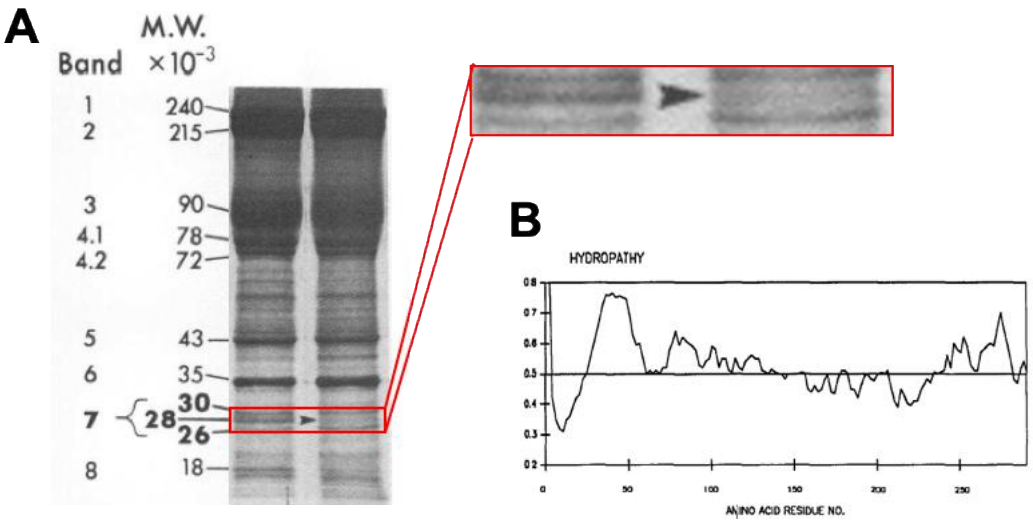

Figure 6: Original identification of the protein absent in patients with stomacytosis. A, One-dimensional SDS gel electrophoresis of the erythrocyte membrane proteins. Band 7 is resolved into three components with approximate molecular weights of 30,000, 28,000, and 26,000. The 28,000-dalton component is present in normal patients, left column, and it is absent in patients with stomacytosis, right column (image modified from Lande et al., 1982). B, Kyte-Doolittle hydrophobicity plot using the predicted amino acid sequence from the original report about the sequence identification of the human *Stomatin* gene involved in stomacytosis and that correspond to the band of 28,000-dalton in A (image modified from Stewart et al., 1992).

1.4.2. Evolutionary and structural features of the stomatin proteins

Stomatin-like proteins have been identified in all three domains of life. The conservation among these proteins is notable, indeed bacterial and human homologs share up to 50 % identity. The distinctive feature of stomatin proteins is the presence of a conserved domain of ~120 aa residues, called stomatin domain which has an even higher conservation with respect to the entire sequence of the proteins (Figure 7). The stomatin domain is further related to the SPFH domain (stomatin/prohibitin/flotillin/HflK/ domain), which is found also in prokaryotes and eukaryotes.

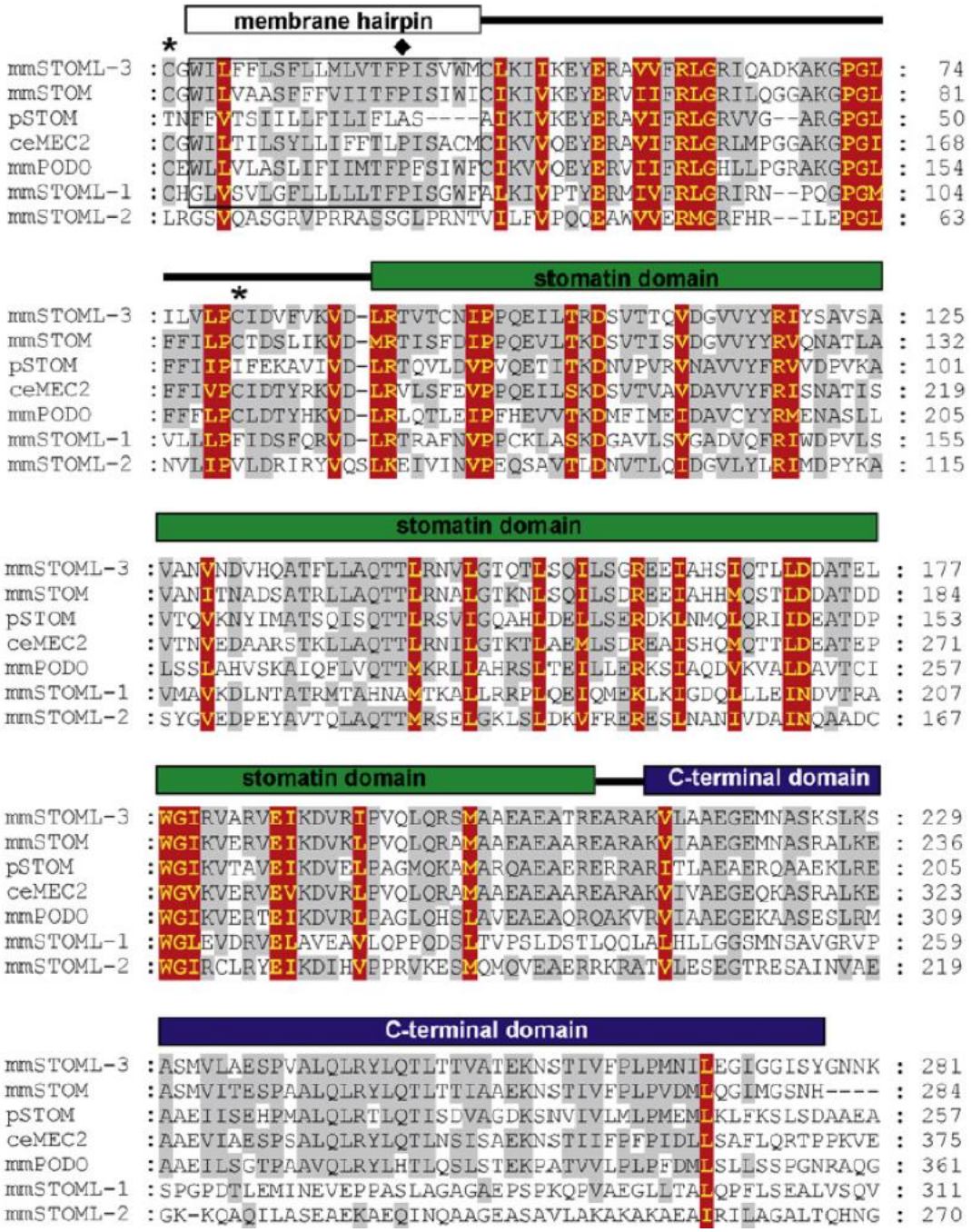

Figure 7: Sequence conservation of the stomatin-domain proteins. Sequence alignment of mouse stomatin-like protein 3 (mmSTOML-3, expasy accession # Q6PE84), mouse Stomatin (mmSTOM, expasy accession # P54116), *Pyrococcus horikoshii* stomatin-like protein

(pSTOM, expasy accession # O59180), *C. elegans* MEC2 (ceMEC2, expasy accession # Q27433), mouse Podocin (mmPODO, expasy accession # Q91X05), mouse stomatin-like protein 1 (mmSTOML-1 , expasy accession # Q8CI66) and mouse stomatin-like protein 2 (mmSTOM-2, expasy accession # Q99JB2). The sequence alignment contains the region starting from the membrane hairpin (boxed) and ending at the C-terminal domain of stomatin. Cysteines shown to be palmitoylated are indicated by * and the proline in the membrane hydrophobic domain required for hairpin formation is indicated by ◆. The amino acids in yellow letters correspond to extremely conserved amino acids. In gray, there are other very conserved amino acids among the different stomatin-domain proteins in this alignment (image modified from Lapatsina et al., 2012).

The conservation in the SPFH domain also is observed at the structural level. Mammalian family members of the SPFH domain proteins include the prohibitins, flotillins, stomatins and the erlins. SPFH domain-containing proteins are all anchored to cellular membranes, including the plasma membrane, endosomes, the Golgi apparatus, mitochondria and the endoplasmic reticulum. This wide distribution also has been accompanied with implication in diverse cellular function, for example in vesicle and protein trafficking, ion channel regulation, cell proliferation, apoptosis and mitochondrial function (Browman et al., 2007; Green and Young, 2008; Tavernarakis et al., 1999).

In mammals, the stomatin family is composed by 5 members: stomatin, stomatin-like protein 1 (STOML-1), stomatin-like protein 2 (STOML-2), stomatin-like protein 3 (STOML-3) and podocin. Stomatin-domain proteins are composed by about 300 amino acids and are organized in 3 domains: harpin hydrophobic domain in the N-terminal, the stomatin domain in the middle and a C-terminal domain (Figure 8A). All stomatin proteins share the same basic topology. A typical stomatin-domain protein is an integral membrane protein localized at the inner leaflet of the membrane with a single, relatively short (around 30 aa), hydrophobic membrane hairpin insertion domain. A single conserved proline residue in the hydrophobic region is required for the formation of the hairpin structure. Stomatin-domain proteins also have conserved cysteine residues close to or in the hydrophobic region, which can be palmitoylated. This modification contributes to the localization of these proteins to mainly lipid rafts. The stomatin domain follows the hydrophobic domain and constitutes most of the protein, followed by a 60 amino acid C-terminal domain, which is less conserved with respect to the other domains. Biochemical membrane fractioning in combination with mutational studies have revealed that residues in the C-terminal domain also contribute to the association to the lipid rafts on the cell membrane (Umlauf et al., 2006). Both N- and C-terminals of the stomatin protein are intracellular.

The stomatin domain is composed by about 120 amino acids and corresponds to the most conserved portion of the protein (Figure 7). It is composed by both α-helices and β-sheets. The N-terminus of stomatin domain is organized in two β-sheets (β1 and β2) followed by four α-helices (α1, α2, α3 and α4). An additional β-sheet (β3) is located at the C-terminus. The β-strands form a curved β-sheet while the α-helices are located inside the groove generated by the β-sheet (Figure 8B). This structural arrangement is highly conserved even from bacteria and in other members of the SPFH domain family. A characteristic of the stomatin-domain

proteins is their ability to oligomerize among themselves, forming homo or hetero oligomers. Biochemical studies have revealed that the stomatin-domain proteins can form high order oligomers composed of more than 10 single monomers (Mairhofer et al., 2009; Snyers et al., 1998; Umlauf et al., 2006). Some amino acid residues the C-terminal domain are essential for oligomerization. Structural studies also have further supported the oligomerization of these proteins. It has been possible to determine the structure of the stomatin-domain proteins forming dimers, trimers and recently high order ring-like structures composed by more than 10 monomers (Figure 9; Brand et al., 2012; Takekawa et al., 2019; Yokoyama et al., 2008). These structural studies have further supported the hypothesis that residues in the C-terminal of the stomatin domain could contribute to oligomerization.

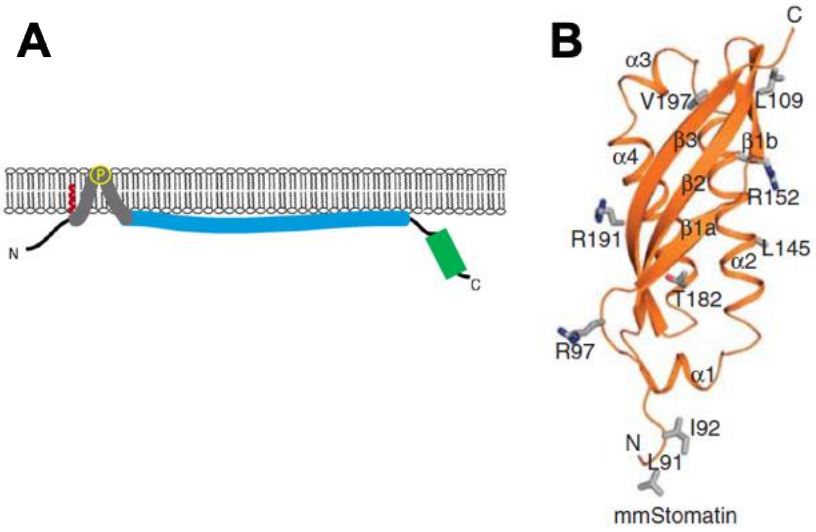

Figure 8: Topology of stomatin-domain proteins and the stomatin domain structure. A, stomatin-domain proteins are ~300 aa integral-membrane proteins. They locate in the inner leaflet of the cell membrane. These proteins contain 3 domains: a short hydrophobic domain in the N-terminal (in gray), a ~120 aa stomatin domain in the middle (in blue) and a C-terminal domain (green). They have some conserved cysteine residues in the N-terminal region that can be palmitoylated (red twist). The stomatin-domain proteins also have a conserved proline residue in the hydrophobic domain important in determine the hairpin topology of this domain (modified from Browman et al., 2007). B, crystal structure of the stomatin domain of mouse Stomatin. This domain is composed by 3 β-strands forming an anti-parallel, curved β -sheet and 4 α-helices. N-and C-termini are located at opposing sides of this domain (modified from Brand et al., 2012).

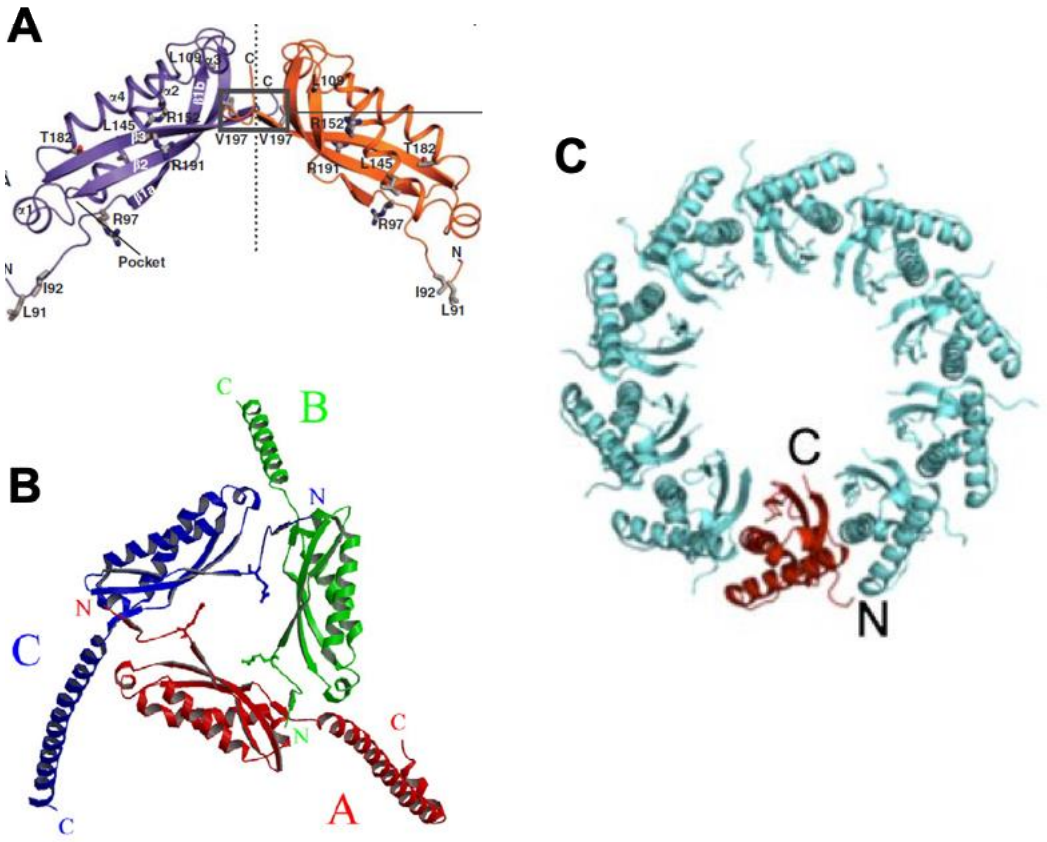

Figure 9: Crystal structures of some stomatin domains forming oligomers. A, structure of mouse stomatin domain forming dimers, one monomer is in purple and another monomer in orange (Brand et al., 2012). B, structure of *Pyrococcus horikoshii* p-stomatin forming trimers, the monomers are represented in blue, green and red (Yokoyama et al., 2008). C, structure of FliL, a stomatin-like protein in *Vibrio alginolyticus* which form ring-like assemblies, one monomer in red and the rest of them in cyan (Takekawa et al., 2019).

STOML1 and STOML-2 have some differences regarding the canonical domain composition and subcellular localization of the stomatin family. STOML-1 has a C-terminal sterol carrier protein-2 (SCP2) domain that is absent in other mammalian stomatin-like proteins (Mairhofer et al., 2009). From the original molecular identification study of *STOML-1* (Seidel and Prohaska, 1998), it was found that STOML-1 has a broad expression in cells and tissues and it is specially enriched in the brain and the heart. The physiological role of STOML-1 is less known. It has been found that STOML-1 is located in the cell membrane and intracellular vesicles, mainly in late endosomes, but is especially enriched in the latter (Kozlenkov et al., 2014; Mairhofer et al., 2009). In fact, it has been found that targeting of STOML-1 to late endosomes is caused by a sorting signal at the N-terminus and mutation of this signal results in plasma membrane localization of STOML-1 (Mairhofer et al., 2009). STOML-2 is the most sequence divergent member of the stomatin family, and also it has a wide expression like

STOML-1 (Wang and Morrow, 2000). STOML-2 has been found predominantly in mitochondria; in fact, this protein has a mitochondrial localization sequence at its N-terminus (Da Cruz et al., 2008). STOML-2 also lacks the N-terminal hydrophobic domain. Because of the wide expression of STOML-2 and its particular localization on mitochondria, STOML-2 could play a role in an important basal cell function. In fact, mutations that lead to loss the expression STOML-2 are lethal (Lapatsina et al., 2012).

1.4.3. Physiology of the stomatin proteins

1.4.3.1. Stomatin proteins in the erythrocyte membrane

Regulation of ion channels and transporters is one of the main functions associated with the stomatin-domain proteins. The first hint for this role comes from the finding that the erythrocytes from patients affected by hereditary stomacytosis are leaky to cations (Oski et al., 1969). As mentioned before, despite that the *stomatin* gene of patients with hereditary stomacytosis does not have mutations, in some of these patients have been found mutations in the anion exchanger 1 gene (*Slc4a1*; Bruce et al., 2005). Recently, it was shown that stomatin and SLC4A1 can interact directly in the membranes of erythrocytes (Rungaldier et al., 2013). Some recent indirect measures suggest this interaction also has a functional impact on the activity of SLC4A1 (Genetet et al., 2017). A stopped-flow spectrofluorometer was used in combination with pH- or chloride-sensitive fluorescent indicators to indirectly determine the flow of bicarbonate and chloride in erythrocyte membranes in normal patients and patients with hereditary stomacytosis. Bicarbonate and chloride flow were slower in membranes from patients with stomacytosis (Genetet et al., 2017). Similar findings were obtained using a cell heterologous expression system. However, the link between this modulation on the SLC4A1 and the defects observed in the erythrocytes in stomacytosis is still unclear.

1.4.3.2. Stomatin proteins in mechanotransduction

A better characterization of the regulation of ion channels by stomatin-domain proteins has been obtained by investigation of mechanotransduction in *Caenorhabditis elegans*. Mutant screenings allowed the identification of proteins involved in the mechanical transduction by mechanoreceptor sensory neurons. From 302 neurons of this organism, around 30 are considered mechanoreceptors. A subset of these mechanoreceptors in *Caenorhabditis elegans* uses a DEG/ENaC channel complex to transduce mechanical forces (Chalfie, 2009; Geffeney and Goodman, 2012). The complex contains two pore-forming subunits, MEC-4 and MEC-10, as well as other accessory subunits such as MEC-2, MEC-6, MEC-7 and others (Figure 10A). This complex localizes in regular *puncta* along the touch receptor neurons. MEC-4 and MEC-10, which belong to the DEG/ENaC ion channel family, form an amiloride-sensitive sodium channel that transduce the mechanical force (Chalfie, 2009; Geffeney and Goodman, 2012).

They form the ion channel that allows the generation of the mechanoreceptor current induced by mechanical stimulation (Chalfie, 2009; Geffeney and Goodman, 2012). MEC-2, a stomatin like protein, has been found essential for mechanotransduction in *C. elegans* (Huang et al., 1995; Zhang et al., 2004). MEC-2 interacts by the stomatin domain with MEC-4 and has the same pattern of localization in the touch receptor neurons (Huang et al., 1995; Zhang et al., 2004). Several mutated MEC-2 alleles have been identified that cause touch insensitivity. Some of these mutations are on the stomatin domain. They disrupt the MEC-2 *puncta* pattern of localization in the touch neurons and these neurons become insensitive (Zhang et al., 2004, 2004). In oocytes, the amiloride sensitive current is abolished by co-expression of MEC-4 with various forms of MEC-2 with mutations in the stomatin domain (Zhang et al., 2004). Moreover, several mutated MEC-2 alleles, which causes insensitivity, produce mutated proteins lacking the ability to bind cholesterol (Huber et al., 2006). For example, the MEC-2(P134S) mutant, which has a substitution of a serine for a proline in the hydrophobic region that precedes the stomatin domain, cannot bind cholesterol even though it can oligomerize and interact properly with the MEC-4 (Huber et al., 2006). These data suggest that loss of touch sensitivity results from the loss of cholesterol binding by MEC-2 and demonstrate the importance of the *in vivo* binding to cholesterol (Huber et al., 2006). Single channel recordings of the MEC-4/10 expressed in oocytes showed that co-expression with MEC-2 does not alter dramatically the open probability of the channel, but produces a small increase in the amplitude of single channel conductance (Brown et al., 2008). At the macroscopic level, MEC2 increases the current mediated by MEC-4/10 without altering their membrane expression. This current increase is lost in the MEC-2(P134S) mutant, unable to bind to cholesterol, but also in the MEC-2(C140/174A) mutant that has a substitution in two conserved cysteine residues that are palmitoylated and contribute to cholesterol binding. These findings further support a role of MEC-2 as a positive regulator of MEC-4 by placing this channel in a particular lipid environment (Brown et al., 2008).

The role of stomatin-domain proteins in mechanotransduction and touch sensitivity is conserved during the evolution. For example in mammals, STOML-3 is expressed in a subset of dorsal root ganglion (DRG) neurons and studies of mutant mice lacking STOML-3 showed that STOML-3 is an important determinant of the skin mechanoreceptor functions. Indeed, about 35% of skin mechanoreceptors do not respond to mechanical stimuli in STOML-3 knock out mice (Figure 10B). At the behavioral level, the loss of STOML-3 impairs tactile discrimination capability and touch-evoked pain following neuropathic injury (Wetzel et al., 2007). It is still unclear the precise molecular mechanisms by which STOML-3 controls the response of skin mechanoreceptors. However, it has been found that STOML-3 functionally interacts with the mechanosensitive ion channels Piezo-1 and Piezo-2, increasing the sensitivity of these channels to mechanical stimulations (Figure 10C; Poole et al., 2014). In addition, repetitive mechanical stimulations lead to a reduction of the amplitude of the Piezo currents and this phenomenon is partially prevented by the presence of STOML-3 (Figure 10D; Poole et al., 2014a). Finally, mutations in residues important for oligomerization and in the stomatin domain of STOML-3 lead to lose this effect (Poole et al., 2014).

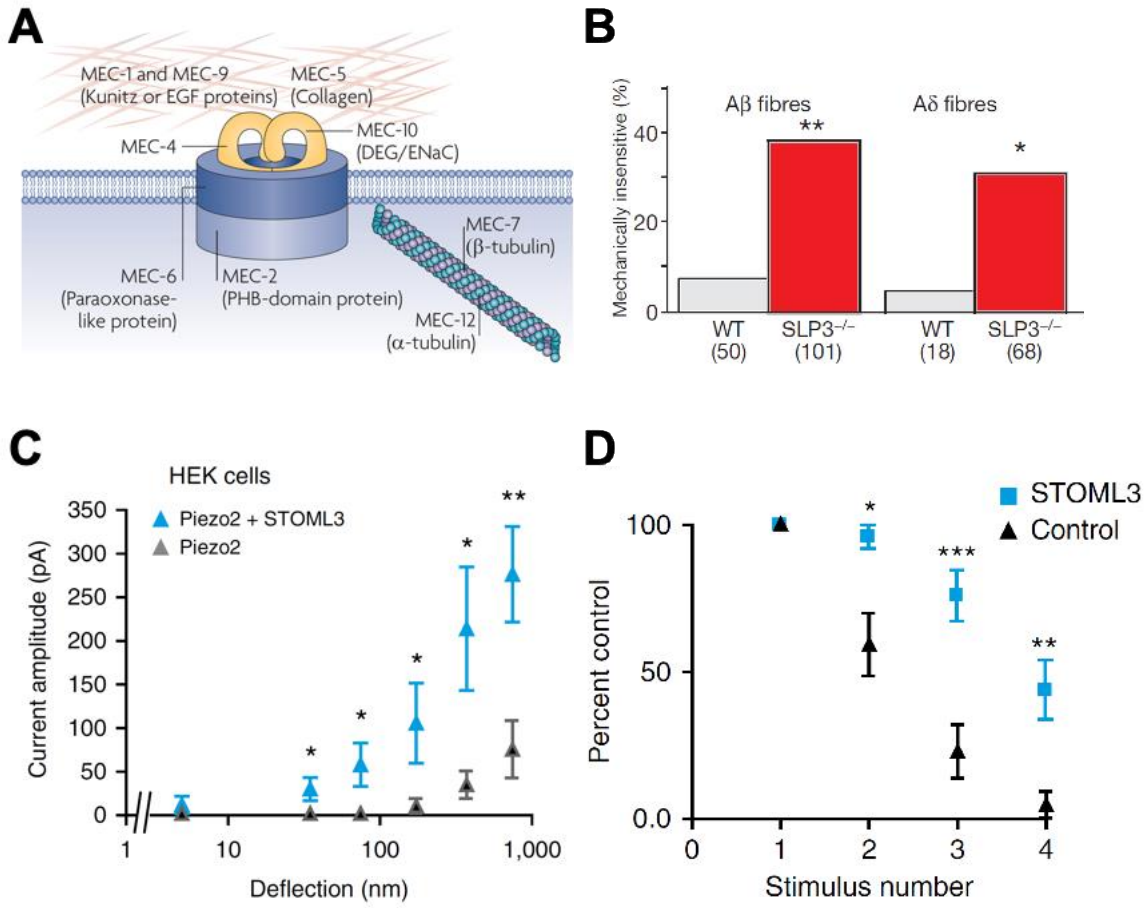

Figure 10: Stomatin-domain proteins are involved in mechanotrasduction in different species. A, A subset of mechanosensory neurons *Caenorhabditis elegans* uses a DEG/ENaC channel complex to transduce mechanical stimuli. Multiple proteins compose this complex. MEC-4 and MEC-10 are the pore-forming subunits of the channel that allows the generation of the mechanoreceptor current induced by mechanical stimulation. MEC-2 is a stomatin-like protein, which is essential for mechanosensitivity. In particular MEC-2 can interact and regulate MEC-4 (modified from Chalfie, 2009). B, normally, more than 90% of sensory fibers innervating the skin of mouse are mechanoreceptors. The percentage of fibers that become insensitive to mechanical stimulation increase in STOML-3 knock out mice to around 35% (modified from Wetzel et al., 2007). C, Co-expression Piezo2 with STOML-3 decrease the threshold of mechanical stimuli that induces the current (modified from Poole et al., 2004). D, Overexpression of STOML-3 in N2a cells prevents the desensitization of Piezo-1 mediated currents (modified from Poole et al., 2004).

1.4.3.3. Regulation of the acid-sensing ion channel family (ASIC) by stomatin proteins

Stomatin-domain proteins also modulate the acid-sensing ion channel family (ASIC). In vertebrates, 6 members compose the ASIC family: ASIC1a, ASIC1b, ASIC2a, ASIC2b, ASIC3 and ASIC4. ASIC1a/ASIC1b and ASIC2a/ASIC2b are splice variants. These channels express broadly and are implicated in several functions, for example pain perception (Bianchi and Driscoll, 2002). Stomatin, STOML-1 and STOML-3 can interact with the ASIC channels and regulate them in diverse ways.

In particular, Stomatin has been found to interact with ASIC1a, ASIC2a and ASIC3 in heterologous systems (Figure 11A; Brand et al., 2012; Price et al., 2004). Co-expression of stomatin with ASIC3 abolishes the proton-sensitive current by ASIC3 (Figure 11C), whereas co-expression of stomatin with ASIC2a does not alter the amplitude of the proton sensitive current. However, the speed of desensitization of the channel in a sustained stimulus of low pH increases (Figure 11D). Co-expression of stomatin with ASIC1a does not alter the amplitude of the proton evoked current or the time constant of desensitization (Brand et al., 2012; Price et al., 2004).

STOML-3 can interact directly with ASIC2a, ASIC2b and ASIC3 (Figure 11B; Lapatsina et al., 2012; Wetzel et al., 2007) and a decrease in the proton induced current by the presence of STOML-3 in CHO cells expressing ASIC2a has been measured (Figure 11E; Lapatsina et al., 2012). This STOML-3 regulation observed in heterologous system could also have an impact on DRG neurons. In fact, DRG neurons from STOML-3 knock out mice also have an increase in the current induced by stimulation of low pH (Figure 11F; Wetzel et al., 2007).

STOML-1 expresses broadly in tissues and cells, including a subset of DRG neurons (Figure 12A). In DRG neurons, STOML-1 proteins localize in the cell membrane and mostly in intracellular vesicles. STOML-1 is expressed in approximately half of the DRG neurons, mainly in small diameter ones (Kozlenkov et al., 2014). Using heterologous expression systems, it was found that STOML-1 decreases and almost abolishes the ASIC1a current induced by stimulation at low pH (Figure 12B). This effect was not observed using a version of STOML-1 that loses the SCP2 domain, pointing out a possible divergent mechanism of regulation by STOML-1 respect to other stomatin family members. STOML-1 does not have any effect in the amplitude of the pH-induced current of ASIC1b, ASIC2a ASIC3; however, it accelerates the inactivation time constant when the stimulus is removed in the case of ASIC3 (Kozlenkov et al., 2014). Additionally, in DRG neurons from STOML-1 knock out mice, showed a tendency to have a smaller amplitude of the currents induced by stimulation with low pH (Kozlenkov et al., 2014). These findings support that STOML-1 have different modulatory roles depending on the target.

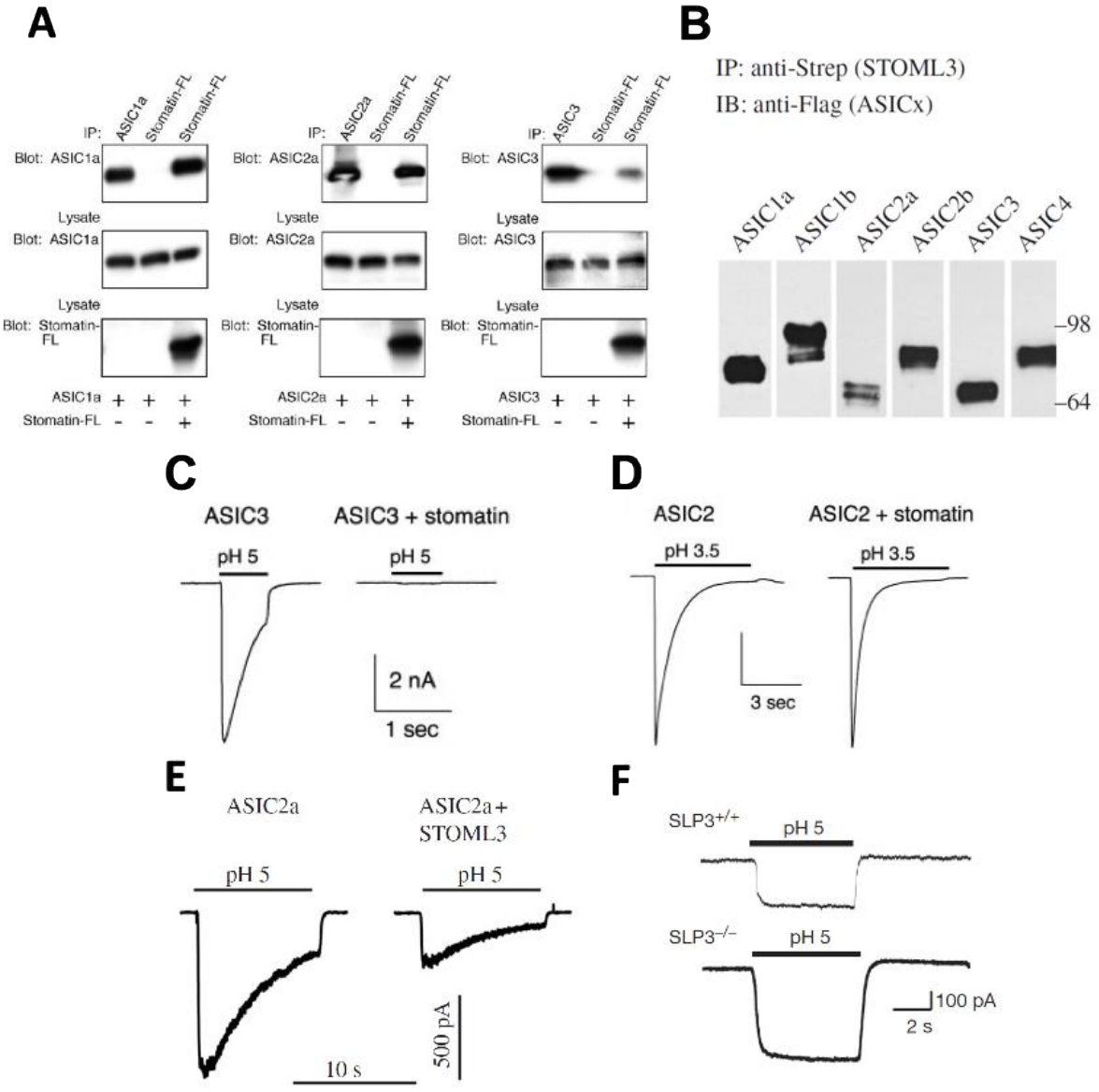

Figure 11: Stomatin-domain proteins interact and modulate the acid sensitive ion channels ASICS. A, COS-7 cells were transfected with ASIC1a, ASIC2a, or ASIC3 and stomatin-Flag (FL). Immunoprecipitated was performed with anti-Flag antibody and the immunoprecipitates were probed with either ASIC1a, ASIC2a, or ASIC3 antibodies as indicated. ASIC1a, ASIC2a, and ASIC3 co-immunoprecipitate with stomatin (modified from Price et al., 2004). B, CHO cells were transfected with Flag-ASIC1a, Flag-ASIC1b, Flag-ASIC2a, Flag-ASIC2b, Flag-ASIC3 and Flag-ASIC4 and STOML-3-Strep. Immunoprecipitated was performed with anti-Strep antibodies and they were probed with anti-Flag antibodies as indicated. All ASIC channels were found to interact with STOML-3 (modified from Lapatsina et al., 2012b). C, representative currents evoked by application of pH 5 to CHO cells expressing ASIC3 or co-expressing ASIC3 and stomatin. Stomatin inhibits ASIC3 acid-evoked current (modified from Price et al., 2004). D, representative currents evoked by application of pH 3.5 to CHO cells expressing ASIC2a or co-expressing ASIC2a and stomatin. Stomatin increases the rate of ASIC2 desensitization (modified from Price et al., 2004). E, representative currents evoked by application of pH 5 to CHO cells expressing ASIC2a or co-expressing ASIC2a and STOML-3. STOML-3 reduces the amplitude of the

ASIC2a-mediated current (modified from Lapatsina et al., 2012b). F, Proton gated currents in DRG neurons from STOML-3 WT (STOML-$3^{+/+}$) and STOML-3 KO (STOML-$3^{-/-}$) mice. Amplitude of sustained current at pH 5 was larger in KO animals (Wetzel et al., 2007).

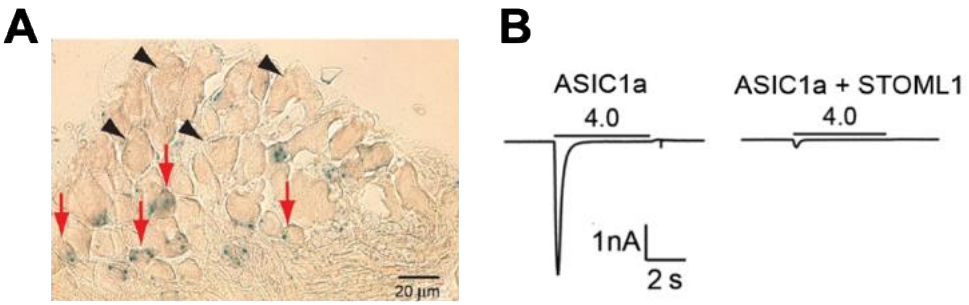

Figure 12: STOML-1 inhibits ASIC1a currents. A, thoracic DRG neuron section illustrating that STOML1 (by X-gal staining in blue) is present in small diameter DRG neurons (red arrows) and absent in large diameter DRG neurons (black arrowheads) (modified from Kozlenkov et al., 2014). B, representative currents evoked by application of pH 4.0 to CHO cells expressing ASIC1a or co-expressing ASIC1a and STOML-1. STOML-1 almost completely ablated the ASIC1a-mediated current (modified from Kozlenkov et al., 2014).

1.4.3.4. TRPC6 regulation by podocin

Finally, some evidence supports also Podocin, the last mammalian member of the stomatin family, as an ion channel regulator. Podocin localizes specifically in the podocytes of kidney in mammals and could be involved in the formation of the filtration barrier. In humans, mutations in the Podocin gene cause congenital nephrotic syndrome, which is a severe genetic kidney disorders characterized by disruption of the filtration barrier. Mutations in some other identified genes that express in the podocytes also can lead to similar kidney defects, for example, alterations on the transient receptor potential channel 6 (TRPC6) gene. TRPC6 and Podocin share the same location in the podocytes and it was found that they can physically interact. Moreover, this physical interaction also leads to changes in the functional properties of TRPC6 (Huber et al., 2006). Co-expression of TRPC6 and Podocin in oocytes increase the current of TRPC6 induced by stimulation with OAG (oleoyl-2-acetyl-sn-glycerol). It was found that the stomatin domain of podocin is required for the binding to TRPC6, and additionally that the stomatin domain can bind cholesterol and substitution mutation in residues in the stomatin domain that allow the binding to cholesterol also impair the modulation of podocin on the TRPC6. Therefore, this finding further supports a cholesterol dependence in the regulation of Podocin on TRPC6 (Huber et al., 2006).

1.4.4. Expression of the stomatin family in the olfactory system

As already mentioned in section 1.3.2, the *STOML-3* promoter region contained specific sequences for the binding of olfactory-specific transcription factors (Goldstein et al., 2003; Wang et al., 1993). In 2002/3, two research groups, Goldstein et al. and Kobayakawa et al. reported the expression of STOML-3 in the OE. Northern blot experiments revealed the presence of *STOML-3* transcripts in the OE from adult mice and no in other tissues such as brain, eyes, liver, spleen, lung, thymus and testis (Figure 13A; Goldstein et al., 2003; Kobayakawa et al., 2002). The expression of *STOML-3* transcripts in the OE from mouse was confirmed by RT-PCR. It was found to be absent in the VNO, retina and tongue, further supporting the very restricted expression of *STOML-3* to the OE (Figure 13B; Kobayakawa et al., 2002). Moreover, by RT-PCR Kobayakawa et al., (2002) found that also *Stomatin* is expressed in the OE as well as in the VNO, retina and the tongue (Figure 13B). By *in situ* hybridization, *STOML-3* and *Stomatin* transcripts were found present in the layer of the OSNs in the OE and were found absent in the supporting cells (Figure 13 C and D; Goldstein et al., 2003; Kobayakawa et al., 2002).

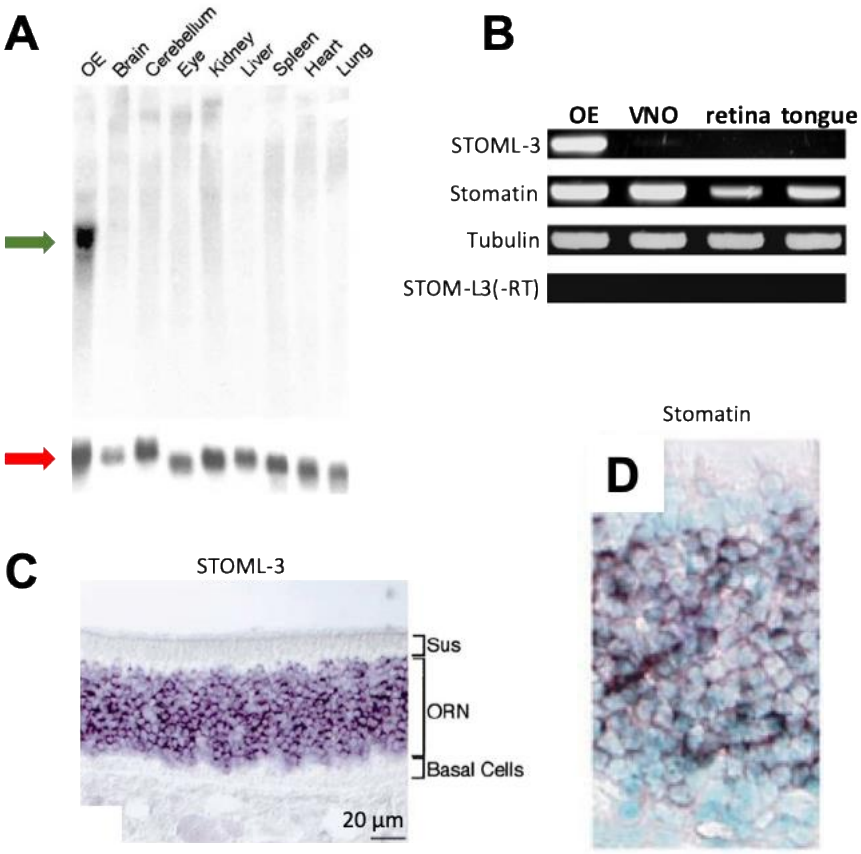

Figure 13: Expression of *STOML-3* and *Stomatin* transcripts in the olfactory epithelium of mouse. A, Northern blot using total RNA isolated from different tissues from adult mice and tested with a *STOML-3* antisense probe. The green arrow indicates the *STOML-3* band. The red arrow indicates the bands obtained by the use of a probe to target the ribosomal protein S26 as positive control of presence of RNA (modified from Goldstein et al., 2003). B, Total RNA was isolated from the OE, VNO, retina, and tongue. Samples were treated with RNase-free DNase I and then reverse transcribed. PCR was performed with *STOML-3*, *stomatin* and tubulin (positive control) primers. Last line corresponds to negative control, adding *STOML-3* primers and, as template, a sample with no retro-transcriptase added during template synthesis. *STOML-3* mRNA expresses only in the OE. *Stomatin* mRNA expresses in the OE, VNO, retina and tongue (modified from Kobayakawa et al., 2002). C and D, high magnification image of *in situ* hybridization using an antisense probe to target *STOML-3* and *Stomatin* transcripts in the OE. *STOML-3* and *Stomatin* transcripts are express in the OSNs and are absent in the supporting cells (C, modified from Goldstein et al., 2003. D, modified from Kobayakawa et al., 2002).

By using antibodies against STOML-3 and immunohistochemistry, it was found that STOML-3 protein was preferentially localized in the apical portions of OSNs in adult mice, possibly in the cilia and knobs of the OSNs (Figure 14A; Goldstein et al., 2003; Kobayakawa et al., 2002). STOML-3 protein was absent in the axons emerging from the basal region of the OE or in the glomeruli in the MOB (Goldstein et al., 2003; Kobayakawa et al., 2002). Goldstein et al. (2003) also found STOML-3 protein expression in dendrites and soma. Similar findings

have been confirmed by later reports, however they showed that STOML-3 protein was enriched in the apical portion of the OSNs (Kulaga et al., 2004; Tadenev et al., 2011). The STOML-3 enrichment in the cilia has been confirmed by Western blot comparing the signal obtained using the cilia fraction of the OE respect to total OE as sample source (Kurtenbach et al., 2017). Tadenev et al. (2011) additionally showed, by immunohistochemistry, the colocalization of STOML-3 with the ORI7, further supporting the localization of STOML-3 protein in the cilia of the OSNs. The expression of STOML-3 also was studied in genetically modified mice which express STOML-3 fused to the green fluorescent protein GFP (STOML-3-GFP). In this type of mice, using whole mount *en face* preparations, the signal of STOML-3-GFP was observed in the base of the cilia of the OSNs, complementing the apical localization of STOML-3 observed in the previous immunohistochemical experiments (Figure 14C).

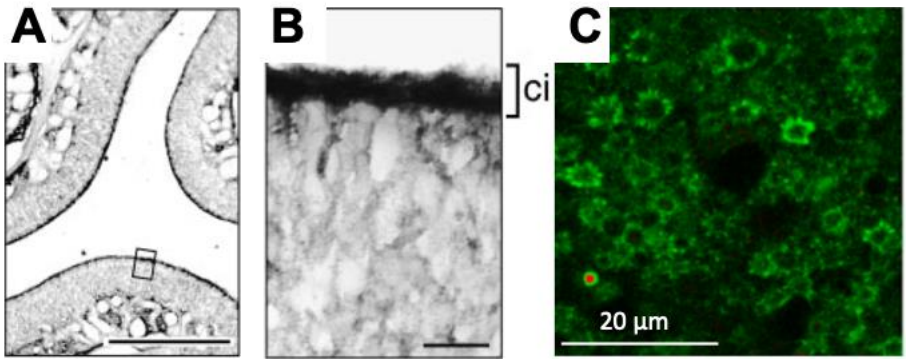

Figure 14: Localization of STOML-3 proteins in the olfactory epithelium of mouse. A, Guinea pig antiserum was produced using peptides based on the sequence of mouse *STOML-3* gene. Peptides correspond to the 19 N-terminal residues of the deduced STOML-3 amino-acid sequence. Antiserum was used in immunohistochemistry in coronal sections of the OE of adult mice. Immunoreactivity is mainly present in the cilia of the OSNs. B, magnified view of a small portion of the image in A (modified from Kobayakawa et al., 2002). C, on face whole mount of OE preparation from a mouse expressing the fusion protein STOML-3-GFP. Fluorescent signal of GFP is present mainly in the basal part of the cilia of the OSNs (modified from Tadenev et al., 2011).

In recent years, transcriptomic and proteomic research in the mouse OE have supported the expression of other stomatin family members such as STOML-1 and STOML-2, in addition to STOML-3 and Stomatin (Ibarra-Soria et al., 2014; Kanageswaran et al., 2015; Saraiva et al., 2015). Although, there are some discrepancies among the results of these studies, they all agree in the absence of podocin in the OE. Moreover, the transcriptomic data show that *Stomatin* and *STOML-3* are among the highest expressed transcripts in the mouse OE, while STOML-1 and STOML-2 expression levels seems lower. The high expression of *Stomatin* and *STOML-3* transcripts in the OE has been confirmed by qRT-PCR by Wetzel et al. (2007), and also pointing out that among several tissues tested, the OE has the highest expression levels for these two transcripts.

Several proteomics studies have been focused on the detection of the proteins in the cilia of the OSNs using biochemically isolated cilia extracts from the OE of mice and rats. All these studies agreed in the presence of Stomatin and STOML-3 in the cilia extracts, and one in particular suggested the presence of STOML-2 (Klimmeck et al., 2008; Kuhlmann et al., 2014; Mayer et al., 2008; Stephan et al., 2009).

The possible role of stomatin-domain proteins in OSNs is still very unclear. Kobayakawa et al. (2002) found that STOML-3 was enriched in the lipid raft fraction of the membrane from OE, colocalizing with caveolin-1, a lipid raft associated protein that organizes signaling complexes in this submembrane structure. In fact, using immunoprecipitation and Western blot, caveolin-1 has been shown to interact with components of the transduction machinery like the $G\alpha_{olf}$ and ACIII (Schreiber et al., 2000). Interestingly, by biochemical experiments the amount of cyclic AMP in ciliary membrane extracts from mouse OE produced by ACIII activators (forskolin and GTPγS) was increased upon the incubation with antibodies against STOML-3 (Kobayakawa et al., 2002).

2. Materials and methods

2.1 Animals

To study the role of the stomatin-domain proteins in the development and function of the olfactory system, we used two knock-out mouse lines for stomatin protein genes provided by professor Gary Lewin (Max Delbrück Center for Molecular Medicine, Berlin, Germany). The first mouse line named in this study KO, which is knock-out for STOML-3 (Wetzel et al., 2007) and the second mouse line named in this study TKO, which is knock-out for Stomatin, STOML-1 and STOML-3 (Kozlenkov et al., 2014; Moshourab et al., 2013; Wetzel et al., 2007). Animals were used at 2 ages: 2 months or 6 months old. The mouse colonies were maintained in the animal house facility at the International School for Advances studies (SISSA) in Trieste. Animals were maintained in temperature-controlled environment with a twelve-hour light/dark cycle and continues supply of food and water. All animals were handled in accordance with the Italian Guidelines for the Use of Laboratory Animals (Decreto Legislativo 24/14) and European Union guidelines on animal research (2010/63/UE). To obtain the OE for the different experiments the mice were sacrificed by CO_2 inhalation, decapitated, and then the skin and posterior part of the head were removed and separated from the most apical part which contain the nasal cavity with the whole olfactory epithelium.

2.2 mRNA isolation and polymerase chain reaction PCR

mRNA was extracted from 10-20 mg of the olfactory epithelium of wild type (WT) mice using magnetic beads mRNA isolation kit (New England Biolabs). cDNA was synthetized using the Protoscript First-Strand DNA Synthesis Kit from 100-500 ng of mRNA (New England Biolabs). PCR was performed in thermocycler ThermaCycler2720 (LifeTechnologies) using Taq DNA polymerase and Thermopol buffer (New England Biolabs), 0.2 mM for each dNTPs and 200 pmol forward/reverse target-specific primers. Cycling parameters were: an initial denaturation step (95 °C, 2 minutes) followed by 35 cycles, each of these cycles included a denaturation step (95 °C, 30 seconds), a primer annealing step (62-64 °C, 30 seconds), and an extension step (72 °C, 60 seconds). Reaction was completed by a final extension step at 72 °C for 5 minutes. Contamination from genomic DNA was tested by using a sample of the mRNA without retrotranscription step. Quality of the olfactory epithelium cDNA was tested by using primers for targets expressed in this tissue such as *Gapdh*, olfactory receptor 73 (*OLFR73*), *Tmem16B* or $G_{\alpha olf}$. All amplicons were purified and sent to sequencing to confirm the molecular identity of the respective targets. cDNA from testis (Clontech Laboratories) was used to set a positive control for PCR amplification to confirm that the primers of podocin are properly working. The sequences of all primers used are listed in Table 1.

Target	Primer forward	Primer reverse	Tm (°C)	Amplicon length (bp)	Accession number
GAPDH	TGCTGAGTATGTCGTGGAGTCT	TGCTGTAGCCGTATTCATTGTC	62	691	NM_008084.
OLFR73	GCTGGTATTGGGATCCTATGCTT	CGTCCACTTGCTGACTTCATCTT	62	272	NM_054090.1
$G\alpha_{olf}$	CTGCACGTCAATGGCTTCAA	TCACGGCAATCGTTGAACAC	64	910	NM_177137.5
Tmem16B	GCAGAAAGTCCAGTGAATTCC	GCCCAGCAGCCATCAGGTTG	64	385	NM_153589.2
Stomatin	AAGACAGAACTGGGAGCTTGTG	TGATAACCATGGACGCTTCTTTC	64	654	X91043.1
STOML-1	GGATGATTGTGTTTCGACTGG	TTATCATCTCCAAGGTGTCTGG	64	548	BC037074.1
STOML-2	TACAAGGCAAGTTACGGTGTGG	GAGAATGCGCTGACATACTGCT	64	523	AK002793.1
STOML-3	CCCAATCTCAGTATGGATGTGC	AGGCTTTAGCAGTGACCTTCTTAT	64	745	BC138667.1
Podocin	CATCAAGCCCTCTGGATTAGG	AGCGACTGAAGAGTGTGCAAGT	64	713	AJ302048.1

Table 1. Primers used to perform PCR amplification and temperature of annealing during PCR reactions.

2.3 Immunohistochemistry

The head containing the nasal cavity was fixed in 4% paraformaldehyde in PBS pH 7.4 for 4 hours at 4 ◦C. After fixing, heads of adult mice were incubated in 0.5 M EDTA for 2 days or 4 days for 2 months or 6 months old mice respectively. The tissues were cryoprotected by incubation in 30% sucrose in PBS pH 7.4 overnight. Tissue was immersed in cryostat embedding medium (BioOptica) and immediately frozen at −80 ◦C. 18 µm coronal sections were cut on a cryostat and mounted on Superfrost Plus Adhesion Microscope Slides (ThermoFisher Scientific). The sections were air-dried for 3 hours. To wash the cryostat embedding medium from tissue, slices were incubated 15 minutes with PBS. Tissue was treated for 15 minutes with 0.5 % sodium dodecyl sulphate in PBS for antigen retrieval, then washed and incubated in blocking solution (2% normal goat serum, 0.2% Triton X-100 in PBS) for 90 minutes and finally overnight at 4 ◦C in primary antibodies diluted in blocking solution. The antibodies used in this study are listed in Table 2 together with the dilutions used. After removal of the excess of primary antibodies with PBS washes, sections were incubated with Alexa Fluor-conjugated secondary antibodies (1:500 dilution) in TPBS (Tween 20 0.2% in PBS) for 2 hours at room temperature, washed and mounted with Vectashield (Vector Laboratories) or FluoromontG (ThermoFisher). DAPI (5 µg/ml) was added in solution containing secondary antibody to stain the nuclei. Secondary antibodies used were Alexa 594-conjugated donkey anti-goat, Alexa-594 conjugated chicken anti-rabbit Alexa 488-conjugated goat anti-rabbit, Alexa 488-conjugated donkey anti-mouse (ThermoFisher). For antibodies anti-Ki67 and anti-p63 we used heat antigen retrieval protocol instead of treatment with SDS. Tissue was put in a container with sodium citrate buffer (10 mM Sodium Citrate, 0.05% Tween 20, pH 6.0) and heated at 100 ºC with microwave for 5 min. After cool down, sodium citrate buffer was washed and the rest of procedure was the same as mentioned before. To reveal antibodies anti STOML-1 and STOML-3 we applied the tyramide signal amplification method using the Tyramide SuperBoost™ Kit (ThemoFisher; Hunyady et al., 1996). Immunoreactivity was visualized with

a confocal microscope (Nikon A1R or C1). Images were acquired using NIS Element software (Nikon) at 1,204x1,1024-pixel resolution and were not modifies other than to balance brightness and contrast.

Antibody	Company	Catalog number	Dilution
Acetylated Tubulin	Sigma	T7451	1:100
Active Caspase3	BD Pharmigen	559565	1:250
ACIII	Santa Cruz	sc-588	1:100
CNGA2	Santa Cruz	sc-13700	1:100
Ki67	Santa Cruz	sc-7846	1:250
OMP	WAKO	544-10001	1:1000
p63	Biocare Medical	CM 163	1:250
Stomatin	Santa Cruz	sc-48309	1:200
STOML-1	Proteintech	12852-1-AP	1:200
STOML-2	Abcam	ab191883	1:200
STOML-3	Proteintech	13316-1-AP	1:200
TMEM16B	Novus	NBP1-90739	1:250

Table 2. Primary antibodies and dilutions used in this study

2.4 Cell culture and transfection

HEK-293T (Sigma) cells were grown in DMEM medium supplemented with 10% fetal bovine serum, 100 IU/ml penicillin and 100 µg/ml streptomycin at 37 °C in a humidified CO_2 incubator. Transfection of HEK-293T cells was made with X-tremeGENE 9 DNA Transfection Reagent (Roche) following the protocol recommended by the supplier. mCherry or EGFP-fusion stomatin-domain protein constructs were used to transfect the cells. In particular we used, Stomatin-mCherry, STOML-1-mCherry, STOML-2-EGFP and STOML-3-mCherry. Plasmids were kindly provided by professor Gary Lewin (Max Delbrück Center for Molecular Medicine ,Berlin, Germany; Lapatsina et al., 2012). After 24-48 hours from transfection the cells were plated on circular coverslips coated with poly-L-lysine to improve the adhesion and used for immunocytochemistry experiments.

2.5 Immunocytochemistry

Transfected cells were grown for around 12 hours on the coverslips. They were fixed with 4% paraformaldehyde in PBS pH 7.4 for 20 min at room temperature. After washes with PBS, cells were incubated in quenching solution (0.1 M of glycine) for 15 minutes at room temperature and then washed again with PBS. Then cells were permeabilized 0.01% Triton X-100 in PBS for 15 min and then washed again. In some cases, alternative antigen retrieval

treatment was performed before permeability step treating the cells 0.05% SDS in PBS for 10 minutes and then washed. After incubation with blocking solution (2% FBS, 0.2% Triton X100 in PBS) for 15 minutes, cells were incubated in primary antibodies diluted in blocking solution for 4 hours at 4 °C. Cells were incubated with Alexa Fluor-conjugated secondary antibodies (1:500 dilution) in TPBS (Tween 20 0.2% in PBS) for 45 minutes at room temperature, washed and mounted with Vectashield (Vector Laboratories) or Fluoromont-G (ThemoFisher). DAPI (5 μg/ml) was added in solution containing secondary antibody to stain the nuclei.

2.6 Whole mount cilia staining

The olfactory turbinates were exposed by bisecting the head along the midline and removing the septum. The tissues were fixed with 4% paraformaldehyde in PBS pH 7.4 for 20 min at room temperature and then washed with PBS. Endogenous biotin was blocked by using Avidin/Biotin Blocking Kit (Vector Laboratories) following the according to the manufacturer's protocol. Then, the preparation was incubated for 2 hours with the biotinylated lectin *Dolichos biflorus* agglutinin (VectorLabs) at 20 μg/ml concentration in PBS. Then tissue was washed at least 3 times with PBS, 10 minutes each wash. Tissue was incubated for 3 hours with Streptavidin-Alexa Fluor594 (ThermoFisher) diluted 1:500 in PBS and washed again. Then turbinates were dissected out from the nasal cavity and mounted on FluoroDishes (World Precision Instruments) with Vectashield (Vector Laboratories) or Fluoromont-G (ThemoFisher). A coverslip was gently placed on the tissue to press and close the cilia to the glass bottom of the FluoroDish.

2.7 Electro-olfactogram recordings

Experimental procedure was similar as described by Zhao et al. (1998). Briefly, after sacrifice of the mouse, the olfactory turbinates were exposed by bisecting the head along the midline and removing the septum. The turbinate preparation was then attached on the stage of a dissecting microscope and a recording electrode was placed at the surface of the olfactory epithelium on one of the medial turbinates (Figure 15). The recording electrode was made with borosilicate glass (WPI) with tip diameter of about 10-20 μm. The tip of the pipette was filled with Ringer's solution with 0.5 % agar and finally back filled with Ringer's solution. Ringer's solution contain (in mM) 140 NaCl, 5 KCl, 2 $CaCl_2$, 1 $MgCl_2$, 10 Hepes, pH 7.4 with NaOH. The pipette was mounted in a pipette holder with a silver chloride electrode for electrical recording and placed on the surface of the olfactory epithelium. The ground electrode was located directly in the brain of the mouse.

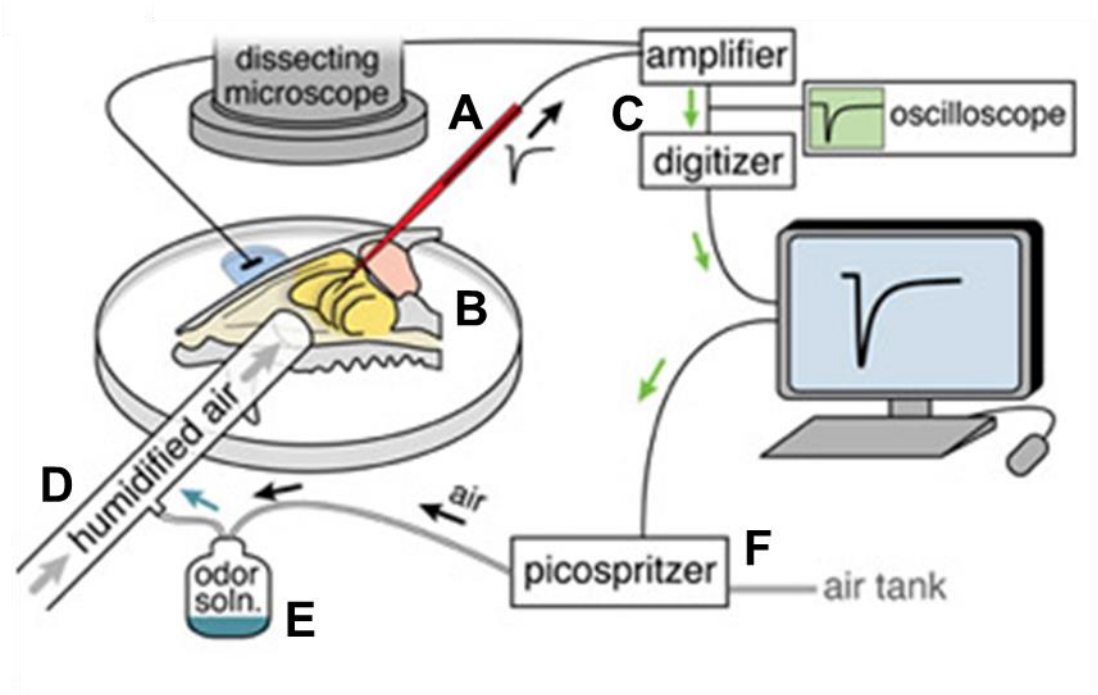

Figure 15: Experimental setup for air-phase EOG recording. EOG is a field potential recording that measures the extracellular changes on the potential induced by application of a stimulus. The recording electrode (A) is placed on the surface of the OE (B) and is connected to an amplifier and digitizer (C) to record a negative change in the voltage when an odorant is applied. OE is continuously expose to a flux of humidified air (D). Odorant in air-phase is generated using vial containing odorant solution at different concentrations (E) and it is delivered to the OE by injecting pressured air using a picospritzer system (F) (from Cygnar et al., 2010).

A continuous flow of humidified air controlled by a Picospritzer (around 2 psi) was blown over the surface of the epithelium to keep it humid. The vapor of odorant stimuli solutions was puffed into the stream of humidified air to stimulate the epithelium. The odorant stimuli were delivered by 10 psi pulse. The pulse of stimuli was controlled by a Picospritzer controlled valve. Pulses of 100 milliseconds were used to make the stimulation. Isoamyl acetate (IAA, Sigma) was used as stimuli. Odorant solutions were prepared as 5 M stocks in dimethyl sulfoxide (DMSO) and then were diluted with water. Odorants were prepared at a liquid concentration from 10^{-7} M to 1 M. The recordings were made in 3 distal points from the olfactory epithelium, in the anterior region of turbinate II, in the posterior region of turbinate II and ventrally in the turbinate IV (Figure 16). Responses were recorded and digitized for further analysis. The data were collected with an Axopatch 1D amplifier controlled by Clampex 9.2 (Axon Instruments, USA). The signals were recorded at a sampling rate of 1 kHz and low-pass filtered at 20 Hz. Data were further analyzed using IgorPro 6.3.7.2 software (Wavemetrics). Data are given as mean ± sem.

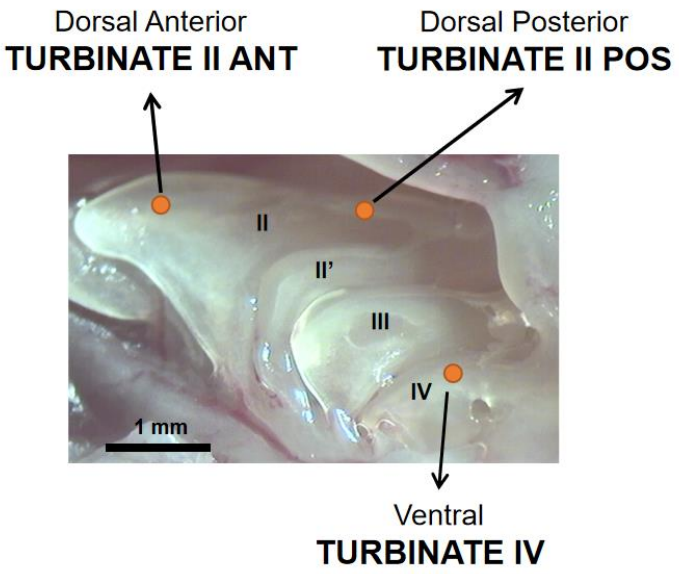

Figure 16: View from turbinates exposed in sagittal sections of the mouse head. In this preparation the different turbinates can be identified II, II', III and IV. Recordings were obtained from the regions indicated with orange points.

3. Aims

The specific aims of this work were:

- To investigate in detail the expression of all stomatin proteins in the olfactory epithelium.

- To study the development of the olfactory epithelium and olfactory sensory neurons in STOML-3 single KO mice and Stomatin/STOML-1/STOML-3 triple KO mice.

- To study the physiological response to odorants of the olfactory epithelium in these two stomatin KO models and in WT using electro-olfactogram recordings.

4. Results

4.1 Knockout of Stomatin-domain protein STOML-3 reduces the odorant response of mouse olfactory sensory neurons

Knockout of Stomatin-domain protein STOML-3 reduces the odorant response of mouse olfactory sensory neurons

Manuscript in preparation

Kevin Y. Gonzalez-Velandia performed and analyzed all the experiments.

Devendra Kumar Maurya (Department of Molecular Biology, Umeå University, Umeå, Sweden)

contributed and analyzed some immunohistochemical experiments.

Kevin Y. Gonzalez-Velandia, Anna Menini and Simone Pifferi designed research, contributed to data analysis and writing of the manuscript.

Christiane Wetzel, Valérie Bégay, Gary R Lewin (Department of Neuroscience, Max Delbrück Center for Molecular Medicine, Berlin, Germany) provided STOML-3 KO mice and plasmids.

ABSTRACT

Olfactory sensory neurons use a cAMP-based signal cascade to transduce the chemosensory signal in neuronal activation. Here, we focused on the stomatin-domain proteins to find possible new regulators of olfactory transduction. Using RT-PCR and immunohistochemical approaches, we confirmed the localization of STOML-3 in the cilia of the olfactory sensory neurons. Interestingly, we found that also Stomatin is present only in the cilia. In contrast, we revealed that STOML-1 and STOML-2 localize in the central layer of the olfactory epithelium, in the soma of the neurons. Then we compared the development of the olfactory epithelium and the physiological response to odorants in wild-type (WT) and knockout (KO) mice for STOML-3. We did not find significant differences in the number of olfactory neurons, apoptotic, globose or horizontal basal cells, in the morphology of the cilia of the neurons. We also did not observe changes in the expression and localization of several members of the transduction machinery and potential targets of stomatin-domain proteins. Using electro-olfactogram recordings, we found a reduction in the amplitude of the response to odorants in several regions of the olfactory epithelium providing the first evidence that the stomatin protein STOML-3 modulates the odorant response in mice and the foundation for future work aimed at clarifying the physiological role of stomatin proteins in the olfactory system.

INTRODUCTION

Sensory receptors cells are devoted to detect and transduce the properties of sensory stimuli generating cellular electrical signals depending on the type, amplitude and temporal profile of the stimulus. These signals are relayed to specific areas of the brain to further processing leading to behavioral response.

In vertebrates, the initial steps of olfaction occur in olfactory sensory neurons (OSNs), located in the olfactory epithelium (OE) in upper reaches of the nasal cavity (Firestein, 2001; Menini et al., 2004; Tirindelli et al., 2009). The OSNs are bipolar neurons with a single dendrite that terminates with a knob, from which protrude several tiny cilia, where the transduction takes place. Odorant molecules bind to olfactory receptor proteins, and this interaction triggers an increase in the ciliary concentration of cAMP through the activation of receptor-coupled G-protein and adenylate cyclase. Cyclic nucleotide-gated (CNG) channels located in the ciliary membrane are directly activated by cAMP, causing a depolarizing influx of Na^+ and Ca^{2+} ions (Bönigk et al., 1999; Brunet et al., 1996). Ca^{2+} inside the cilia play many roles, both excitatory and inhibitory. Indeed, Ca^{2+} can gate the TMEM16B/Ano-2 Ca^{2+}- activated Cl^- channel, which in the presence of high intracellular Cl^- contributes to depolarize the cell; on the other hand, Ca^{2+} can modulate, via calmodulin and other unidentified mechanisms, the CNG channels, contributing to the response termination and adaptation (Billig et al., 2011; Matthews and Reisert, 2003; Pifferi et al., 2010; Stephan et al., 2009; Tirindelli et al., 2009). Ca^{2+} handling is regulated by Na^+/ Ca^{2+} exchangers (both dependent and independent on K^+), Ca^{2+}-ATPase pump and by mitochondrial buffering system (Castillo et al., 2007; Fluegge et al., 2012; Reisert and Matthews, 1998).

Despite a well-established knowledge of basic components of the olfactory transduction cascade, it is still missing a complete understanding of the regulatory mechanisms allowing a precise coding of the stimuli properties. To obtain a clearer view of the olfactory transduction, we focused on stomatin-domain proteins.

Proteins of the stomatin family are membrane protein characterized by the presence of a structurally conserved core domain called stomatin-domain of near 120 residues, that is further related to the SPFH domain (Stomatin, Prohibitin, Flotillin, HflK/HflC; Green and Young, 2008; Lapatsina et al., 2012; Tavernarakis et al., 1999). Stomatin proteins are found in all three domains of life with a remarkable conservation, with bacterial and human homologous sharing 50% identity. In the mammal genome 5 members have been identified (*Stomatin*, stomatin-like protein-1 or *STOML-1*, stomatin-like protein-2 or *STOML-2*, stomatin-like protein-3 or *STOML-3* and *Podocin*), all sharing 40/84% sequence similarity in the stomatin-domain and having similar membrane topology characterized by a single, relatively short, hydrophobic membrane insertion domain, followed by the core stomatin domain (Green and Young, 2008; Lapatsina et al., 2012). A single conserved proline residue (known to be a potent helix breaker) is required to form the membrane interacting hairpin. Both N- and C-termini of the proteins are intracellular and unique for every protein (Boute et al., 2000; Owczarek et al., 2001; Salzer et al., 1993; Seidel and Prohaska, 1998; Snyers et al., 1998). Several recent studies began to reveal some common aspects of the physiology of the stomatin proteins. In particular, it has been demonstrated that they can form oligomers, they mostly localize to membrane domains and they can modulate ion channel activity, even if the precise mechanisms of this regulation is still unclear (Brand et al., 2012; Lapatsina et al., 2012; Poole et al., 2014). Interestingly, data obtained from different approaches have shown that stomatin proteins are expressed by olfactory sensory neurons. In particular, two independent differential screening found that *STOML-3* mRNA was expressed by OSNs and STOML-3 protein localizes primarily on the olfactory cilia, the site of olfactory transduction (Goldstein et al., 2003; Kobayakawa et

al., 2002). Moreover, proteomics data have shown that also stomatin and STOML-2 are expressed on olfactory cilia and intriguingly Stomatin and STOML-3 have been detected by screening for protein complex binding Ca^{2+}-calmodulin that it is well known directly modulates several components of the olfactory signaling transduction (Klimmeck et al., 2008; Mayer et al., 2008, 2009; Pifferi et al., 2010).

Here, we analyzed in details the expression and the subcellular localization of the stomatin-domain proteins in the olfactory epithelium revealing that Stomatin and STOML-3 are targeted to the cilia of OSNs, the site of the olfactory transduction. Then, by using a knock-out (KO) mouse line for STOML-3 protein, we found that, although KO mice have a normal development and neurogenesis of OSNs, they show a reduced odorant response in specific regions of the OE especially at older age.

MATERIALS AND METHODS

Animals

All animals were handled in accordance with the Italian Guidelines for the Use of Laboratory Animals (Decreto Legislativo 24/2014) and European Union guidelines on animal research (63/2013). To obtain the OE the mice were sacrificed by CO_2 inhalation, decapitated, and then the skin and posterior part of the head were removed and separated from the most apical part, which contains the olfactory cavity.

mRNA extraction and RT-PCR

mRNA was extracted from 10-20 mg of the olfactory epithelium of WT mice using magnetic beads mRNA isolation kit (New England Biolabs). cDNA was synthetized using the Protoscript First-Strand DNA Synthesis Kit from 100-500 ng of mRNA (New England Biolabs). PCR was performed in thermocycler ThermaCycler2720 (LifeTechnologies) using Taq DNA polymerase and Thermopol buffer (New England Biolabs), 0.2 mM for each dNTPs and 200 pmol forward/reverse target-specific primers. Cycling parameters were: an initial denaturation step (95 °C, 2 minutes) followed by 35 cycles, each of these cycles included a denaturation step (95 °C, 30 seconds), a primer annealing step (62-64 °C, 30 seconds), and an extension step (72 °C, 60 seconds) step. Reaction was completed by a final extension step at 72 °C for 5 minutess. cDNA from testis (Clontech Laboratories) was used as positive control for podocin PCR amplification.

The following primer sequences were used to amplify target DNAs: *GAPDH* fwd 5'-TGCTGAGTATGTCGTGGAGTCT-3' rev 5'-TGCTGTAGCCGTATTCATTGTC-3' (Tm=62 °C; 691 bp; GenBank. accession no. NM_008084.3); *OLFR73* fwd 5'-GCTGGTATTGGGATCCTATGCTT-3' rev 5'- CGTCCACTTGCTGACTTCATCTT-3' (Tm=62 °C; 272 bp; GenBank. accession no. NM_054090.1); *$G\alpha_{olf}$* fwd 5'-CTGCACGTCAATGGCTTCAA-3' rev 5'-TCACGGCAATCGTTGAACAC-3' (Tm=64 °C; 910 bp; GenBank. accession no. NM_177137.5); *Tmem16B* fwd 5'-GCAGAAAGTCCAGTGAATTCC-3' rev 5'-GCCCAGCAGCCATCAGGTTG-3' (Tm=64 °C; 385 bp; GenBank. accession no. NM_153589.2); *Stomatin* fwd 5'-AAGACAGAACTGGGAGCTTGTG-3' rev 5'- TGATAACCATGGACGCTTCTTTC-3' (Tm=64 °C; 654 bp; GenBank. accession no. X91043.1); *STOML-1* fwd 5'-GGATGATTGTGTTTCGACTGG-3' rev 5'- TTATCATCTCCAAGGTGTCTGG-3' (Tm=64 °C; 548 bp; GenBank. accession no. BC037074.1); *STOML-2* fwd 5'-TACAAGGCAAGTTACGGTGTGG-3' rev 5'-GAGAATGCGCTGACATACTGCT-3' (Tm=64 °C; 523 bp; GenBank. accession no. NM_054090.1 AK002793.1); *STOML-3* fwd 5'-CCCAATCTCAGTATGGATGTGC-3' rev 5'-AGGCTTTAGCAGTGACCTTCTTAT-3' (Tm=62 °C; 745 bp; GenBank. accession no. BC138667.1); *Podocin* fwd 5'-CATCAAGCCCTCTGGATTAGG-3' rev 5'-AGCGACTGAAGAGTGTGCAAGT -3' (Tm=62 °C; 713 bp; GenBank. accession no. AJ302048.1). The products were visualized following agarose gel electrophoresis (1.5%) and DNA was stained with Midori Green Advance (Nippongenetics).

Immunohistochemistry and cell counting

The head containing the nasal cavity was fixed in 4% paraformaldehyde in PBS pH 7.4 for 4 hours at 4 °C. After fixing, heads of adult mice were incubated in 0.5 M EDTA for 2 days or 4 days for 2 months or 6 months old mice respectively. The tissues were cryoprotected by

incubation in 30% sucrose in PBS pH 7.4 overnight. Tissue was immersed in cryostat embedding medium (BioOptica) and immediately frozen at −80 °C. 18 μm coronal sections were cut on a cryostat and mounted on Superfrost Plus Adhesion Microscope Slides (ThermoFisher Scientific). The sections were air-dried for 3 hours. To wash the cryostat embedding medium from tissue, slices were incubated 15 minutes with PBS. Tissue was treated for 15 minutes with 0.5 % sodium dodecyl sulphate in PBS for antigen retrieval, then washed and incubated in blocking solution (2% normal goat serum, 0.2% Triton X-100 in PBS) for 90 minutes and finally overnight at 4 °C in primary antibodies diluted in blocking solution. The following primary antibodies (catalog number, dilution; company) were used: mouse monoclonal anti-acetylated tubulin (T7451; 1:100; Sigma); polyclonal rabbit anti-active caspase-3 (559565; 1:250; BD Pharmigen); polyclonal rabbit anti-ACIII (sc-588; 1:100, Santa Cruz Biotechnology); polyclonal goat anti-CNGA2 (sc-13700; 1:100, Santa Cruz Biotechnology); polyclonal rabbit anti-Ki67 (sc-7846, 1:250, Santa Cruz Biotechnology); polyclonal goat anti-OMP (544-10001, 1:1000, Wako); mouse monoclonal anti-p63 (CM163, 1:250, Biocare Medical); polyclonal goat anti-Stomatin (sc-48309, 1:200, Santa Cruz Biotechnology); polyclonal rabbit anti-STOML-1 (12852-1-AP, 1:200, Proteintech); polyclonal rabbit anti-STOML-2 (ab191883,1:200, Abcam); polyclonal rabbit anti-STOML-3 (13316-1-AP, 1:200, Proteintech), polyclonal rabbit anti-TMEM16B (NBP1-90739,1:250, Novus). After removal of the excess of primary antibodies with PBS washes, sections were incubated with Alexa Fluor-conjugated secondary antibodies (1:500 dilution) in TPBS (Tween 20 0.2% in PBS) for 2 hours at room temperature, washed and mounted with Vectashield (Vector Laboratories) or FluoromontG (ThermoFisher). DAPI (5 μg/ml) was added in solution containing secondary antibody to stain the nuclei. Secondary antibodies used were Alexa 594-conjugated donkey anti-goat, Alexa-594 conjugated chicken anti-rabbit Alexa 488-conjugated goat anti-rabbit, Alexa 488-conjugated donkey anti-mouse (ThermoFisher). For antibodies anti-Ki67 and anti-p63 we used heat antigen retrieval protocol instead of treatment with SDS. Tissue was put in a container with sodium citrate buffer (10 mM Sodium Citrate, 0.05% Tween 20, pH 6.0) and heated at 100 ºC with microwave for 5 min. After cool down, sodium citrate buffer was washed and the rest of procedure was the same as mentioned before. To reveal antibodies anti STOML-1 and STOML-3 we applied the tyramide signal amplification method using the Tyramide SuperBoost™ Kit (ThemoFisher; Hunyady et al., 1996). Immunoreactivity was visualized with a confocal microscope (Nikon A1R or C1). Images were acquired using NIS Element software (Nikon) at 1,204x1,1024-pixel resolution and were not modifies other than to balance brightness and contrast. For the cell counting we used three mice for each genotype, we collected three adjacent sections from three different OE regions (anterior part of turbinate II, II Ant, posterior part of turbinate II, II Post, and turbinate IV) and for each section we selected two areas to count the cells. Number of cells are reported as average ± SEM. Statistical significance was determined using unpaired Student's t-tests and p values <0.05 were considered significant.

Cell culture, transfection and immunocytochemistry

HEK-293T cells (Sigma) were grown in DMEM medium supplemented with 10% fetal bovine serum, 100 IU/ml penicillin and 100 μg/ml streptomycin at 37°C in a humidified CO_2 incubator. Transfection of HEK-293T cells was made with X-tremeGENE 9 DNA Transfection Reagent (Roche) following the protocol recommended by the supplier. mCherry or EGFP-fusion stomatin protein constructs were used to transfect the cells. In particular we used, Stomatin-mCherry, STOML-1-mCherry, STOML-2-EGFP and STOML-3-mCherry (Lapatsina et al., 2012). After 24-48 hours from transfection the cells were plated on coverslips

coated with poly-L-lysine to improve the adhesion and used for immunocytochemistry experiments the day after. The cells were fixed with 4% paraformaldehyde in PBS pH 7.4 for 20 minutes at room temperature. After washes with PBS, cells were incubated in quenching solution (0.1 M of glycine) for 15 minutes and then washed again with PBS. Then cells were permeabilized with 0.01% Triton X-100 in PBS for 15 min and then washed. In some cases, antigen retrieval treatment was performed before permeabilization step treating the cells with 0.05% SDS in PBS for 10 minutes and then washed. After incubation with blocking solution (2% FBS, 0.2% tritonX100) for 15 minutes, cells were incubated in primary antibodies diluted in blocking solution for 4 hours at 4 °C. After washes, the cells were incubated with Alexa Fluor-conjugated secondary antibodies (1:500 dilution) in TPBS (Tween 20 0.2% in PBS) for 45 minutes at room temperature, washed and mounted with Vectashield (Vector Laboratories) or Fluoromont-G (ThemoFisher). DAPI (5 μg/ml) was added in solution containing secondary antibody to stain the nuclei.

Whole mount cilia staining

The olfactory turbinates were exposed by bisecting the head along the midline and removing the septum. The tissues were fixed with 4% paraformaldehyde in PBS pH 7.4 for 20 min at room temperature and then washed with PBS. Endogenous biotin were blocked by using Avidin/Biotin Blocking Kit (Vector Laboratories) following the according to the manufacturer's protocol. Then, the preparation was incubated for 2 hours with the biotinylated lectin *Dolichos biflorus* agglutinin (VectorLabs) at 20 μg/ml concentration in PBS. Then tissue was washed at least 3 times with PBS, 10 minutes each wash. Tissue was incubated for 3 hours with Streptavidin-Alexa Fluor594 (ThermoFisher) diluted 1:500 in PBS and washed again. Then turbinates were dissected out from the nasal cavity and mounted on FluoroDishes (World Precision Instruments) with Vectashield (Vector Laboratories) or Fluoromont-G (ThemoFisher). A coverslip was gently placed on the tissue to press and close cilia to the glass bottom of the FluoroDish.

Electro-olfactogram recordings

Experimental procedure was similar as described by (Zhao et al., 1998). Briefly, after sacrifice of the mouse, the olfactory turbinates were exposed by bisecting the head along the midline and removing the septum. The turbinate preparation was then attached on the stage of a dissecting microscope and a recording electrode was placed at the surface of the olfactory epithelium on one of the medial turbinates. The recording electrode was made with borosilicate glass (WPI) with tip diameter of about 10-20 μm. The tip of the pipette was filled with Ringer's solution with 0.5 % agar and finally back filled with Ringer's solution. Ringer's solution contain (in mM) 140 NaCl, 5 KCl, 2 $CaCl_2$, 1 $MgCl_2$, 10 Hepes, pH 7.4 with NaOH. The pipette was mounted in a pipette holder with a silver chloride electrode for electrical recording and placed on the surface of the olfactory epithelium. The ground electrode was located directly in the brain of the mouse.

A continuous flow of humidified air was blown over the surface of the epithelium to keep it humid. The vapor of odorant stimuli solutions was puffed into the stream of humidified air to stimulate the epithelium. The odorant stimuli were delivered by 10 psi pulse. The pulse of stimuli was controlled by a Picospritzer controlled valve. Pulses of 100 milliseconds were used to make the stimulation. Isoamyl acetate (IAA, Sigma) was used as stimuli. Odorant solutions were prepared as 5 M stocks in dimethyl sulfoxide (DMSO) and were then diluted with water. Odorants were prepared at a liquid concentration from 10^{-7} M to 1 M. The recordings were made in 3 distal points from the olfactory epithelium, in the anterior region of

turbinate II, in the posterior region of turbinate II and ventrally in the turbinate IV. Responses were recorded and digitized for further analysis. The data were collected with an Axopatch 1D amplifier controlled by Clampex 9.2 (Axon Instruments, USA). The signals were recorded at a sampling rate of 1 kHz and low-pass filtered at 20 Hz. Data were further analyzed using IgorPro 6.3.7.2 software (WaveMetrics). Data were given as mean ± sem.

RESULTS

Expression and localization of stomatin-domain proteins in the olfactory epithelium.

We screened the expression of stomatin-domain proteins by RT-PCR on mRNA from the OE. We detected the expression of mRNA of *Stomatin, STOML-1, STOML-2, STOML-3* but not *Podocin* (Fig. 1A). As controls, we could amplified *Podocin* from cDNA from testis (data not shown) and we detected the housekeeping gene *GAPDH* only from OE cDNA but not from retrotranscriptase free sample (Fig. 1B). As expected, we also observed in the OE the expression of the olfactory receptor *OLFR-73*, $G\alpha_{olf}$ and *Tmem16B* (Fig. 1C). The identity of amplicons were verified by sequencing.

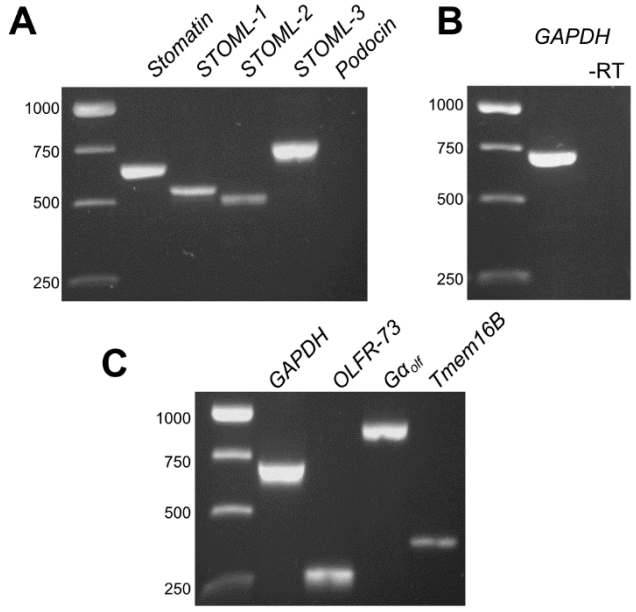

Figure 1. Stomatin-domain proteins are expressed in the olfactory epithelium. (A) Primers specific for *Stomatin, STOML-1, STOML-2, STOML-3* and *Podocin* were used to amplify cDNA obtained from mRNA of OE. (B) Negative control experiment showing the lack of the amplification of the housekeeping gene *GAPDH* from retrotranscriptase free sample (-RT). (C) Positive control experiments showing the expression of genes specifically expressed in the OE.

Then we analyzed the localization of stomatin-domain proteins in OE by immunochemistry experiments. We first tested the specificity of commercially available antibodies against stomatin-domain proteins on HEK 293T cells transiently transfected with plasmids containing the cDNA sequence of *Stomatin, STOML-1, STOML-2* or *STOML-3* fused with EGFP or mCherry. Figures 2-5 show that cells transfected with of *Stomatin, STOML-1, STOML-2* and *STOML-3* produced a strong and specific immunoreactivity exclusively to their respective antibody.

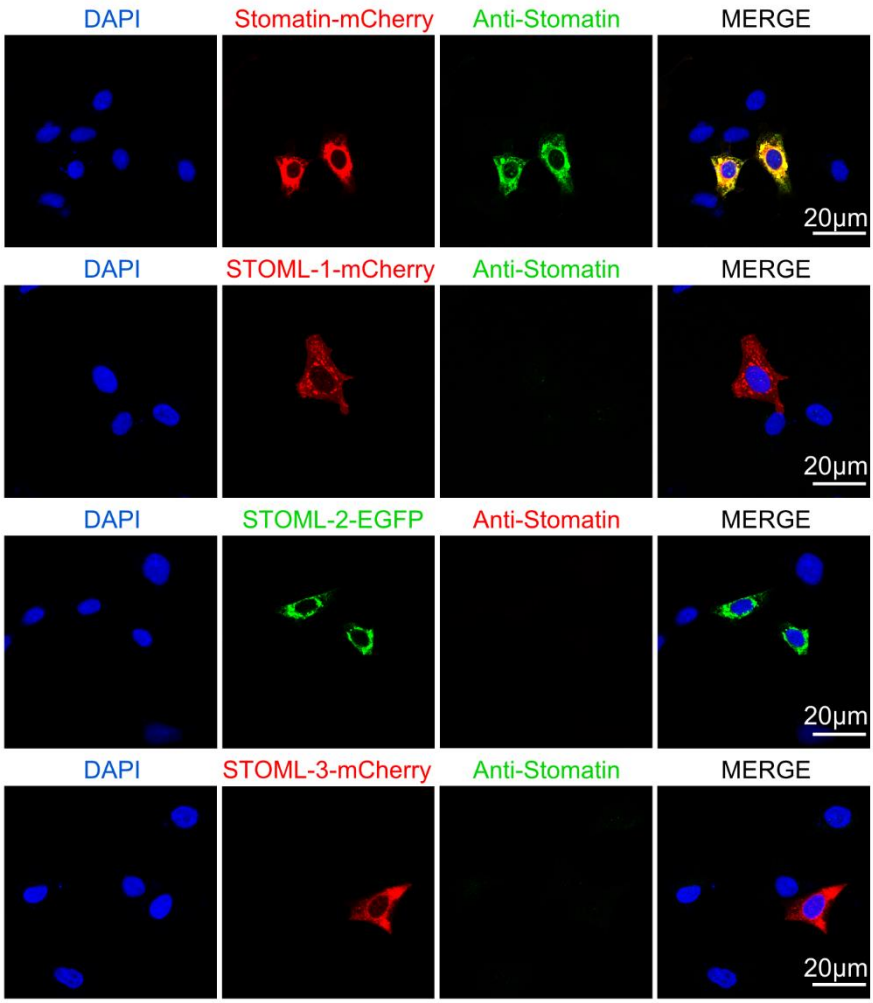

Figure 2. Specificity of goat anti-Stomatin antibody in HEK 293T cells expressing stomatin-domain proteins. Fluorescence images of the staining with anti-Stomatin antibody of HEK 293T cells transiently transfected with plasmid containing the cDNA of the indicated stomatin-domain proteins fused with EGFP or mCherry. Specific staining was observed only in Stomatin-expressing cells whereas no immunoreactivity was detected in cells transfected with other stomatin-domain proteins.

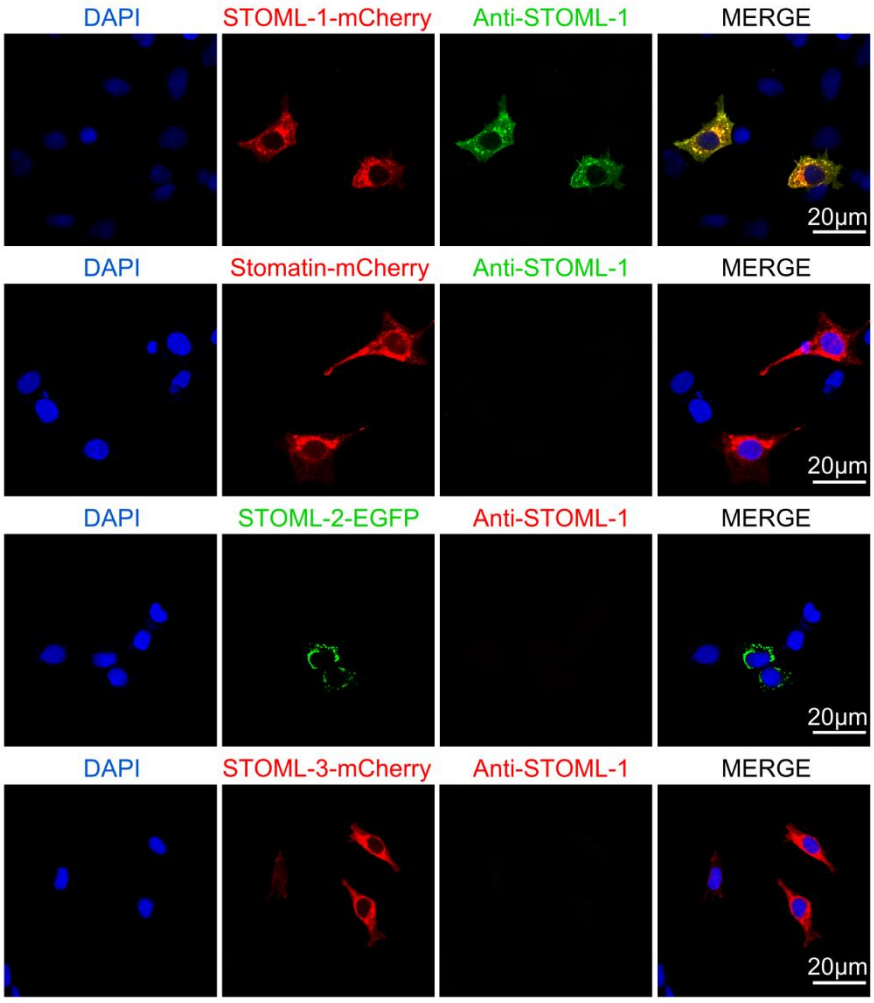

Figure 3. Specificity of rabbit anti-STOML-1 antibody in HEK 293T cells expressing stomatin-domain proteins. (A) Fluorescence images of the staining with anti-STOML-1 antibody of HEK 293T cells transiently transfected with plasmid containing the cDNA of the indicated stomatin-domain proteins fused with EGFP or mCherry. Specific staining was observed only in STOML-1-expressing cells whereas no immunoreactivity was detected in cells transfected with other stomatin-domain proteins.

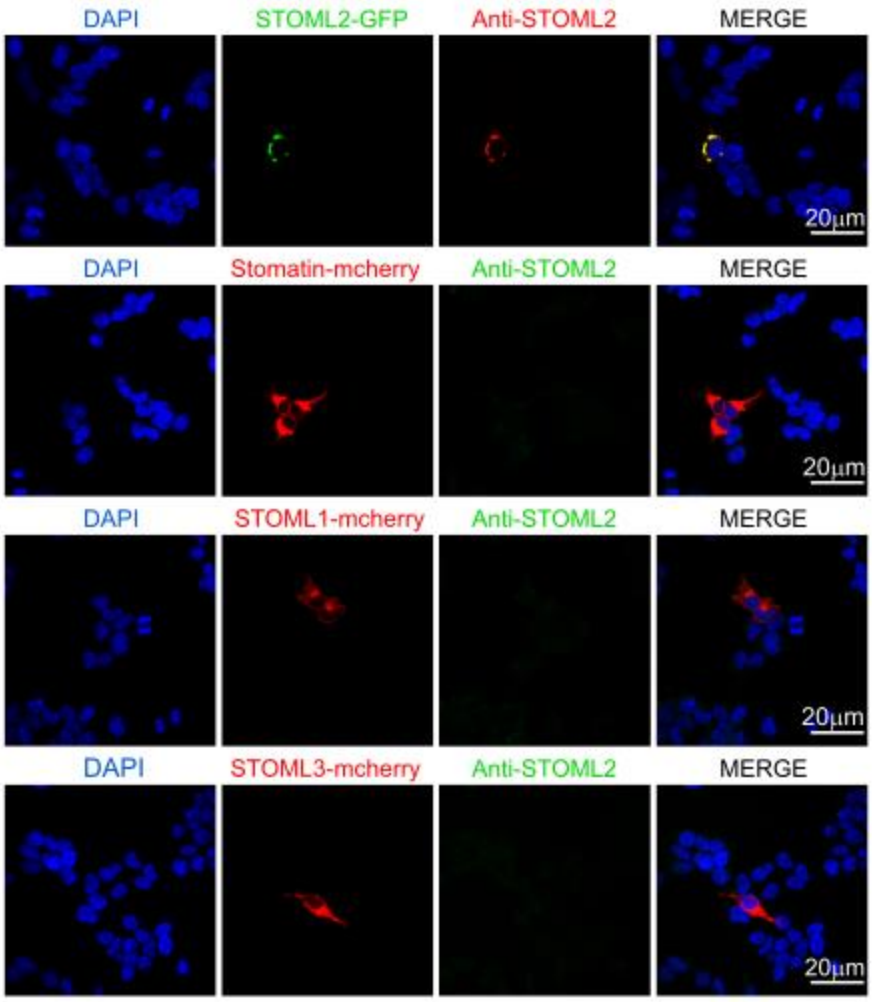

Figure 4. Specificity of rabbit anti-STOML-2 antibody in HEK 293T cells expressing stomatin-domain proteins. (A) Fluorescence images of the staining with anti-STOML-2 antibody of HEK 293T cells transiently transfected with plasmid containing the cDNA of the indicated stomatin-domain proteins fused with EGFP or mCherry. Specific staining was observed only in STOML-2-expressing cells whereas no immunoreactivity was detected in cells transfected with other stomatin-domain proteins.

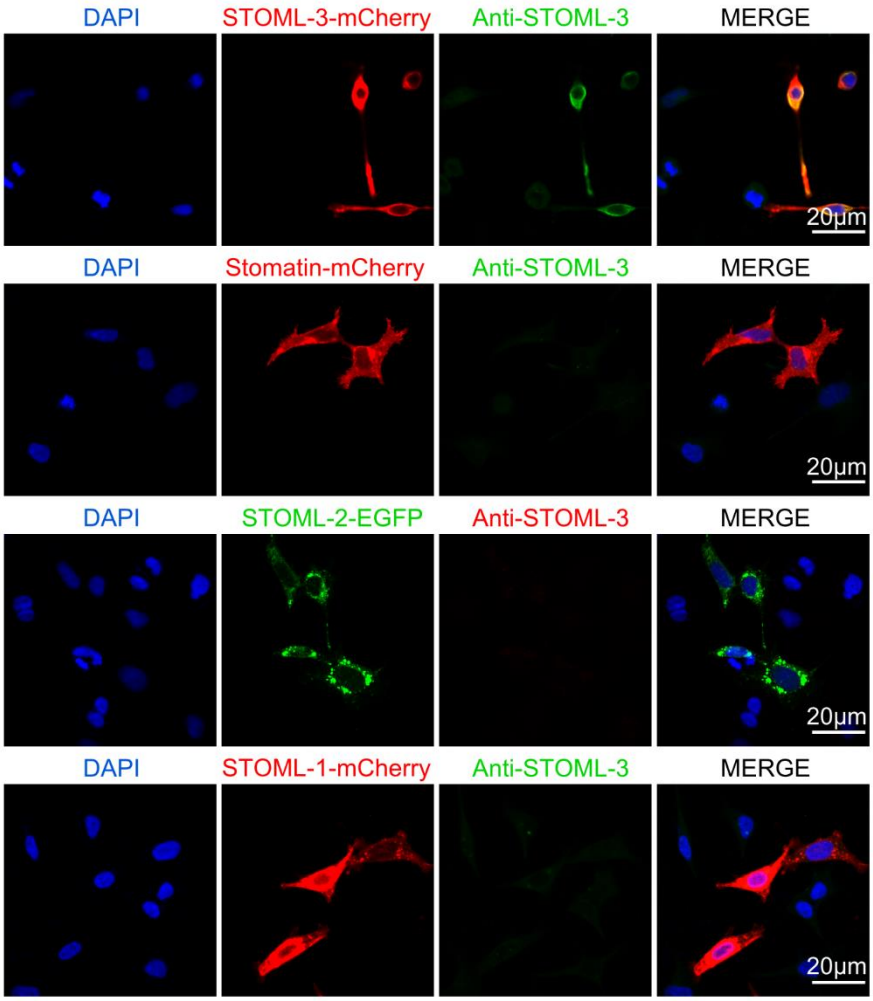

Figure 5. Specificity of rabbit anti-STOML-3 antibody in HEK 293T cells expressing stomatin-domain proteins. (A) Fluorescence images of the staining with anti-STOML-3 antibody of HEK 293T cells transiently transfected with plasmid containing the cDNA of the indicated stomatin-domain proteins fused with EGFP or mCherry. Specific staining was observed only in STOML-3-expressing cells whereas no immunoreactivity was detected in cells transfected with other stomatin-domain proteins. (B) Confocal micrographs of coronal sections of the olfactory epithelium from STOML-3 KO mice immunostained for STOML-3 and for the cilia marker acetylated tubulin (AcTb). Cell nuclei were stained with DAPI (blue).

We therefore used the same antibodies to examine the localization of stomatin-domain proteins in the OE. We detected a strong immunoreactivity for Stomatin and STOML-3 at the luminal surface of the sensory epithelium (Fig. 6). Double staining for Stomatin or STOML-3 and acetylated tubulin (AcTb), a canonical marker for cilia (Piperno and Fuller, 1985), showed that Stomatin and STOML-3 are localized on the cilia at the site of olfactory transduction. In the olfactory epithelium of STOML-3 KO mice, STOML-3 immunoreactivity was absent, while AcTb was normally expressed at the level of the ciliary layer (Fig. 7). These results demonstrate the loss of the STOML-3 protein in the olfactory epithelium of KO mice and confirm the specificity of the antibody against this protein. Interestingly, in STOML-3 KO mice, Stomatin is mislocalized, and it does not reach the ciliary layer remaining trapped in the knobs of the OSNs (Fig. 7). Moreover, we found that STOML-1 and STOML-2 were expressed

by OSNs, but they do not localize to the cilia. Immunostaining of STOML-1 showed a diffuse distribution in the soma of the OSNs, whereas STOML-2 is localized in small puncta around the OSN nuclei (Fig. 6). The subcellular localization of STOML-1 and STOML-2 was not altered in STOML-3 KO mice (Fig. 7).

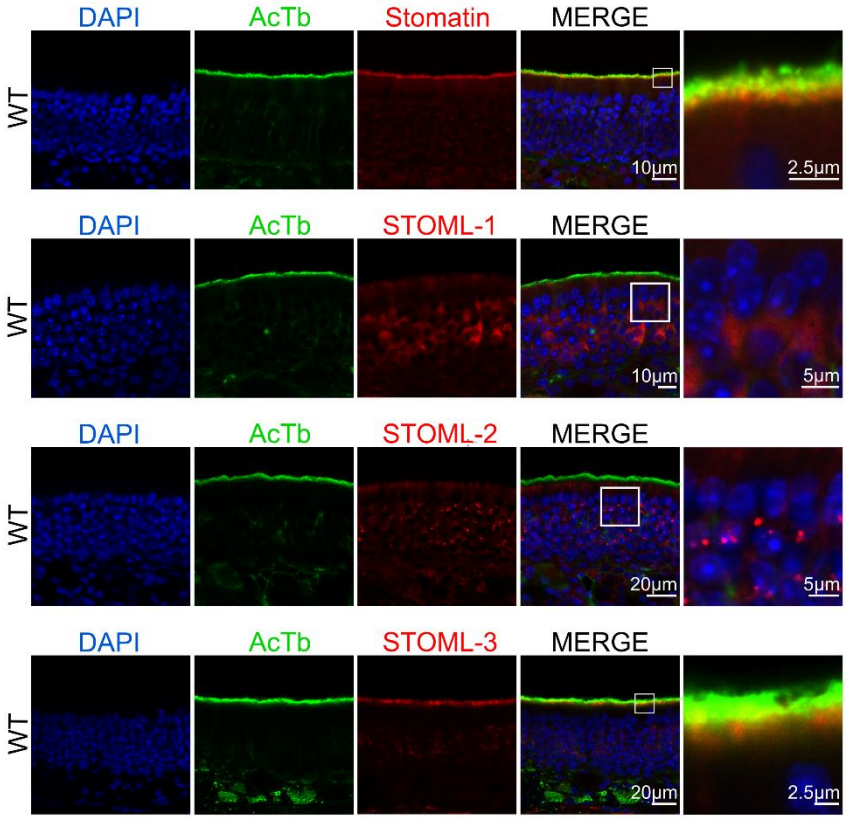

Figure 6. Stomatin-domain protein expression in the olfactory epithelium. Confocal images of coronal section of the olfactory epithelium immunostained for Stomatin, STOML-1, STOML-2 or STOML-3 (red) and acetylated tubulin (AcTb, green). Stomatin and STOML-3 were expressed in the ciliary layer at the luminal surface of the epithelium, while STOML-1 and STOML-2 localized in the soma of the olfactory sensory neurons. Cell nuclei were stained with DAPI (blue).

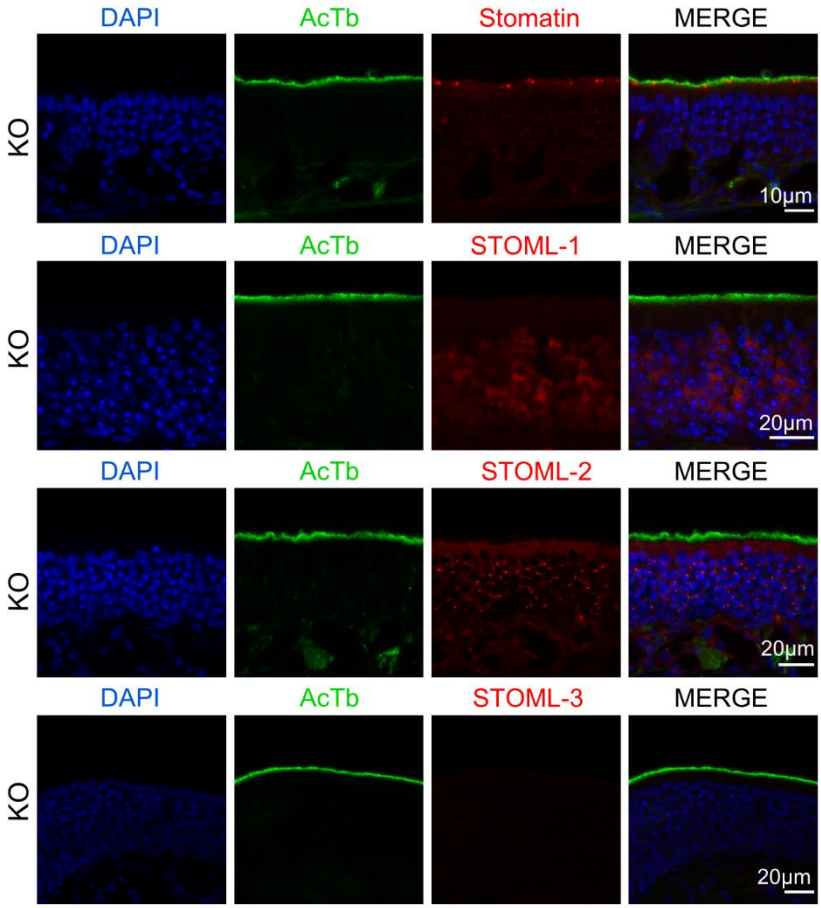

Figure 7. Stomatin-domain protein expression in the olfactory epithelium from STOML-3 KO mice. Confocal images of coronal section of the olfactory epithelium immunostained for Stomatin, STOML-1, STOML-2 or STOML-3 (red) and acetylated tubulin (AcTb, green). STOML-3 is not expressed in KO mice. STOML-1 and STOML-2 are normally localized in the soma of the olfactory sensory neurons, while Stomatin does not reach the ciliary layer. Cell nuclei were stained with DAPI (blue).

Development of the Olfactory Epithelium in STOML-3 KO mice.

We evaluated whether STOML-3 has an influence on the development of the OE, therefore we performed immunostaining to identify most of the different cell types present in the OE. We used the olfactory marker protein (OMP) as the typical marker for mature olfactory sensory neurons (Keller and Margolis, 1975); active Caspase-3 for apoptotic cells (Thornberry and Lazebnik, 1998); Ki-67 and p63 to stain the globose and horizontal basal cells respectively (Fletcher et al., 2011). To obtain a quantitative comparison between WT and STOML-3 KO mice we counted the immunopositive cells in three different regions of the OE: anterior part of turbinate II (II Ant), posterior part of turbinate II (II Post) and turbinate IV. Finally, we performed experiment both in 2 and 6 months old mice. We did not find significant differences between WT and STOML-3 KO mice in all the regions of the OE both in 2 and 6 months old

mice indicating that STOML-3 is not involved in the controlling the proliferation and the development of OSNs (Fig. 8).

Then we analyzed the localization of several protein involved in the olfactory transduction in STOML-3 KO mice such as ACIII (Bakalyar and Reed, 1990), the main subunit of CNG channel, CNGA2 (Bönigk et al., 1999) and the Ca^{2+} activated Cl^{-} channel TMEM16B (Billig et al., 2011; Stephan et al., 2009). Figure 9A shows that ACIII, CNGA2 and TMEM16B are localized at the luminal surface of the OE both in WT and in STOML-3 KO mice. No significant differences were found between different OE regions. Moreover, double immunohistochemical labeling with the ciliary marker AcTb shows that all the components of the olfactory transduction we have investigated were normally targeted to the cilia also in STOML-3 KO mice (Fig. 9B).

Finally, we used whole mount preparation to analyze the ciliary structure using the *Dolichos biflorus* agglutinin that stains a subset of OSNs (Lipscomb et al., 2002; Talaga et al., 2017). Figure 10 shows that the number of cilia per OSN and the total length of the cilia for each OSN was not significantly different between WT and STOML-3 KO mice and no significant difference were found between different OE regions (Fig. 11). Overall, we observed no overt structural alterations in the OE of STOML-3 KO mice.

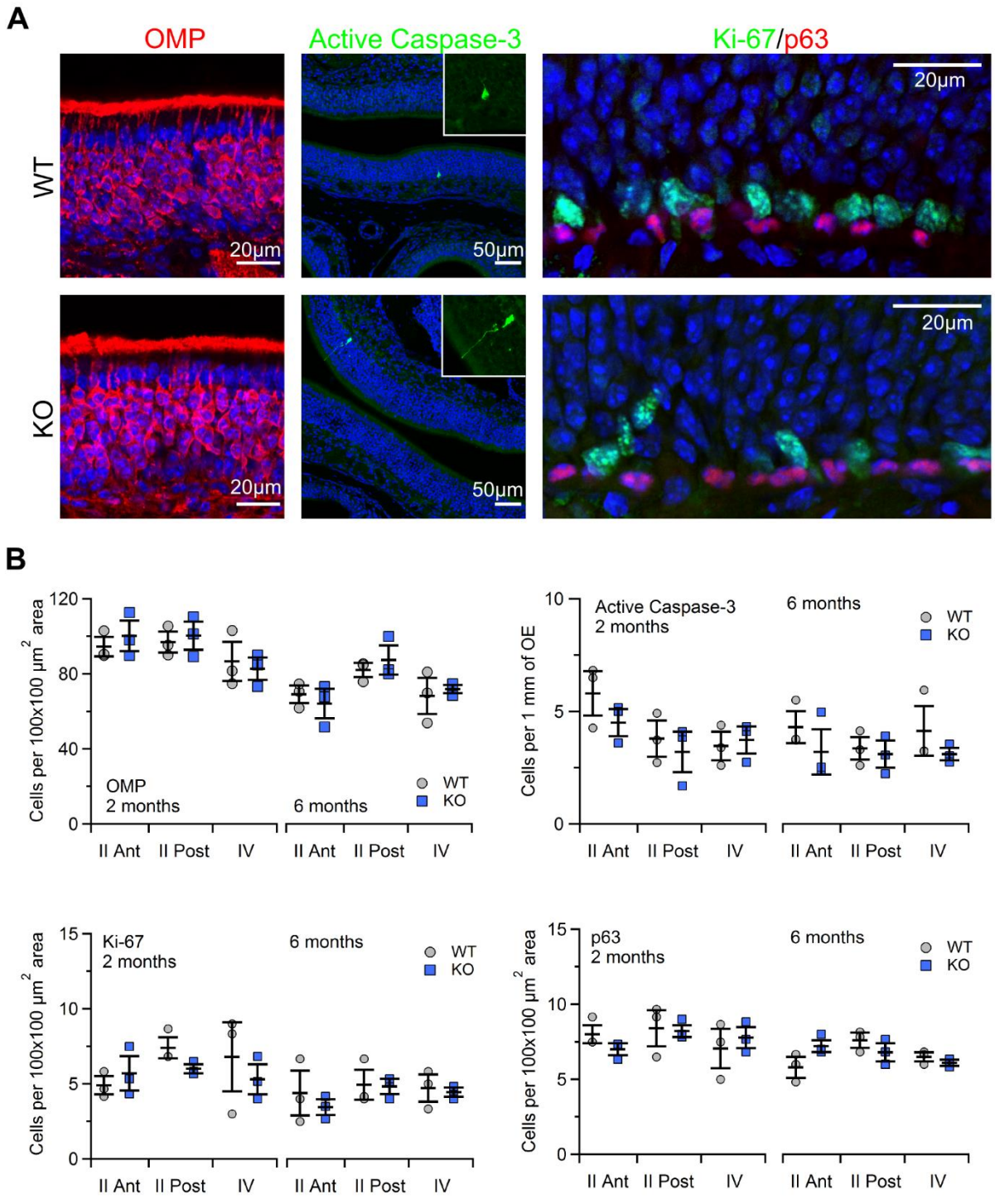

Figure 8. STOML-3 KO mice do not show defects in the development of OSNs. (A) Confocal images of coronal section of the olfactory epithelium from WT and STOML-3 KO mice immunostained for OMP, active Caspase-3, Ki-67 and p63. Cell nuclei were stained with DAPI (blue). (B) Scatter dot plot with average ± sem showing the number of OMP, active Caspase-3, Ki-67 and p63 immunopositive cells in different OE regions from WT and STOML-3 KO mice at age of 2 and 6 months (mice, n=3).

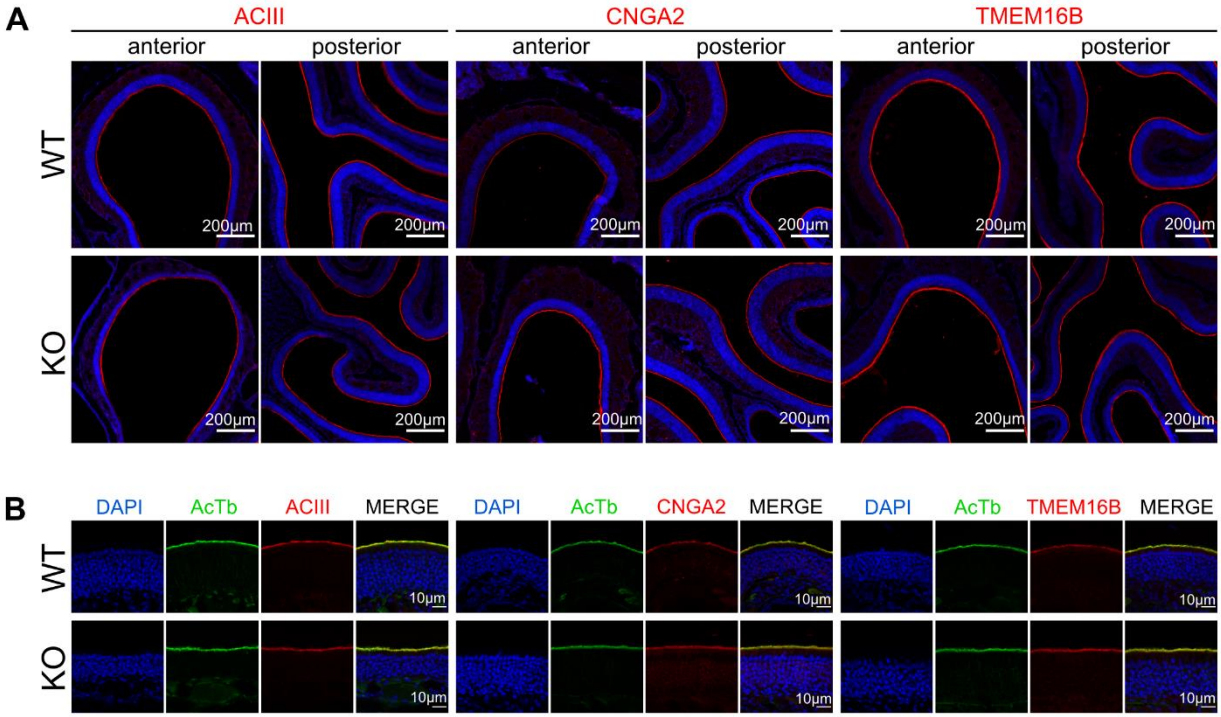

Figure 9. Localization of ACIII, CNGA2 and TMEM16B in olfactory epithelium from WT and STOML-3 KO mice. (A) Confocal images of coronal section of anterior and posterior region the olfactory epithelium from WT and STOML-3 KO mice immunostained for ACIII (left), CNGA2 (middle) and TMEM16B (right). (B) Confocal images of coronal section of the olfactory epithelium from WT and STOML-3 KO mice double immunostained for Acetylated tubulin (AcTb) and ACIII (left), CNGA2 (middle) or TMEM16B (right). Cell nuclei were stained with DAPI (blue).

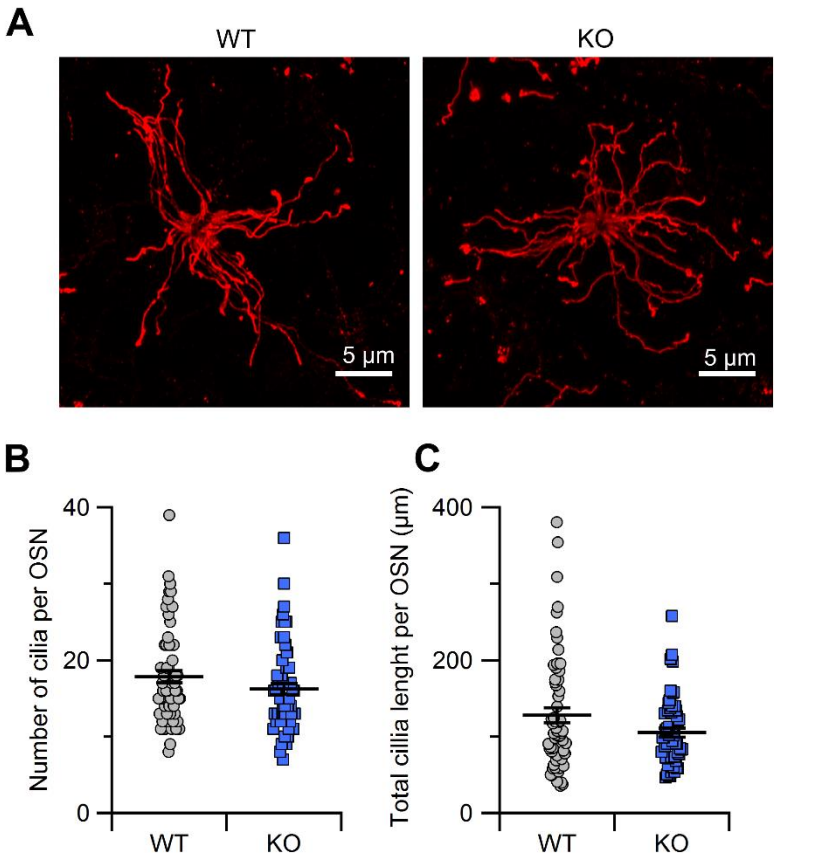

Figure 10. OSN cilia organization in WT and STOML-3 KO mice. (A) Whole-mount preparation of OE from WT and STOML-3 KO mice with the cilia of an OSN labeled by *Dolichos biflorus* agglutinin. Scatter dot plot with average ± sem showing the number of cilia per OSN (B) and the total length of the cilia for each OSN (C) from WT and STOML-3 KO mice.

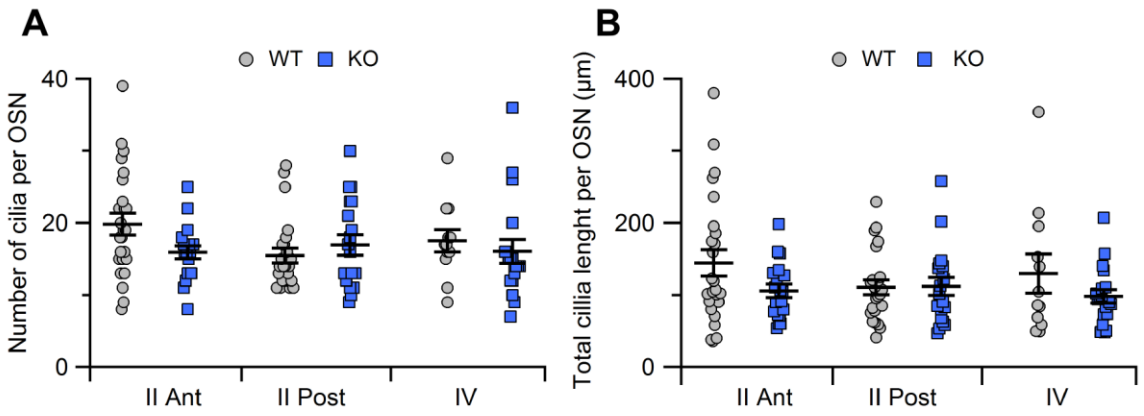

Figure 11. OSN cilia organization in WT and STOML-3 KO mice. Scatter dot plot with average ± sem showing the number of cilia per OSN (A) and the total length of the cilia for each OSN (B) located in different region of OE from WT and STOML-3 KO mice.

Odorant response in STOML-3 KO mice.

To test whether the lack of STOML-3 alters the odorant response of the OSNs, we performed electro-olfactogram (EOG) recordings. Using this approach, we measured odorant-induced changes in voltage across the olfactory epithelium monitoring the electrical activity of a population of OSNs close to recording electrode (Scott and Scott-Johnson, 2002). In a similar way to the experiments investigating the OE development, we measured the EOG responses in three different regions of the OE: anterior part of turbinate II (II Ant), posterior part of turbinate II (II Post) and turbinate IV. Moreover, we performed experiment both in 2 and 6 months old mice. Figure 12A shows representative EOG responses induced by 100 ms long pulse of vapor phase of isomyl acetate (IAA) solutions with concentration ranging 10^{-7} to 1 M in 2 months old WT and STOML-3 KO mice. We found that the amplitude of the odorant response from II Ant region is significantly smaller in STOML-3 KO. Indeed, upon stimulation with vapor from 1 M IAA solution the EOG amplitude was 16.4 ± 0.7 mV in WT mice and 12 ± 1 mV in STOML-3 KO (n=9-10 *<0.05 Student's t-test, Fig. 12 B). In contrast, recordings from II Post and turbinate IV did not shown statistically significant differences between WT and STOML-3 KO mice. Recordings from 6 months old mice shown a significant reduction in the amplitude in the odorant-evoked response both in II Ant and in II Post region. In particular, stimulation with vapor from 1 M IAA solution in II Ant region induced an EOG response of 18 ± 1 mV and 13 ± 1 mV in WT and STOML-3 KO mice respectively (n=9-10 *<p0.05 Student's t-test, Fig. 12 CD). Similarly, in II Post region the EOG response upon the same stimulation was of 10.6 ± 0.3 mV in WT and 8.3 ± 0.6 mV in STOML-3 KO mice (n=9-10 *<p0.05 Student's t-test, Fig. 12 CD). In addition, recordings from turbinate IV showed a reduced amplitude without reaching the statistically significant level (Fig. 12 CD).

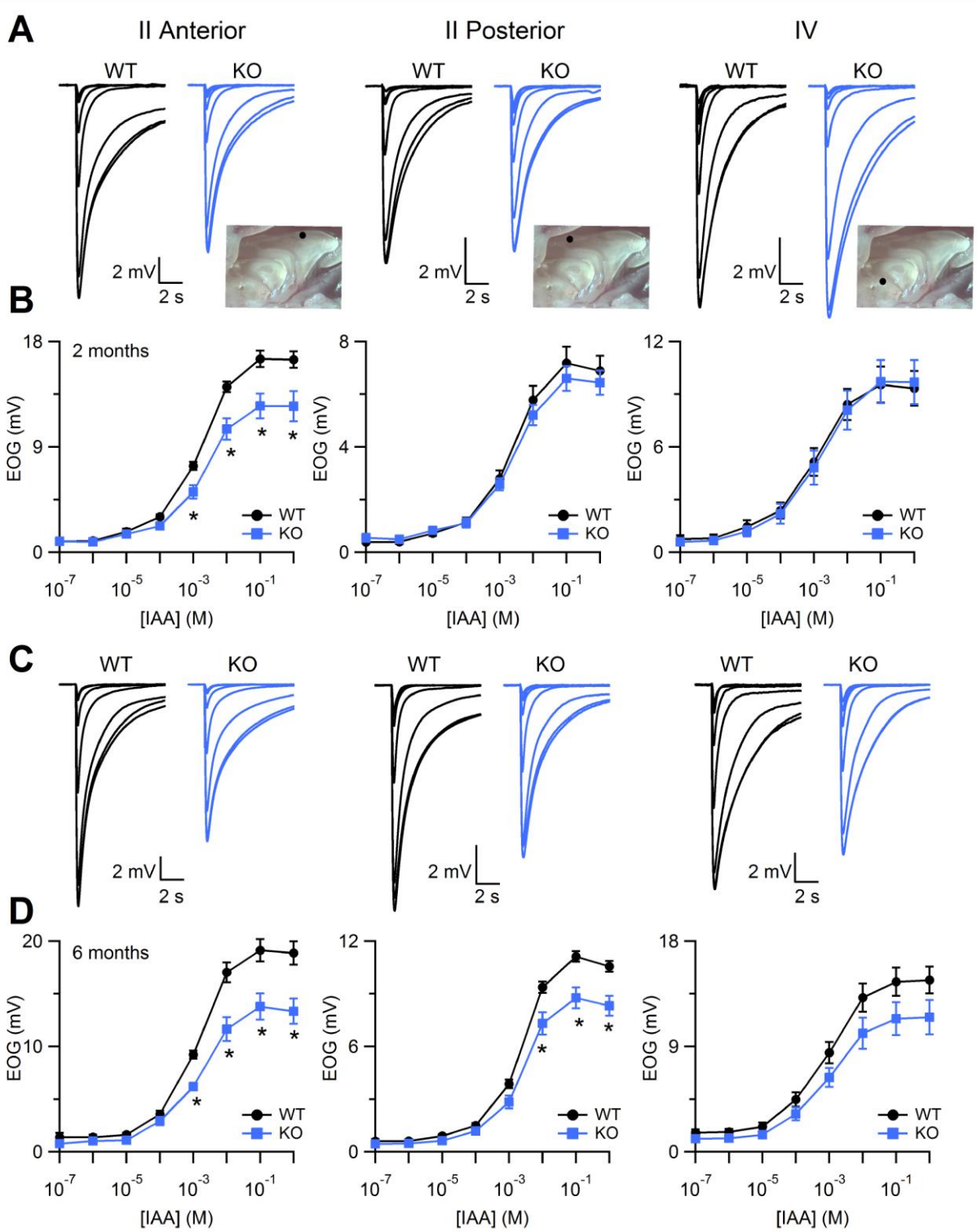

Figure 12. Odorant response in WT and STOML-3 KO mice. Representative EOG recordings from WT (black traces) or STOML-3 KO (blue traces) 2 months (A) or 6 months (C) old mice. The responses were evoked by 100 ms stimulation with isoamyl acetate vapors of increasing concentrations. EOG recordings were obtained from indicated OE locations. Dose–response relationships of average peak EOG amplitudes from WT (black traces) or STOML-3 KO (blue traces) 2 months (B) or 6 months (D) old mice (n=9-10 *<0.05 Student's t-test).

We further analyzed the kinetics of the EOG recordings. We measured the latency as the time between the starting of the stimulus and the time at which the response comes to 1% of its peak value; the rise time as the interval between the beginning of the response and the time of the peak response; the time constant of the monoexponential fit of the recovery phase of the EOG response. We did not find significant differences in the kinetics of the EOG recordings between WT and STOML-3 mice in all tested regions of OE both in 2- and 6-months old animals (Fig. 13).

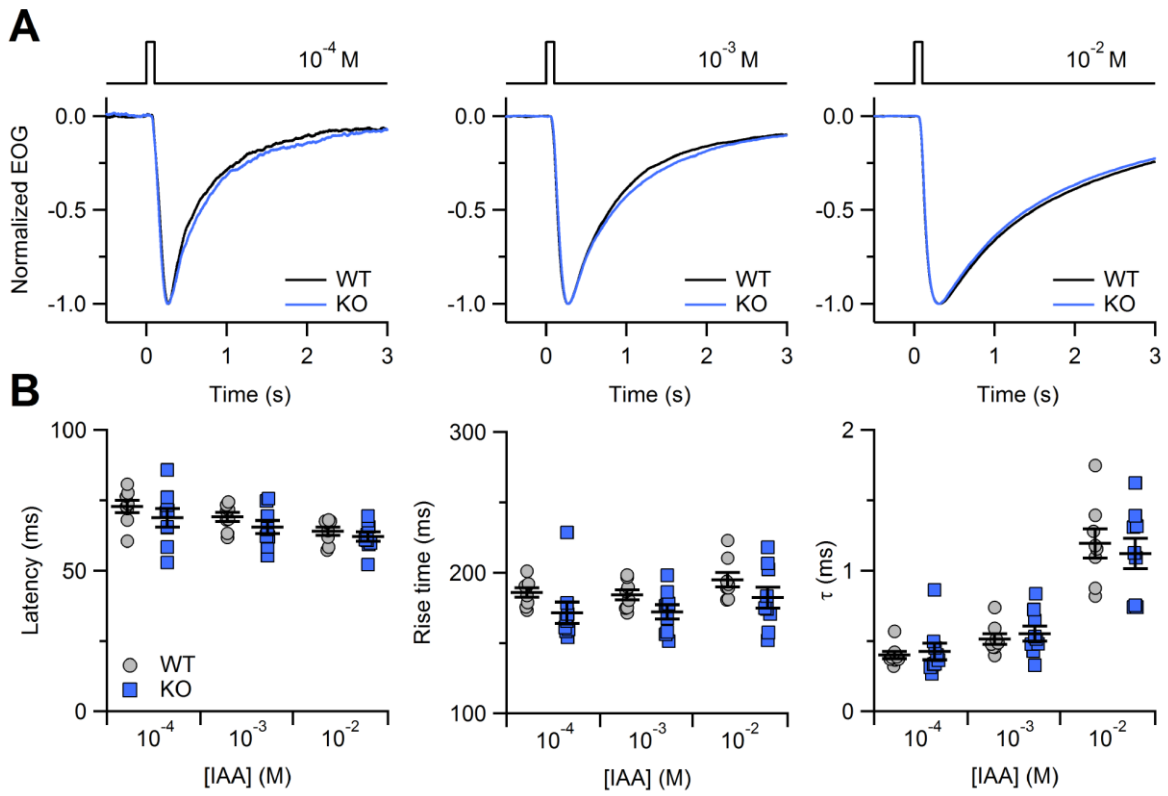

Figure 13. Kinetics of the odorant response in WT and STOML-3 KO mice. Representative normalized EOG recordings from 2 months old WT (black traces) or STOML-3 KO (blue traces) mice in II Ant region. The responses were evoked by 100 ms stimulation of vapors of the indicated IAA solution concentration. (B) Scatter dot plot with average ± sem showing the values of latency (left), rise time (middle) and time constant (right) in WT or STOML-3 KO mice at each odorant concentration (n=9-10).

DISCUSSION

In this study, we have provided a comprehensive investigation of the localization of stomatin-domain proteins in the mouse OE. We found that Stomatin and STOML-3 are targeted to the OSN cilia, while STOML-1 and STOML-2 are localized in the OSN soma. Using knockout for STOML-3 we found that even if the OE development is normal, the lack of STOML-3 causes a reduction in the amplitude of the physiological response to odorants in some OE region especially in older mice.

Expression of stomatin proteins in OE

Several proteomic and transcriptomic studies had pointed out that stomatin proteins are expressed in the OE (Ibarra-Soria et al., 2014; Kanageswaran et al., 2015; Klimmeck et al., 2008, 2008; Kuhlmann et al., 2014; Mayer et al., 2009; Saraiva et al., 2015; Stephan et al., 2009). Here, we reported the first detailed investigation on the expression and subcellular localization of all stomatin proteins in OE. By RT-PCR, we confirmed the expression of *Stomatin*, *STOML-1*, *STOML-2* and *STOML-3* in the OE (Ibarra-Soria et al., 2014; Kanageswaran et al., 2015; Saraiva et al., 2015; Wetzel et al., 2007; Fig. 1). We also found that *Podocin* is not expressed. Using specific antibodies, we confirmed the localization of STOML-3 on the OSN cilia (Goldstein et al., 2002; Kobayakawa et al., 2002; Kulaga et al., 2004; Kurtenbach et al., 2017; Tadenev et al., 2011). We found that also Stomatin is targeted to the cilia confirming previous proteomic data (Klimmeck et al., 2008, 2008; Kuhlmann et al., 2014; Mayer et al., 2009; Stephan et al., 2009). This localization suggests a possible role of Stomatin and STOML-3 in the regulation of olfactory transduction. Moreover, the mislocalization of Stomatin in STOML-3 mice indicates the involvement of STOML-3 in the targeting of Stomatin to the cilia.

Even if some previous studies reported the presence of STOML-1 and STOML-2 in preparations of ciliary proteins, we showed that these two members of stomatin protein family are localized in the soma of the OSNs (Kuhlmann et al., 2014; Mayer et al., 2009, 2009). These results could explain by a possible contamination in the isolation of ciliary proteins.

Physiological role of STOML-3 in olfactory sensory neurons

Previously, it has been shown that absence or alteration in the activity of members of the transduction machinery could lead to alterations in the development of key structures in the olfactory epithelium. This could be due to alterations in the homeostasis of the OSNs or to the role played in OSN development in addition to the involvement into the odorant transduction cascade. For example, the absence of ACIII leads to a decrease in the number of mature OSNs due to an increase of apoptotic cells and without affecting the rate of cell proliferation in the OE the (Zhang et al., 2017). On the other hand, ACIII seems to be also involved in the cilia development. Indeed, in coronal sections of the OE, the immunostaining with AcTb is reduced in ACIII KO mice (Zhang et al., 2017). Using whole mount preparation, Challis et al. (2016) found that ACIII KO mice display a reduction in the length of the cilia. The role of the cAMP signaling on the ciliogenesis have been further supported by observing similar alterations in PDE1C/PDE4 double KO mice (Challis et al., 2016) and in mice with a dominant-negative form of cAMP-dependent protein kinase A (PKA, Kaneko-Goto et al., 2013).

We investigates in detail the development of several structures in the OE of STOML-3 KO animals. They displayed normal formation of the folds of turbinates and they did not have alterations in the density of OSNs, apoptotic, globose or horizontal basal cells.

Previous biochemical data showed an alteration of cAMP production in OE cilia extracts treated with antibodies against STOML-3 (Kobayakawa et al., 2002). Moreover, the expression of STOML-3 is strongly misregulated or mislocalized in KO mice for some Bardet–Biedl Syndrome (BBS) proteins. BBS proteins have been involved in ciliogenesis and transport inside the cilia (Jin and Nachury, 2009; Nachury and Mick, 2019). In humans, mutations in BBS protein leads to multiple symptoms, for example, blindness, obesity and deafness and also causes anosmia (Jin and Nachury, 2009). In mice, the absence BBS proteins also leads to anosmia and an altered development of the olfactory cilia (Kulaga et al., 2004; Tadenev et al., 2011). Therefore, we tested if STOML-3 KO could have alterations in the development of cilia. We did not observe significant differences in the number and the total length of cilia per neuron demonstrating that STOML-3 is not involved in the regulation of ciliogenesis.

We used EOG recordings to study the responsiveness of the olfactory epithelium to odorant stimulation (Scott and Scott-Johnson, 2002). This technique has been used to evaluate the role of several elements of the olfactory transduction process. For example, in CNGA2, ACIII or $G\alpha_{olf}$ KO mice the EOG response is almost completely abolished (Belluscio et al., 1998; Brunet et al., 1996; Wong et al., 2000). Moreover, other type of alterations in the EOG response kinetics have been observed specially in mutants of molecules involved in negative feedback on the odorant transduction. For example, slower decaying phase after a short odorant stimulus, or slower adaptation under prolonged stimulation (Cygnar and Zhao, 2009; Song et al., 2008; Stephan et al., 2012). This suggests that the EOG response represents the electrical activity of the OSNs, in particular the odor-evoked activity of the members of the odor transduction machinery, and therefore support this technique as a valuable tool to test the role in the responsiveness of the olfactory epithelium of uncharacterized proteins and even get some hints about possible functions. We found a reduction in the amplitude of the response to short pulse stimulation with IAA in STOML-3 KO mice, especially at older ages. This reduction is more profound in the anterior-dorsal portion of the OE.

Our results exclude that this reduction of EOG response could be due to a decrease of the number of mature OSNs or to an alteration of their ciliary structure. We also found that in STOML-3 mice key elements of the olfactory transduction are correctly targeted to the cilia. However, quantitative Western blot experiments will better test if STOML-3 controls the expression level of ACIII, CNGA2, TMEM16B or other components of the signaling cascade.

Since, stomatin proteins can physically and functionally interact with different types of ion channels (Lapatsina et al., 2012; Poole et al., 2014), we can speculate that STOML-3 could modulates also CNG and/or TMEM16B. Immunoprecipitation experiment and patch-clamp recording will be necessary to fully investigate this scenario. In STOML-3 mice, we found also a reduction in expression level of Stomatin that remains trapped in knobs of some OSNs without reaching the cilia. This could indicate a possible interaction between Stomatin and STOML-3 with relevant physiological implications, therefore it would be very interesting to investigate by using Stomatin KO and Stomatin and STOML-3 double KO mice to understand the relative role of these proteins in the odorant detection. Finally, additional experiments are need to test is the observed reduction of odorant-responses can give rise to behavioral relevant alterations.

Conclusions

In summary, our data provide a definitive demonstration that STOML-3 is expressed in the cilia of OSNs together with Stomatin. STOML-3 is not involved in OE development, but controls the responsiveness of OSN to odorant. The data will allow to deeper investigation of the physiological role of stomatin proteins in OE.

REFERENCES

Bakalyar, H.A., and R.R. Reed. 1990. Identification of a specialized adenylyl cyclase that may mediate odorant detection. *Science*. 250:1403–1406. doi:10.1126/science.2255909.

Belluscio, L., G.H. Gold, A. Nemes, and R. Axel. 1998. Mice Deficient in Golf Are Anosmic. *Neuron*. 20:69–81. doi:10.1016/S0896-6273(00)80435-3.

Billig, G.M., B. Pál, P. Fidzinski, and T.J. Jentsch. 2011. Ca2+-activated Cl− currents are dispensable for olfaction. *Nat. Neurosci.* 14:763–769. doi:10.1038/nn.2821.

Bönigk, W., J. Bradley, F. Müller, F. Sesti, I. Boekhoff, G.V. Ronnett, U.B. Kaupp, and S. Frings. 1999. The native rat olfactory cyclic nucleotide-gated channel is composed of three distinct subunits. *J. Neurosci. Off. J. Soc. Neurosci.* 19:5332–5347.

Boute, N., O. Gribouval, S. Roselli, F. Benessy, H. Lee, A. Fuchshuber, K. Dahan, M.C. Gubler, P. Niaudet, and C. Antignac. 2000. NPHS2, encoding the glomerular protein podocin, is mutated in autosomal recessive steroid-resistant nephrotic syndrome. *Nat. Genet.* 24:349–354. doi:10.1038/74166.

Brand, J., E.S.J. Smith, D. Schwefel, L. Lapatsina, K. Poole, D. Omerbašić, A. Kozlenkov, J. Behlke, G.R. Lewin, and O. Daumke. 2012. A stomatin dimer modulates the activity of acid-sensing ion channels. *EMBO J.* 31:3635–3646. doi:10.1038/emboj.2012.203.

Brunet, L.J., G.H. Gold, and J. Ngai. 1996a. General anosmia caused by a targeted disruption of the mouse olfactory cyclic nucleotide-gated cation channel. *Neuron*. 17:681–693. doi:10.1016/s0896-6273(00)80200-7.

Brunet, L.J., G.H. Gold, and J. Ngai. 1996b. General anosmia caused by a targeted disruption of the mouse olfactory cyclic nucleotide-gated cation channel. *Neuron*. 17:681–693.

Castillo, K., R. Delgado, and J. Bacigalupo. 2007. Plasma membrane Ca(2+)-ATPase in the cilia of olfactory receptor neurons: possible role in Ca(2+) clearance. *Eur. J. Neurosci.* 26:2524–2531. doi:10.1111/j.1460-9568.2007.05863.x.

Challis, R.C., H. Tian, W. Yin, and M. Ma. 2016. Genetic Ablation of Type III Adenylyl Cyclase Exerts Region-Specific Effects on Cilia Architecture in the Mouse Nose. *PLOS ONE*. 11:e0150638. doi:10.1371/journal.pone.0150638.

Cygnar, K.D., and H. Zhao. 2009. Phosphodiesterase 1C is dispensable for rapid response termination of olfactory sensory neurons. *Nat. Neurosci.* 12:454–462. doi:10.1038/nn.2289.

Firestein, S. 2001. How the olfactory system makes sense of scents. *Nature*. 413:211–218. doi:10.1038/35093026.

Fletcher, R.B., M.S. Prasol, J. Estrada, A. Baudhuin, K. Vranizan, Y.G. Choi, and J. Ngai. 2011. p63 regulates olfactory stem cell self-renewal and differentiation. *Neuron*. 72:748–759. doi:10.1016/j.neuron.2011.09.009.

Fluegge, D., L.M. Moeller, A. Cichy, M. Gorin, A. Weth, S. Veitinger, S. Cainarca, S. Lohmer, S. Corazza, E.M. Neuhaus, W. Baumgartner, J. Spehr, and M. Spehr. 2012. Mitochondrial Ca(2+) mobilization is a key element in olfactory signaling. *Nat. Neurosci.* 15:754–762. doi:10.1038/nn.3074.

Goldstein, B.J., H.M. Kulaga, and R.R. Reed. 2002. Cloning and Characterization of SLP3: a Novel Member of the Stomatin Family Expressed by Olfactory Receptor Neurons. *JARO - J. Assoc. Res. Otolaryngol.* 4:74–82. doi:10.1007/s10162-002-2039-5.

Goldstein, B.J., H.M. Kulaga, and R.R. Reed. 2003. Cloning and characterization of SLP3: a novel member of the stomatin family expressed by olfactory receptor neurons. *J. Assoc. Res. Otolaryngol. JARO*. 4:74–82. doi:10.1007/s10162-002-2039-5.

Green, J.B., and J.P.W. Young. 2008. Slipins: ancient origin, duplication and diversification of the stomatin protein family. *BMC Evol. Biol.* 8:44. doi:10.1186/1471-2148-8-44.

Hunyady, B., K. Krempels, G. Harta, and E. Mezey. 1996. Immunohistochemical signal amplification by catalyzed reporter deposition and its application in double immunostaining. *J. Histochem. Cytochem.* 44:1353–1362. doi:10.1177/44.12.8985127.

Ibarra-Soria, X., M.O. Levitin, L.R. Saraiva, and D.W. Logan. 2014. The Olfactory Transcriptomes of Mice. *PLoS Genet.* 10:e1004593. doi:10.1371/journal.pgen.1004593.

Jin, H., and M.V. Nachury. 2009. The BBSome. *Curr. Biol.* 19:R472–R473. doi:10.1016/j.cub.2009.04.015.

Kanageswaran, N., M. Demond, M. Nagel, B.S.P. Schreiner, S. Baumgart, P. Scholz, J. Altmüller, C. Becker, J.F. Doerner, H. Conrad, S. Oberland, C.H. Wetzel, E.M. Neuhaus, H. Hatt, and G. Gisselmann. 2015. Deep Sequencing of the Murine Olfactory Receptor Neuron Transcriptome. *PLOS ONE*. 10:e0113170. doi:10.1371/journal.pone.0113170.

Kaneko-Goto, T., Y. Sato, S. Katada, E. Kinameri, S. -i. Yoshihara, A. Nishiyori, M. Kimura, H. Fujita, K. Touhara, R.R. Reed, and Y. Yoshihara. 2013. Goofy Coordinates the Acuity of Olfactory Signaling. *J. Neurosci.* 33:12987–12996. doi:10.1523/JNEUROSCI.4948-12.2013.

Keller, A., and F.L. Margolis. 1975. Immunological studies of the rat olfactory marker protein. *J. Neurochem.* 24:1101–1106.

Klimmeck, D., U. Mayer, N. Ungerer, U. Warnken, M. Schnölzer, S. Frings, and F. Möhrlen. 2008a. Calcium-signaling networks in olfactory receptor neurons. *Neuroscience*. 151:901–912. doi:10.1016/j.neuroscience.2007.11.023.

Klimmeck, D., U. Mayer, N. Ungerer, U. Warnken, M. Schnölzer, S. Frings, and F. Möhrlen. 2008b. Calcium-signaling networks in olfactory receptor neurons. *Neuroscience*. 151:901–912. doi:10.1016/j.neuroscience.2007.11.023.

Kobayakawa, K., R. Hayashi, K. Morita, K. Miyamichi, Y. Oka, A. Tsuboi, and H. Sakano. 2002. Stomatin-related olfactory protein, SRO, specifically expressed in the murine olfactory sensory neurons. *J. Neurosci. Off. J. Soc. Neurosci.* 22:5931–5937.

Kuhlmann, K., A. Tschapek, H. Wiese, M. Eisenacher, H.E. Meyer, H.H. Hatt, S. Oeljeklaus, and B. Warscheid. 2014. The Membrane Proteome of Sensory Cilia to the Depth of Olfactory Receptors. *Mol. Cell. Proteomics*. 13:1828–1843. doi:10.1074/mcp.M113.035378.

Kulaga, H.M., C.C. Leitch, E.R. Eichers, J.L. Badano, A. Lesemann, B.E. Hoskins, J.R. Lupski, P.L. Beales, R.R. Reed, and N. Katsanis. 2004. Loss of BBS proteins causes anosmia in humans and defects in olfactory cilia structure and function in the mouse. *Nat. Genet.* 36:994–998. doi:10.1038/ng1418.

Kurtenbach, S., A. Gießl, S. Strömberg, J. Kremers, J. Atorf, S. Rasche, E.M. Neuhaus, D. Hervé, J.H. Brandstätter, E. Asan, H. Hatt, and M.W. Kilimann. 2017. The BEACH Protein LRBA Promotes the Localization of the Heterotrimeric G-protein Golf to Olfactory Cilia. *Sci. Rep.* 7:8409. doi:10.1038/s41598-017-08543-4.

Lapatsina, L., J. Brand, K. Poole, O. Daumke, and G.R. Lewin. 2012a. Stomatin-domain proteins. *Eur. J. Cell Biol.* 91:240–245. doi:10.1016/j.ejcb.2011.01.018.

Lapatsina, L., J. Brand, K. Poole, O. Daumke, and G.R. Lewin. 2012b. Stomatin-domain proteins. *Eur. J. Cell Biol.* 91:240–245. doi:10.1016/j.ejcb.2011.01.018.

Lipscomb, B.W., H.B. Treloar, and C.A. Greer. 2002. Cell surface carbohydrates reveal heterogeneity in olfactory receptor cell axons in the mouse. *Cell Tissue Res.* 308:7–17. doi:10.1007/s00441-002-0532-0.

Matthews, H.R., and J. Reisert. 2003. Calcium, the two-faced messenger of olfactory transduction and adaptation. *Curr. Opin. Neurobiol.* 13:469–475. doi:10.1016/s0959-4388(03)00097-7.

Mayer, U., A. Küller, P.C. Daiber, I. Neudorf, U. Warnken, M. Schnölzer, S. Frings, and F. Möhrlen. 2009. The proteome of rat olfactory sensory cilia. *Proteomics*. 9:322–334. doi:10.1002/pmic.200800149.

Mayer, U., N. Ungerer, D. Klimmeck, U. Warnken, M. Schnölzer, S. Frings, and F. Möhrlen. 2008. Proteomic analysis of a membrane preparation from rat olfactory sensory cilia. *Chem. Senses*. 33:145–162. doi:10.1093/chemse/bjm073.

Menini, A., L. Lagostena, and A. Boccaccio. 2004. Olfaction: from odorant molecules to the olfactory cortex. *News Physiol. Sci. Int. J. Physiol. Prod. Jointly Int. Union Physiol. Sci. Am. Physiol. Soc.* 19:101–104.

Nachury, M.V., and D.U. Mick. 2019. Establishing and regulating the composition of cilia for signal transduction. *Nat. Rev. Mol. Cell Biol.* 20:389–405. doi:10.1038/s41580-019-0116-4.

Owczarek, C.M., H.R. Treutlein, K.J. Portbury, L.M. Gulluyan, I. Kola, and P.J. Hertzog. 2001. A novel member of the STOMATIN/EPB72/mec-2 family, stomatin-like 2 (STOML2), is ubiquitously expressed and localizes to HSA chromosome 9p13.1. *Cytogenet. Cell Genet.* 92:196–203. doi:10.1159/000056902.

Pifferi, S., A. Menini, and T. Kurahashi. 2010. Signal Transduction in Vertebrate Olfactory Cilia. *In* The Neurobiology of Olfaction. A. Menini, editor. CRC Press/Taylor & Francis, Boca Raton (FL).

Piperno, G., and M.T. Fuller. 1985. Monoclonal antibodies specific for an acetylated form of alpha-tubulin recognize the antigen in cilia and flagella from a variety of organisms. *J. Cell Biol.* 101:2085–2094.

Poole, K., R. Herget, L. Lapatsina, H.-D. Ngo, and G.R. Lewin. 2014. Tuning Piezo ion channels to detect molecular-scale movements relevant for fine touch. *Nat. Commun.* 5:3520. doi:10.1038/ncomms4520.

Reisert, J., and H.R. Matthews. 1998. Na+-dependent Ca2+ extrusion governs response recovery in frog olfactory receptor cells. *J. Gen. Physiol.* 112:529–535.

Salzer, U., H. Ahorn, and R. Prohaska. 1993. Identification of the phosphorylation site on human erythrocyte band 7 integral membrane protein: implications for a monotopic protein structure. *Biochim. Biophys. Acta*. 1151:149–152. doi:10.1016/0005-2736(93)90098-k.

Saraiva, L.R., X. Ibarra-Soria, M. Khan, M. Omura, A. Scialdone, P. Mombaerts, J.C. Marioni, and D.W. Logan. 2015. Hierarchical deconstruction of mouse olfactory sensory neurons: from whole mucosa to single-cell RNA-seq. *Sci. Rep.* 5:18178. doi:10.1038/srep18178.

Scott, J.W., and P.E. Scott-Johnson. 2002a. The electroolfactogram: a review of its history and uses. *Microsc. Res. Tech.* 58:152–160. doi:10.1002/jemt.10133.

Scott, J.W., and P.E. Scott-Johnson. 2002b. The electroolfactogram: A review of its history and uses. *Microsc. Res. Tech.* 58:152. doi:10.1002/jemt.10133.

Seidel, G., and R. Prohaska. 1998. Molecular cloning of hSLP-1, a novel human brain-specific member of the band 7/MEC-2 family similar to Caenorhabditis elegans UNC-24. *Gene*. 225:23–29. doi:10.1016/s0378-1119(98)00532-0.

Snyers, L., E. Umlauf, and R. Prohaska. 1998. Oligomeric nature of the integral membrane protein stomatin. *J. Biol. Chem.* 273:17221–17226. doi:10.1074/jbc.273.27.17221.

Song, Y., K.D. Cygnar, B. Sagdullaev, M. Valley, S. Hirsh, A. Stephan, J. Reisert, and H. Zhao. 2008. Olfactory CNG Channel Desensitization by Ca2+/CaM via the B1b Subunit Affects Response Termination but Not Sensitivity to Recurring Stimulation. *Neuron*. 58:374–386. doi:10.1016/j.neuron.2008.02.029.

Stephan, A.B., E.Y. Shum, S. Hirsh, K.D. Cygnar, J. Reisert, and H. Zhao. 2009a. ANO2 is the cilial calcium-activated chloride channel that may mediate olfactory amplification. *Proc. Natl. Acad. Sci. U. S. A.* 106:11776–11781. doi:10.1073/pnas.0903304106.

Stephan, A.B., E.Y. Shum, S. Hirsh, K.D. Cygnar, J. Reisert, and H. Zhao. 2009b. ANO2 is the cilial calcium-activated chloride channel that may mediate olfactory amplification. *Proc. Natl. Acad. Sci.* 106:11776–11781. doi:10.1073/pnas.0903304106.

Stephan, A.B., S. Tobochnik, M. Dibattista, C.M. Wall, J. Reisert, and H. Zhao. 2012. The Na+/Ca2+ exchanger NCKX4 governs termination and adaptation of the mammalian olfactory response. *Nat. Neurosci.* 15:131–137. doi:10.1038/nn.2943.

Tadenev, A.L.D., H.M. Kulaga, H.L. May-Simera, M.W. Kelley, N. Katsanis, and R.R. Reed. 2011. Loss of Bardet-Biedl syndrome protein-8 (BBS8) perturbs olfactory function, protein localization, and axon targeting. *Proc. Natl. Acad. Sci.* 108:10320–10325. doi:10.1073/pnas.1016531108.

Talaga, A.K., F.N. Dong, J. Reisert, and H. Zhao. 2017. Cilia- and Flagella-Associated Protein 69 Regulates Olfactory Transduction Kinetics in Mice. *J. Neurosci. Off. J. Soc. Neurosci.* 37:5699–5710. doi:10.1523/JNEUROSCI.0392-17.2017.

Tavernarakis, N., M. Driscoll, and N.C. Kyrpides. 1999. The SPFH domain: implicated in regulating targeted protein turnover in stomatins and other membrane-associated proteins. *Trends Biochem. Sci.* 24:425–427.

Thornberry, N.A., and Y. Lazebnik. 1998. Caspases: enemies within. *Science*. 281:1312–1316. doi:10.1126/science.281.5381.1312.

Tirindelli, R., M. Dibattista, S. Pifferi, and A. Menini. 2009. From pheromones to behavior. *Physiol. Rev.* 89:921–956. doi:10.1152/physrev.00037.2008.

Wetzel, C., J. Hu, D. Riethmacher, A. Benckendorff, L. Harder, A. Eilers, R. Moshourab, A. Kozlenkov, D. Labuz, O. Caspani, B. Erdmann, H. Machelska, P.A. Heppenstall, and G.R. Lewin. 2007. A stomatin-domain protein essential for touch sensation in the mouse. *Nature*. 445:206–209. doi:10.1038/nature05394.

Wong, S.T., K. Trinh, B. Hacker, G.C. Chan, G. Lowe, A. Gaggar, Z. Xia, G.H. Gold, and D.R. Storm. 2000. Disruption of the type III adenylyl cyclase gene leads to peripheral and behavioral anosmia in transgenic mice. *Neuron*. 27:487–497.

Zhang, Z., D. Yang, M. Zhang, N. Zhu, Y. Zhou, D.R. Storm, and Z. Wang. 2017. Deletion of Type 3 Adenylyl Cyclase Perturbs the Postnatal Maturation of Olfactory Sensory Neurons and

Olfactory Cilium Ultrastructure in Mice. *Front. Cell. Neurosci.* 11. doi:10.3389/fncel.2017.00001.

Zhao, H., L. Ivic, J.M. Otaki, M. Hashimoto, K. Mikoshiba, and S. Firestein. 1998. Functional Expression of a Mammalian Odorant Receptor. *Science*. 279:237–242. doi:10.1126/science.279.5348.237

4.2 Knockout of Stomatin-domain proteins Stomatin, STOML-1 and STOML3 reduces the odorant response of mouse olfactory sensory neurons

In order to obtain a better understanding of the role of the stomatin-domain proteins in the OE, we started to characterize the phenotype of other KO mouse line. We used a triple knock for Stomatin, STOML-1 and STOML-3 (TKO) and we repeated most of the experiment performed on STOML-3 KO mice.

Development of the Olfactory Epithelium in TKO mice.

We evaluated whether the lack of Stomatin, STOML-1 and STOML-3 has an influence on the development of the OE, therefore we performed immunostaining to identify most of the different cell types present in the OE. We used the olfactory marker protein (OMP) as the typical marker for mature olfactory sensory neurons (Keller and Margolis, 1975); active Caspase-3 for apoptotic cells (Thornberry and Lazebnik, 1998); Ki-67 and p63 to stain the globose and horizontal basal cells respectively (Fletcher et al., 2011). To obtain a quantitative comparison between WT and TKO mice we counted the immunopositive cells in three different regions of the OE: anterior part of turbinate II (II Ant), posterior part of turbinate II (II Post) and turbinate IV. Finally, we performed experiment both in 2 and 6 months old mice. We did not find significant differences between WT and T KO mice in all the regions of the OE both in 2 and 6 months old mice indicating that T3 is not involved in the controlling the proliferation and the development of OSNs (Fig. 1).

Then we analyzed the localization of several protein involved in the olfactory transduction in TKO mice such as ACIII (Bakalyar and Reed, 1990), the main subunit of CNG channel, CNGA2 (Bönigk et al., 1999) and the Ca^{2+} activated Cl^{-} channel TMEM16B (Billig et al., 2011; Stephan et al., 2009). Figure 2A shows that ACIII, CNGA2 and TMEM16B are localized at the luminal surface of the OE both in WT and in TKO mice. No significant differences were found between different OE regions. Moreover, double immunohistochemical labeling with the ciliary marker AcTb shows that all the components of the olfactory transduction we investigated were normally targeted to the cilia also in TKO mice (Fig. 2B).

Finally, we used whole mount preparation to analyze the ciliary structure using the *Dolichos biflorus* agglutinin that stains a subset of OSNs (Lipscomb et al., 2002; Talaga et al., 2017). Figure 3 shows that the number of cilia per OSN and the total length of the cilia for each OSN was not significantly different between WT and TKO mice and no significant difference were found between different OE regions (Fig. 3 C-D). Overall, we observed no significant structural alterations in the OE of TKO mice.

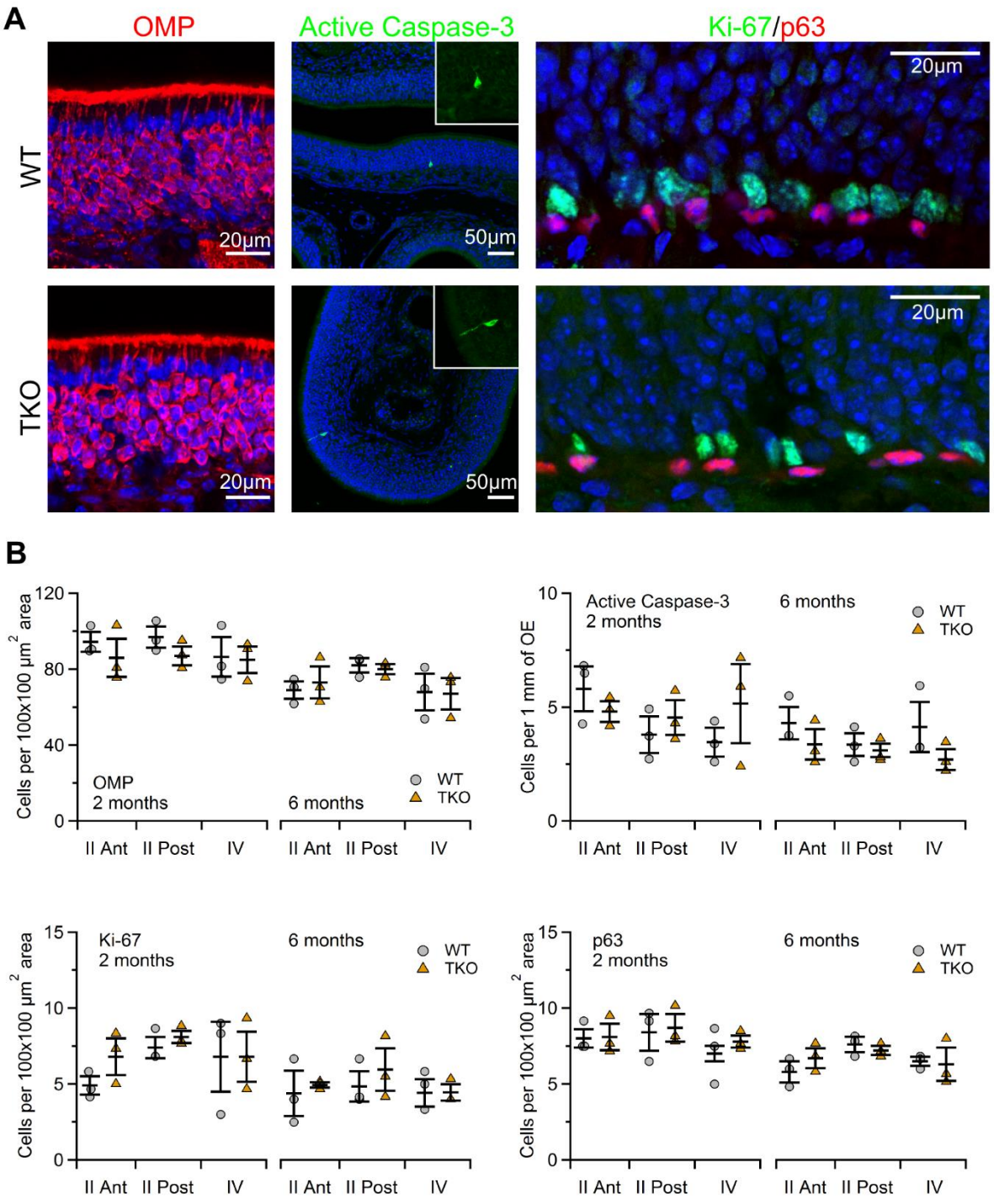

Figure 1. T KO mice do not show defects in the development of OSNs. (A) Confocal images of coronal section of the olfactory epithelium from WT and TKO mice immunostained for OMP, active Caspase-3, Ki-67 and p63. Cell nuclei were stained with DAPI (blue). (B) Scatter dot plot with average ± sem showing the number of OMP, active Caspase-3, Ki-67 and p63 immunopositive cells in different OE regions from WT and TKO mice at age of 2 and 6 months.

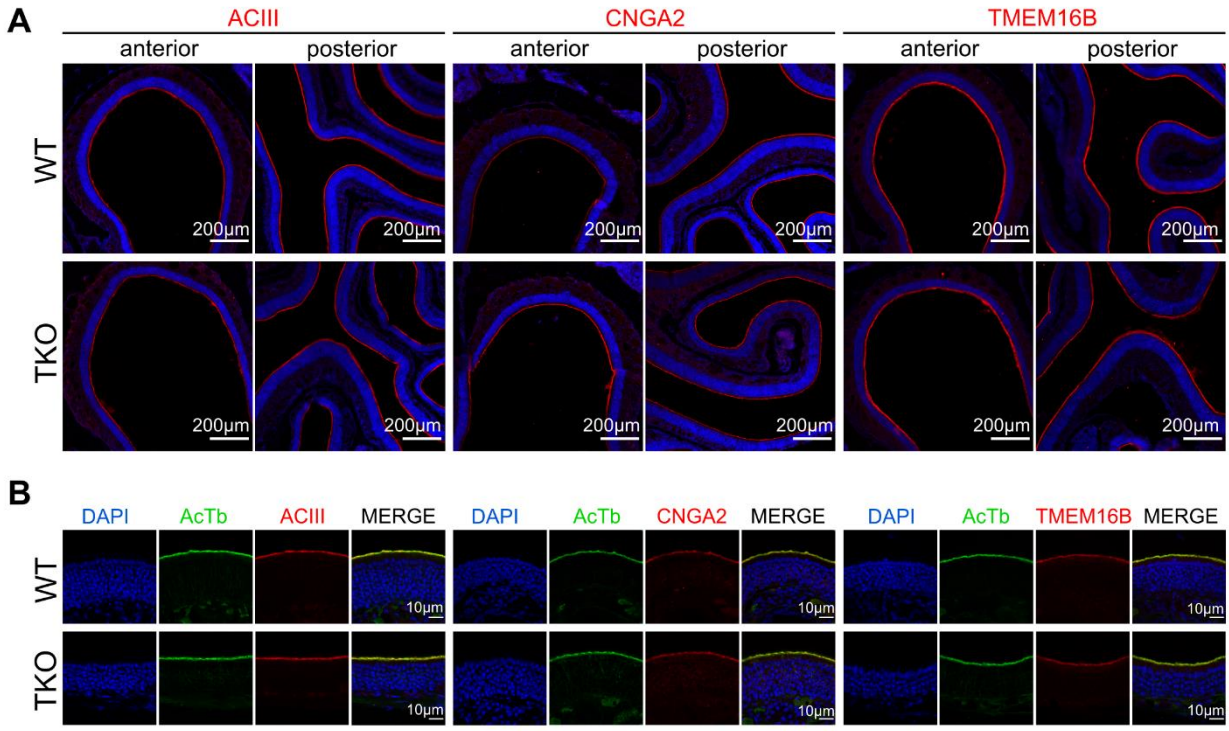

Figure 2. Localization of ACIII, CNGA2 and TMEM16B in olfactory epithelium from WT and TKO mice. (A) Confocal images of coronal section of anterior and posterior region the olfactory epithelium from WT and TKO mice immunostained for ACIII (left), CNGA2 (middle) and TMEM16B (right). (B) Confocal images of coronal section of the olfactory epithelium from WT and TKO mice double immunostained for Acetylated tubulin (AcTb) and ACIII (left), CNGA2 (middle) or TMEM16B (right). Cell nuclei were stained with DAPI (blue).

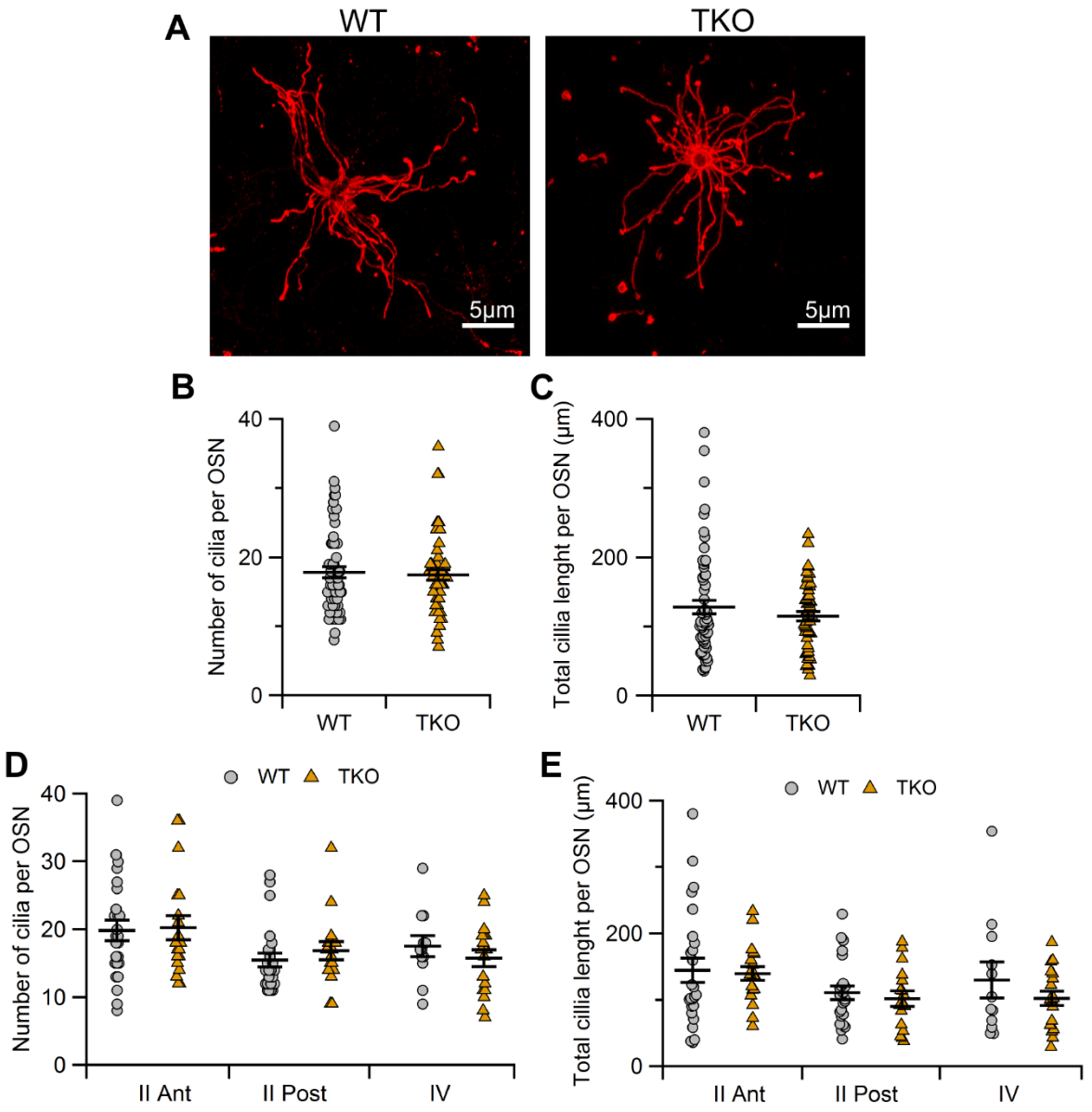

Figure 3. OSN cilia organization in WT and TKO mice. (A) Whole-mount preparation of OE from WT and TKO mice with the cilia of an OSN labeled by *Dolichos biflorus* agglutinin. Scatter dot plot with average ± sem showing the number of cilia per OSN (B) and the total length of the cilia for each OSN (C) from WT and TKO mice. Scatter dot plot with average ± sem showing the number of cilia per OSN (D) and the total length of the cilia for each OSN (E) located in different region of OE from WT and TKO mice.

Odorant response in TKO mice.

To test whether the lack of Stomatin, STOML-1 and STOML-3 alters the odorant response of the OSNs, we performed electro-olfactogram (EOG) recordings. Using this approach, we measured odorant-induced changes in voltage across the olfactory epithelium generated by the electrical activity of a population of OSNs close to recording electrode (Scott and Scott-Johnson, 2002). In a similar way to the experiments investigating the OE

development, we measured the EOG responses in three different regions of the OE: anterior part of turbinate II (II Ant), posterior part of turbinate II (II Post) and turbinate IV. Moreover, we performed experiment both in 2 and 6 months old mice. Figure 4A shows representative EOG responses induced by 100 ms long pulse of vapor phase of isomyl acetate (IAA) solutions with concentration ranging 10^{-7} to 1 M in 2 months old WT and TKO mice. We found that the amplitude of the odorant response from II Ant region is significantly smaller in TKO. Indeed upon stimulation with vapor from 1 M IAA solution the EOG amplitude was 16.4 ± 0.7 mV in WT mice and 10.3 ± 0.9 mV in TKO (n=9-10 *<p0.05 Student's t-test, Fig. 4 B). In contrast, recordings from II Post and turbinate IV did not shown statistically significant differences between WT and TKO mice. Recordings from 6 months old mice shown a significant reduction in the amplitude in the odorant-evoked response both in II Ant and in II Post region. In particular, stimulation with vapor from 1 M IAA solution in II Ant region induced an EOG response of 18 ± 1 mV and 14 ± 2 mV in WT and TKO mice respectively (n=9-10 *<p0.05 Student's t-test, Fig. 6 CD). Similarly, in II Post region the EOG response upon the same stimulation was of 10.6 ± 0.3 mV in WT and 8.5 ± 0.5 mV in TKO mice (n=9-10 *<p0.05 Student's t-test, Fig. 4 CD). In addition, recordings from turbinate IV showed a reduced amplitude without reaching the statistically significant level (Fig. 4 CD).

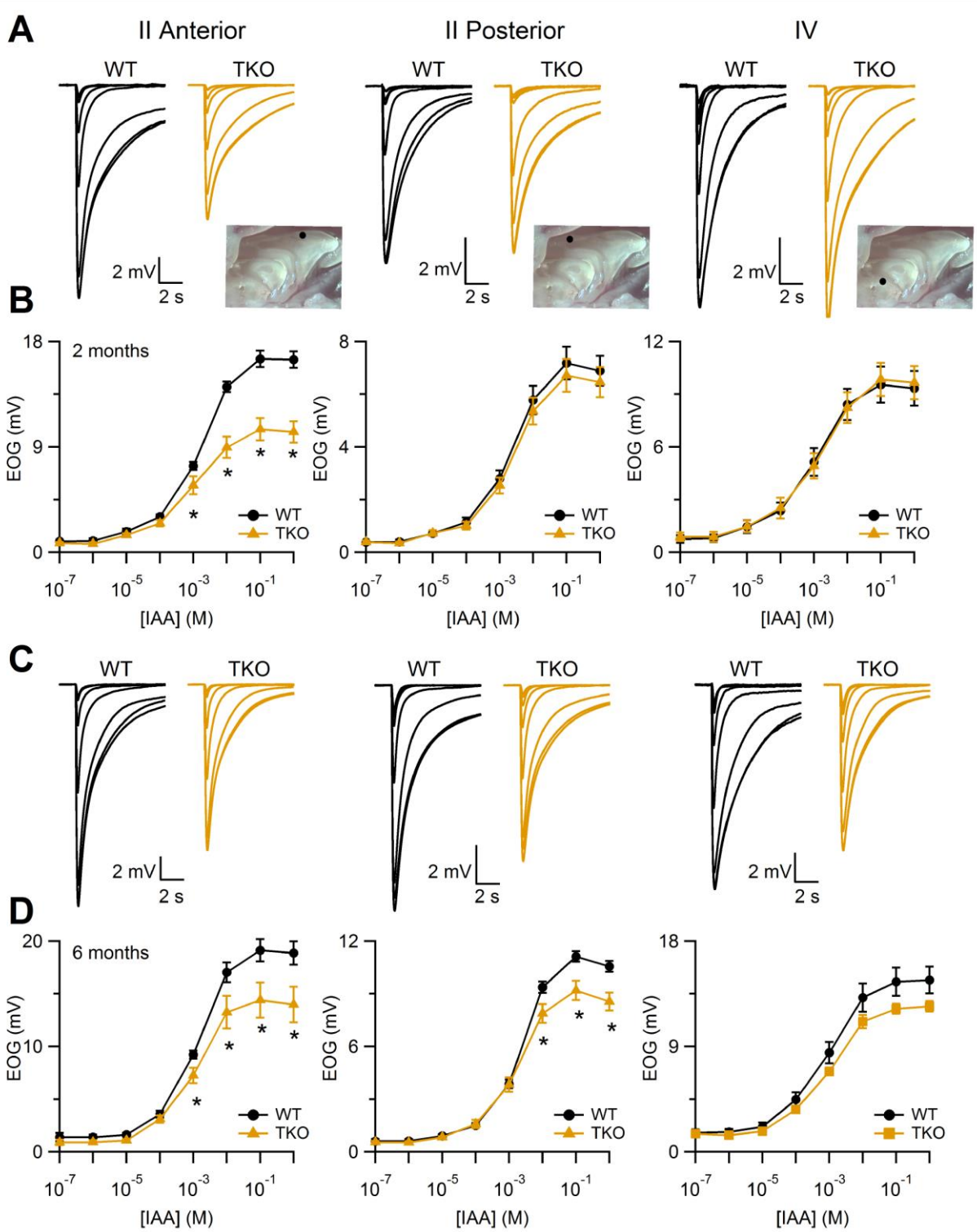

Figure 4. Odorant response in WT and TKO mice. Representative EOG recordings from WT (black traces) or TKO (orange traces) 2 months (A) or 6 months (C) old mice. The responses were evoked by 100 ms stimulation with isoamyl acetate vapors of increasing concentrations. EOG recordings were obtained from indicated OE locations. Dose–response relationships of average peak EOG amplitudes from WT (black traces) or TKO (orange traces) 2 months (B) or 6 months (D) old mice (n=9-10 *<0.05 Student's t-test).

We further analyzed the kinetics of the EOG recordings. We measured the latency as the time between the starting of the stimulus and the time at which the response comes to 1% of its peak value; the rise time as the interval between the beginning of the response and the time of the peak response; the time constant of the monoexponential fit of the recovery phase of the EOG response. We did not find significant differences in the kinetics of the EOG recordings between WT and TKO mice in all tested regions of OE both in 2- and 6-months old animals (Fig 5).

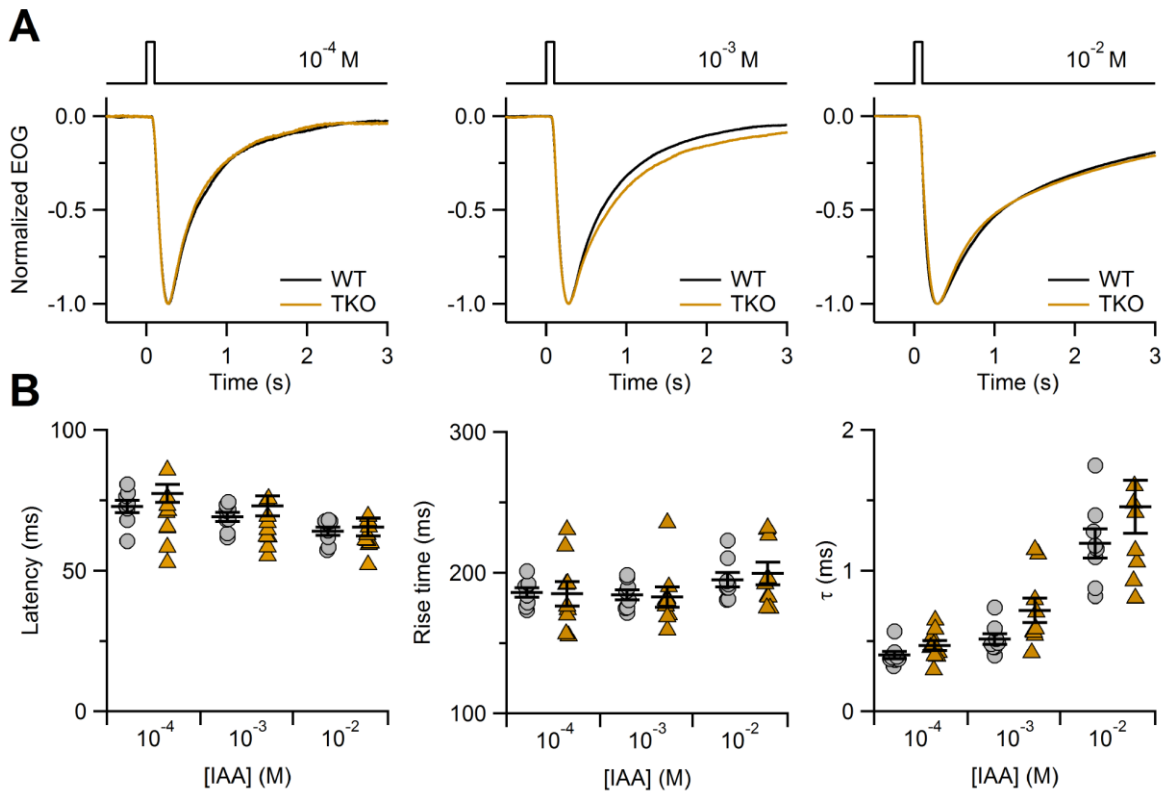

Figure 5. Kinetics of the odorant response in WT and TKO mice. Representative normalized EOG recordings from 2 months old WT (black traces) or TKO (orange traces) mice in II Ant region. The responses were evoked by 100 ms stimulation of vapors of the indicated IAA solution concentration. (B) Scatter dot plot with average ± sem showing the values of latency (left), rise time (middle) and time constant (right) in WT or TKO mice at each odorant concentration (n=9-10).

5. Conclusions

In this work, we provide novel information regarding the expression and localization of all stomatin-domain proteins in the mouse OE. We confirmed the localization of STOML-3 in the cilia of the OSNs, where the sensory transduction takes place. Remarkably, we found that also Stomatin is present only in these structures. In contrast, we revealed that STOML-1 and STOML-2 localize in the soma of the neurons.

To understand the physiological role of these proteins in the OE, we investigated the development of OSNs and other OE cell types in two KO mice models. A first line is a knockout for STOML-3, while the second is a Stomatin/STOML-1/STOML-3 triple knock out (TKO). Then we used the EOG recordings to compare the physiological responses to odorant stimulation in WT with those of mutant mice.

We found that in both, STOML-3 KO and TKO, the number of mature OSNs was not significantly different from WT mice. Moreover, the cilia number and length were not affected in both mutant models. These data strongly suggest that stomatin-domain proteins Stomatin, STOML-1 and STOML-3 are not involved in the regulation of OSN development. Interestingly also several components of the olfactory transduction cascade are normally targeted to the cilia also in the absence of stomatin-domain proteins.

Despite the normal OE development in mutant mice, we found a reduction in the amplitude of the response in both KO animals, especially in older mice. The magnitude of the reduction was similar in both KO mice, suggesting that STOML-3 is the main responsible for this effect. Since stomatin proteins can physically and functionally interact with different types of ion channels (Lapatsina et al., 2012; Poole et al., 2014), we speculate that STOML-3 and/or Stomatin could modulate also CNG and/or TMEM16B. Immunoprecipitation experiment and patch-clamp recordings will be necessary to fully investigate this scenario. In STOML-3 KO mice, we found a reduction in the expression level of Stomatin that remained trapped in knobs of some OSNs without reaching the cilia, suggesting a possible functional interaction between these STOML-3 and Stomatin. Further experiments will be necessary to clarify the relative role of Stomatin and STOML-3 in the regulation of odorant response.

The results in this thesis establish the first evidences that stomatin-domain proteins modulate the odorant response in mice and provide the foundation for future work aimed at clarifying the physiological role of stomatin protein in the olfactory system.

6. References

Ache, B.W., and Young, J.M. (2005). Olfaction: diverse species, conserved principles. Neuron *48*, 417–430.

Antolin, S., Reisert, J., and Matthews, H.R. (2010). Olfactory response termination involves Ca2+-ATPase in vertebrate olfactory receptor neuron cilia. J. Gen. Physiol. *135*, 367–378.

Bakalyar, H.A., and Reed, R.R. (1990). Identification of a specialized adenylyl cyclase that may mediate odorant detection. Science *250*, 1403–1406.

Barnes, T.M., Jin, Y., Horvitz, H.R., Ruvkun, G., and Hekimi, S. (1996). The Caenorhabditis elegans behavioral gene unc-24 encodes a novel bipartite protein similar to both erythrocyte band 7.2 (stomatin) and nonspecific lipid transfer protein. J. Neurochem. *67*, 46–57.

Barrios, A.W., Núñez, G., Sánchez Quinteiro, P., and Salazar, I. (2014). Anatomy, histochemistry, and immunohistochemistry of the olfactory subsystems in mice. Front. Neuroanat. *8*, 63.

Belluscio, L., Gold, G.H., Nemes, A., and Axel, R. (1998). Mice deficient in G(olf) are anosmic. Neuron *20*, 69–81.

Bianchi, L., and Driscoll, M. (2002). Protons at the gate: DEG/ENaC ion channels help us feel and remember. Neuron *34*, 337–340.

Billig, G.M., Pál, B., Fidzinski, P., and Jentsch, T.J. (2011). Ca2+-activated Cl− currents are dispensable for olfaction. Nat. Neurosci. *14*, 763–769.

Boccaccio, A., and Menini, A. (2007). Temporal development of cyclic nucleotide-gated and Ca2+ -activated Cl- currents in isolated mouse olfactory sensory neurons. J. Neurophysiol. *98*, 153–160.

Bolz, F., Kasper, S., Bufe, B., Zufall, F., and Pyrski, M. (2017). Organization and Plasticity of Sodium Channel Expression in the Mouse Olfactory and Vomeronasal Epithelia. Front. Neuroanat. *11*, 28.

Bönigk, W., Bradley, J., Müller, F., Sesti, F., Boekhoff, I., Ronnett, G.V., Kaupp, U.B., and Frings, S. (1999). The native rat olfactory cyclic nucleotide-gated channel is composed of three distinct subunits. J. Neurosci. Off. J. Soc. Neurosci. *19*, 5332–5347.

Borisy, F.F., Ronnett, G.V., Cunningham, A.M., Juilfs, D., Beavo, J., and Snyder, S.H. (1992). Calcium/calmodulin-activated phosphodiesterase expressed in olfactory receptor neurons. J. Neurosci. Off. J. Soc. Neurosci. *12*, 915–923.

Bozza, T., Feinstein, P., Zheng, C., and Mombaerts, P. (2002). Odorant receptor expression defines functional units in the mouse olfactory system. J. Neurosci. Off. J. Soc. Neurosci. *22*, 3033–3043.

Bradley, J., Bönigk, W., Yau, K.-W., and Frings, S. (2004). Calmodulin permanently associates with rat olfactory CNG channels under native conditions. Nat. Neurosci. *7*, 705–710.

Brand, J., Smith, E.S.J., Schwefel, D., Lapatsina, L., Poole, K., Omerbašić, D., Kozlenkov, A., Behlke, J., Lewin, G.R., and Daumke, O. (2012). A stomatin dimer modulates the activity of acid-sensing ion channels. EMBO J. *31*, 3635–3646.

Breipohl, W., Laugwitz, H.J., and Bornfeld, N. (1974). Topological relations between the dendrites of olfactory sensory cells and sustentacular cells in different vertebrates. An ultrastructural study. J. Anat. *117*, 89–94.

Browman, D.T., Hoegg, M.B., and Robbins, S.M. (2007). The SPFH domain-containing proteins: more than lipid raft markers. Trends Cell Biol. *17*, 394–402.

Brown, A.L., Liao, Z., and Goodman, M.B. (2008). MEC-2 and MEC-6 in the Caenorhabditis elegans sensory mechanotransduction complex: auxiliary subunits that enable channel activity. J. Gen. Physiol. *131*, 605–616.

Bruce, L.J., Robinson, H.C., Guizouarn, H., Borgese, F., Harrison, P., King, M.-J., Goede, J.S., Coles, S.E., Gore, D.M., Lutz, H.U., et al. (2005). Monovalent cation leaks in human red cells caused by single amino-acid substitutions in the transport domain of the band 3 chloride-bicarbonate exchanger, AE1. Nat. Genet. *37*, 1258–1263.

Bruce, L.J., Guizouarn, H., Burton, N.M., Gabillat, N., Poole, J., Flatt, J.F., Brady, R.L., Borgese, F., Delaunay, J., and Stewart, G.W. (2009). The monovalent cation leak in overhydrated stomatocytic red blood cells results from amino acid substitutions in the Rh-associated glycoprotein. Blood *113*, 1350–1357.

Brunet, L.J., Gold, G.H., and Ngai, J. (1996). General anosmia caused by a targeted disruption of the mouse olfactory cyclic nucleotide-gated cation channel. Neuron *17*, 681–693.

Buck, L., and Axel, R. (1991). A novel multigene family may encode odorant receptors: a molecular basis for odor recognition. Cell *65*, 175–187.

Carter, L.A., MacDonald, J.L., and Roskams, A.J. (2004). Olfactory horizontal basal cells demonstrate a conserved multipotent progenitor phenotype. J. Neurosci. Off. J. Soc. Neurosci. *24*, 5670–5683.

Castillo, K., Delgado, R., and Bacigalupo, J. (2007). Plasma membrane Ca(2+)-ATPase in the cilia of olfactory receptor neurons: possible role in Ca(2+) clearance. Eur. J. Neurosci. *26*, 2524–2531.

Chalfie, M. (2009). Neurosensory mechanotransduction. Nat. Rev. Mol. Cell Biol. *10*, 44–52.

Chamero, P., Leinders-Zufall, T., and Zufall, F. (2012). From genes to social communication: molecular sensing by the vomeronasal organ. Trends Neurosci. *35*, 597–606.

Courtiol, E., and Wilson, D.A. (2017). The Olfactory Mosaic: Bringing an Olfactory Network Together for Odor Perception. Perception *46*, 320–332.

Cygnar, K.D., and Zhao, H. (2009). Phosphodiesterase 1C is dispensable for rapid response termination of olfactory sensory neurons. Nat. Neurosci. *12*, 454–462.

Cygnar, K.D., Stephan, A.B., and Zhao, H. (2010). Analyzing responses of mouse olfactory sensory neurons using the air-phase electroolfactogram recording. J. Vis. Exp. JoVE.

Da Cruz, S., Parone, P.A., Gonzalo, P., Bienvenut, W.V., Tondera, D., Jourdain, A., Quadroni, M., and Martinou, J.-C. (2008). SLP-2 interacts with prohibitins in the mitochondrial inner membrane and contributes to their stability. Biochim. Biophys. Acta *1783*, 904–911.

Dahl, A.R., and Hadley, W.M. (1991). Nasal cavity enzymes involved in xenobiotic metabolism: effects on the toxicity of inhalants. Crit. Rev. Toxicol. *21*, 345–372.

De Palo, G., Boccaccio, A., Miri, A., Menini, A., and Altafini, C. (2012). A dynamical feedback model for adaptation in the olfactory transduction pathway. Biophys. J. *102*, 2677–2686.

Dhaliwal, G., Cornett, P.A., and Tierney, L.M. (2004). Hemolytic anemia. Am. Fam. Physician *69*, 2599–2606.

Dibattista, M., Pifferi, S., Boccaccio, A., Menini, A., and Reisert, J. (2017). The long tale of the calcium activated Cl- channels in olfactory transduction. Channels Austin Tex *11*, 399–414.

Dibattista, M., and Reisert, J. (2016). The Odorant Receptor-Dependent Role of Olfactory Marker Protein in Olfactory Receptor Neurons. Journal of Neuroscience 36, 2995–3006.

Dulac, C., and Torello, A.T. (2003). Molecular detection of pheromone signals in mammals: from genes to behaviour. Nat. Rev. Neurosci. *4*, 551–562.

Feinstein, P., and Mombaerts, P. (2004). A contextual model for axonal sorting into glomeruli in the mouse olfactory system. Cell *117*, 817–831.

Firestein, S. (2001). How the olfactory system makes sense of scents. Nature *413*, 211–218.

Fletcher, R.B., Prasol, M.S., Estrada, J., Baudhuin, A., Vranizan, K., Choi, Y.G., and Ngai, J. (2011). p63 regulates olfactory stem cell self-renewal and differentiation. Neuron *72*, 748–759.

Fletcher, R.B., Das, D., Gadye, L., Street, K.N., Baudhuin, A., Wagner, A., Cole, M.B., Flores, Q., Choi, Y.G., Yosef, N., et al. (2017). Deconstructing Olfactory Stem Cell Trajectories at Single-Cell Resolution. Cell Stem Cell *20*, 817-830.e8.

Geffeney, S.L., and Goodman, M.B. (2012). How we feel: ion channel partnerships that detect mechanical inputs and give rise to touch and pain perception. Neuron *74*, 609–619.

Genetet, S., Desrames, A., Chouali, Y., Ripoche, P., Lopez, C., and Mouro-Chanteloup, I. (2017). Stomatin modulates the activity of the Anion Exchanger 1 (AE1, SLC4A1). Sci. Rep. *7*, 46170.

Goldstein, B.J., Kulaga, H.M., and Reed, R.R. (2003). Cloning and characterization of SLP3: a novel member of the stomatin family expressed by olfactory receptor neurons. J. Assoc. Res. Otolaryngol. JARO *4*, 74–82.

Graziadei, P.P., and Graziadei, G.A. (1979). Neurogenesis and neuron regeneration in the olfactory system of mammals. I. Morphological aspects of differentiation and structural organization of the olfactory sensory neurons. J. Neurocytol. *8*, 1–18.

Graziadei, P.P., Levine, R.R., and Monti Graziadei, G.A. (1979). Plasticity of connections of the olfactory sensory neuron: regeneration into the forebrain following bulbectomy in the neonatal mouse. Neuroscience *4*, 713–727.

Green, J.B., and Young, J.P.W. (2008). Slipins: ancient origin, duplication and diversification of the stomatin protein family. BMC Evol. Biol. *8*, 44.

Hengl, T., Kaneko, H., Dauner, K., Vocke, K., Frings, S., and Möhrlen, F. (2010). Molecular components of signal amplification in olfactory sensory cilia. Proc. Natl. Acad. Sci. U. S. A. *107*, 6052–6057.

Herrick, D.B., Lin, B., Peterson, J., Schnittke, N., and Schwob, J.E. (2017). Notch1 maintains dormancy of olfactory horizontal basal cells, a reserve neural stem cell. Proc. Natl. Acad. Sci. U. S. A. *114*, E5589–E5598.

Hiebl-Dirschmied, C.M., Entler, B., Glotzmann, C., Maurer-Fogy, I., Stratowa, C., and Prohaska, R. (1991). Cloning and nucleotide sequence of cDNA encoding human erythrocyte band 7 integral membrane protein. Biochim. Biophys. Acta *1090*, 123–124.

Huang, M., Gu, G., Ferguson, E.L., and Chalfie, M. (1995). A stomatin-like protein necessary for mechanosensation in C. elegans. Nature *378*, 292–295.

Huber, T.B., Schermer, B., Müller, R.U., Höhne, M., Bartram, M., Calixto, A., Hagmann, H., Reinhardt, C., Koos, F., Kunzelmann, K., et al. (2006). Podocin and MEC-2 bind cholesterol to regulate the activity of associated ion channels. Proc. Natl. Acad. Sci. U. S. A. *103*, 17079–17086.

Ibarra-Soria, X., Levitin, M.O., Saraiva, L.R., and Logan, D.W. (2014). The olfactory transcriptomes of mice. PLoS Genet. *10*, e1004593.

Imai, T. (2014). Construction of functional neuronal circuitry in the olfactory bulb. Semin. Cell Dev. Biol. *35*, 180–188.

Iwai, N., Zhou, Z., Roop, D.R., and Behringer, R.R. (2008). Horizontal basal cells are multipotent progenitors in normal and injured adult olfactory epithelium. Stem Cells Dayt. Ohio *26*, 1298–1306.

Jones, D.T., and Reed, R.R. (1989). Golf: an olfactory neuron specific-G protein involved in odorant signal transduction. Science *244*, 790–795.

Kanageswaran, N., Demond, M., Nagel, M., Schreiner, B.S.P., Baumgart, S., Scholz, P., Altmüller, J., Becker, C., Doerner, J.F., Conrad, H., et al. (2015). Deep sequencing of the murine olfactory receptor neuron transcriptome. PloS One *10*, e0113170.

Kaneko, H., Nakamura, T., and Lindemann, B. (2001). Noninvasive measurement of chloride concentration in rat olfactory receptor cells with use of a fluorescent dye. Am. J. Physiol. Cell Physiol. *280*, C1387-1393.

Kaneko, H., Putzier, I., Frings, S., Kaupp, U.B., and Gensch, T. (2004). Chloride accumulation in mammalian olfactory sensory neurons. J. Neurosci. Off. J. Soc. Neurosci. *24*, 7931–7938.

Kaupp, U.B. (2010). Olfactory signalling in vertebrates and insects: differences and commonalities. Nat. Rev. Neurosci. *11*, 188–200.

Keller, A., and Margolis, F.L. (1975). Immunological studies of the rat olfactory marker protein. J. Neurochem. *24*, 1101–1106.

Kleene, S.J. (2008). The electrochemical basis of odor transduction in vertebrate olfactory cilia. Chem. Senses *33*, 839–859.

Kleene, S.J., and Gesteland, R.C. (1981). Dissociation of frog olfactory epithelium with N-ethylmaleimide. Brain Res. *229*, 536–540.

Klimmeck, D., Mayer, U., Ungerer, N., Warnken, U., Schnölzer, M., Frings, S., and Möhrlen, F. (2008). Calcium-signaling networks in olfactory receptor neurons. Neuroscience *151*, 901–912.

Kobayakawa, K., Hayashi, R., Morita, K., Miyamichi, K., Oka, Y., Tsuboi, A., and Sakano, H. (2002). Stomatin-related olfactory protein, SRO, specifically expressed in the murine olfactory sensory neurons. J. Neurosci. Off. J. Soc. Neurosci. *22*, 5931–5937.

Kozlenkov, A., Lapatsina, L., Lewin, G.R., and Smith, E.S.J. (2014). Subunit-specific inhibition of acid sensing ion channels by stomatin-like protein 1. J. Physiol. *592*, 557–569.

Kuhlmann, K., Tschapek, A., Wiese, H., Eisenacher, M., Meyer, H.E., Hatt, H.H., Oeljeklaus, S., and Warscheid, B. (2014). The membrane proteome of sensory cilia to the depth of olfactory receptors. Mol. Cell. Proteomics MCP *13*, 1828–1843.

Kulaga, H.M., Leitch, C.C., Eichers, E.R., Badano, J.L., Lesemann, A., Hoskins, B.E., Lupski, J.R., Beales, P.L., Reed, R.R., and Katsanis, N. (2004). Loss of BBS proteins causes anosmia in humans and defects in olfactory cilia structure and function in the mouse. Nat. Genet. *36*, 994–998.

Kurahashi, T., and Menini, A. (1997). Mechanism of odorant adaptation in the olfactory receptor cell. Nature *385*, 725–729.

Kurahashi, T., and Yau, K.W. (1993). Co-existence of cationic and chloride components in odorant-induced current of vertebrate olfactory receptor cells. Nature *363*, 71–74.

Kurtenbach, S., Gießl, A., Strömberg, S., Kremers, J., Atorf, J., Rasche, S., Neuhaus, E.M., Hervé, D., Brandstätter, J.H., Asan, E., et al. (2017). The BEACH Protein LRBA Promotes the Localization of the Heterotrimeric G-protein Golf to Olfactory Cilia. Sci. Rep. *7*, 8409.

Lande, W.M., Thiemann, P.V., and Mentzer, W.C. (1982). Missing band 7 membrane protein in two patients with high Na, low K erythrocytes. J. Clin. Invest. *70*, 1273–1280.

Lapatsina, L., Brand, J., Poole, K., Daumke, O., and Lewin, G.R. (2012). Stomatin-domain proteins. Eur. J. Cell Biol. *91*, 240–245.

Laska, M., and Shepherd, G.M. (2007). Olfactory discrimination ability of CD-1 mice for a large array of enantiomers. Neuroscience *144*, 295–301.

Leung, C.T., Coulombe, P.A., and Reed, R.R. (2007). Contribution of olfactory neural stem cells to tissue maintenance and regeneration. Nat. Neurosci. *10*, 720–726.

Li, R.-C., Lin, C.-C., Ren, X., Wu, J.S., Molday, L.L., Molday, R.S., and Yau, K.-W. (2018). Ca2+-activated Cl current predominates in threshold response of mouse olfactory receptor neurons. Proc. Natl. Acad. Sci. U. S. A. *115*, 5570–5575.

Liman, E.R., and Buck, L.B. (1994). A second subunit of the olfactory cyclic nucleotide-gated channel confers high sensitivity to cAMP. Neuron *13*, 611–621.

Ling, G., Gu, J., Genter, M.B., Zhuo, X., and Ding, X. (2004). Regulation of cytochrome P450 gene expression in the olfactory mucosa. Chem. Biol. Interact. *147*, 247–258.

Lipscomb, B.W., Treloar, H.B., and Greer, C.A. (2002). Cell surface carbohydrates reveal heterogeneity in olfactory receptor cell axons in the mouse. Cell Tissue Res. *308*, 7–17.

Lock, S.P., Smith, R.S., and Hardisty, R.M. (1961). Stomatocytosis: a hereditary red cell anomally associated with haemolytic anaemia. Br. J. Haematol. *7*, 303–314.

Lowe, G., and Gold, G.H. (1993). Nonlinear amplification by calcium-dependent chloride channels in olfactory receptor cells. Nature *366*, 283–286.

Lux, S.E. (2016). Anatomy of the red cell membrane skeleton: unanswered questions. Blood 127, 187–199.

Mackay-Sim, A., and Kittel, P. (1991). Cell dynamics in the adult mouse olfactory epithelium: a quantitative autoradiographic study. J. Neurosci. Off. J. Soc. Neurosci. *11*, 979–984.

Mainland, J.D., Lundström, J.N., Reisert, J., and Lowe, G. (2014). From molecule to mind: an integrative perspective on odor intensity. Trends Neurosci. *37*, 443–454.

Mairhofer, M., Steiner, M., Salzer, U., and Prohaska, R. (2009). Stomatin-like protein-1 interacts with stomatin and is targeted to late endosomes. J. Biol. Chem. *284*, 29218–29229.

Mayer, U., Ungerer, N., Klimmeck, D., Warnken, U., Schnölzer, M., Frings, S., and Möhrlen, F. (2008). Proteomic analysis of a membrane preparation from rat olfactory sensory cilia. Chem. Senses *33*, 145–162.

Menco, B.P., Birrell, G.B., Fuller, C.M., Ezeh, P.I., Keeton, D.A., and Benos, D.J. (1998). Ultrastructural localization of amiloride-sensitive sodium channels and Na+,K(+)-ATPase in the rat's olfactory epithelial surface. Chem. Senses *23*, 137–149.

Michalakis, S., Reisert, J., Geiger, H., Wetzel, C., Zong, X., Bradley, J., Spehr, M., Hüttl, S., Gerstner, A., Pfeifer, A., et al. (2006). Loss of CNGB1 protein leads to olfactory dysfunction and subciliary cyclic nucleotide-gated channel trapping. J. Biol. Chem. *281*, 35156–35166.

Mombaerts, P. (2004). Genes and ligands for odorant, vomeronasal and taste receptors. Nat. Rev. Neurosci. *5*, 263–278.

Mombaerts, P., Wang, F., Dulac, C., Chao, S.K., Nemes, A., Mendelsohn, M., Edmondson, J., and Axel, R. (1996). Visualizing an olfactory sensory map. Cell *87*, 675–686.

Morrison, E.E., and Costanzo, R.M. (1990). Morphology of the human olfactory epithelium. J. Comp. Neurol. *297*, 1–13.

Moshourab, R.A., Wetzel, C., Martinez-Salgado, C., and Lewin, G.R. (2013). Stomatin-domain protein interactions with acid-sensing ion channels modulate nociceptor mechanosensitivity. J. Physiol. *591*, 5555–5574.

Munger, S.D., Leinders-Zufall, T., and Zufall, F. (2009). Subsystem organization of the mammalian sense of smell. Annu. Rev. Physiol. *71*, 115–140.

Nagayama, S., Homma, R., and Imamura, F. (2014). Neuronal organization of olfactory bulb circuits. Front. Neural Circuits *8*, 98.

Nakamura, T., and Gold, G.H. (1987). A cyclic nucleotide-gated conductance in olfactory receptor cilia. Nature *325*, 442–444.

Nakamura, T., Kaneko, H., and Nishida, N. (1997). Direct measurement of the chloride concentration in newt olfactory receptors with the fluorescent probe. Neurosci. Lett. *237*, 5–8.

Nickell, W.T., Kleene, N.K., Gesteland, R.C., and Kleene, S.J. (2006). Neuronal chloride accumulation in olfactory epithelium of mice lacking NKCC1. J. Neurophysiol. *95*, 2003–2006.

Nickell, W.T., Kleene, N.K., and Kleene, S.J. (2007). Mechanisms of neuronal chloride accumulation in intact mouse olfactory epithelium. J. Physiol. *583*, 1005–1020.

Nomura, T., Takahashi, S., and Ushiki, T. (2004). Cytoarchitecture of the normal rat olfactory epithelium: light and scanning electron microscopic studies. Arch. Histol. Cytol. *67*, 159–170.

Oski, F.A., Naiman, J.L., Blum, S.F., Zarkowsky, H.S., Whaun, J., Shohet, S.B., Green, A., and Nathan, D.G. (1969). Congenital hemolytic anemia with high-sodium, low-potassium red cells. Studies of three generations of a family with a new variant. N. Engl. J. Med. *280*, 909–916.

Pace, U., Hanski, E., Salomon, Y., and Lancet, D. (1985). Odorant-sensitive adenylate cyclase may mediate olfactory reception. Nature *316*, 255–258.

Pietra, G., Dibattista, M., Menini, A., Reisert, J., and Boccaccio, A. (2016). The Ca2+-activated Cl- channel TMEM16B regulates action potential firing and axonal targeting in olfactory sensory neurons. J. Gen. Physiol. *148*, 293–311.

Pifferi, S., Boccaccio, A., and Menini, A. (2006). Cyclic nucleotide-gated ion channels in sensory transduction. FEBS Lett. *580*, 2853–2859.

Pifferi, S., Cenedese, V., and Menini, A. (2012). Anoctamin 2/TMEM16B: a calcium-activated chloride channel in olfactory transduction. Exp. Physiol. *97*, 193–199.

Poole, K., Herget, R., Lapatsina, L., Ngo, H.-D., and Lewin, G.R. (2014). Tuning Piezo ion channels to detect molecular-scale movements relevant for fine touch. Nat. Commun. *5*, 3520.

Price, M.P., Thompson, R.J., Eshcol, J.O., Wemmie, J.A., and Benson, C.J. (2004). Stomatin modulates gating of acid-sensing ion channels. J. Biol. Chem. *279*, 53886–53891.

Rajaram, S., Sedensky, M.M., and Morgan, P.G. (1998). Unc-1: a stomatin homologue controls sensitivity to volatile anesthetics in Caenorhabditis elegans. Proc. Natl. Acad. Sci. U. S. A. *95*, 8761–8766.

Reisert, J., and Reingruber, J. (2019). Ca2+-activated Cl- current ensures robust and reliable signal amplification in vertebrate olfactory receptor neurons. Proc. Natl. Acad. Sci. U. S. A. *116*, 1053–1058.

Reisert, J., Lai, J., Yau, K.-W., and Bradley, J. (2005). Mechanism of the excitatory Cl- response in mouse olfactory receptor neurons. Neuron *45*, 553–561.

Reithmeier, R.A.F., Casey, J.R., Kalli, A.C., Sansom, M.S.P., Alguel, Y., and Iwata, S. (2016). Band 3, the human red cell chloride/bicarbonate anion exchanger (AE1, SLC4A1), in a structural context. Biochim. Biophys. Acta *1858*, 1507–1532.

Ressler, K.J., Sullivan, S.L., and Buck, L.B. (1993). A zonal organization of odorant receptor gene expression in the olfactory epithelium. Cell *73*, 597–609.

Ressler, K.J., Sullivan, S.L., and Buck, L.B. (1994). Information coding in the olfactory system: evidence for a stereotyped and highly organized epitope map in the olfactory bulb. Cell *79*, 1245–1255.

Reuter, D., Zierold, K., Schröder, W.H., and Frings, S. (1998). A depolarizing chloride current contributes to chemoelectrical transduction in olfactory sensory neurons in situ. J. Neurosci. Off. J. Soc. Neurosci. *18*, 6623–6630.

Rungaldier, S., Oberwagner, W., Salzer, U., Csaszar, E., and Prohaska, R. (2013). Stomatin interacts with GLUT1/SLC2A1, band 3/SLC4A1, and aquaporin-1 in human erythrocyte membrane domains. Biochim. Biophys. Acta *1828*, 956–966.

Saidu, S.P., Weeraratne, S.D., Valentine, M., Delay, R., and Van Houten, J.L. (2009). Role of plasma membrane calcium ATPases in calcium clearance from olfactory sensory neurons. Chem. Senses *34*, 349–358.

Saraiva, L.R., Ibarra-Soria, X., Khan, M., Omura, M., Scialdone, A., Mombaerts, P., Marioni, J.C., and Logan, D.W. (2015). Hierarchical deconstruction of mouse olfactory sensory neurons: from whole mucosa to single-cell RNA-seq. Sci. Rep. *5*, 18178.

Schild, D., and Restrepo, D. (1998). Transduction mechanisms in vertebrate olfactory receptor cells. Physiol. Rev. *78*, 429–466.

Schreiber, S., Fleischer, J., Breer, H., and Boekhoff, I. (2000). A possible role for caveolin as a signaling organizer in olfactory sensory membranes. J. Biol. Chem. *275*, 24115–24123.

Scott, J.W., and Scott-Johnson, P.E. (2002). The electroolfactogram: a review of its history and uses. Microsc. Res. Tech. *58*, 152–160.

Seidel, G., and Prohaska, R. (1998). Molecular cloning of hSLP-1, a novel human brain-specific member of the band 7/MEC-2 family similar to Caenorhabditis elegans UNC-24. Gene *225*, 23–29.

Snyers, L., Umlauf, E., and Prohaska, R. (1998). Oligomeric nature of the integral membrane protein stomatin. J. Biol. Chem. *273*, 17221–17226.

Song, Y., Cygnar, K.D., Sagdullaev, B., Valley, M., Hirsh, S., Stephan, A., Reisert, J., and Zhao, H. (2008). Olfactory CNG channel desensitization by Ca2+/CaM via the B1b subunit affects response termination but not sensitivity to recurring stimulation. Neuron *58*, 374–386.

Stephan, A.B., Shum, E.Y., Hirsh, S., Cygnar, K.D., Reisert, J., and Zhao, H. (2009). ANO2 is the cilial calcium-activated chloride channel that may mediate olfactory amplification. Proc. Natl. Acad. Sci. U. S. A. *106*, 11776–11781.

Stephan, A.B., Tobochnik, S., Dibattista, M., Wall, C.M., Reisert, J., and Zhao, H. (2011). The Na(+)/Ca(2+) exchanger NCKX4 governs termination and adaptation of the mammalian olfactory response. Nat. Neurosci. *15*, 131–137.

Stewart, G.W., Hepworth-Jones, B.E., Keen, J.N., Dash, B.C., Argent, A.C., and Casimir, C.M. (1992). Isolation of cDNA coding for an ubiquitous membrane protein deficient in high Na+, low K+ stomatocytic erythrocytes. Blood *79*, 1593–1601.

Su, C.-Y., Menuz, K., and Carlson, J.R. (2009). Olfactory perception: receptors, cells, and circuits. Cell *139*, 45–59.

Sullivan, S.L., Bohm, S., Ressler, K.J., Horowitz, L.F., and Buck, L.B. (1995). Target-independent pattern specification in the olfactory epithelium. Neuron *15*, 779–789.

Suzuki, Y., Takeda, M., and Farbman, A.I. (1996). Supporting cells as phagocytes in the olfactory epithelium after bulbectomy. J. Comp. Neurol. *376*, 509–517.

Tadenev, A.L.D., Kulaga, H.M., May-Simera, H.L., Kelley, M.W., Katsanis, N., and Reed, R.R. (2011). Loss of Bardet-Biedl syndrome protein-8 (BBS8) perturbs olfactory function, protein localization, and axon targeting. Proc. Natl. Acad. Sci. U. S. A. *108*, 10320–10325.

Takekawa, N., Isumi, M., Terashima, H., Zhu, S., Nishino, Y., Sakuma, M., Kojima, S., Homma, M., and Imada, K. (2019). Structure of Vibrio FliL, a New Stomatin-like Protein That Assists the Bacterial Flagellar Motor Function. MBio *10*.

Talaga, A.K., Dong, F.N., Reisert, J., and Zhao, H. (2017). Cilia- and Flagella-Associated Protein 69 Regulates Olfactory Transduction Kinetics in Mice. J. Neurosci. Off. J. Soc. Neurosci. *37*, 5699–5710.

Tavernarakis, N., Driscoll, M., and Kyrpides, N.C. (1999). The SPFH domain: implicated in regulating targeted protein turnover in stomatins and other membrane-associated proteins. Trends Biochem. Sci. *24*, 425–427.

Thornberry, N.A., and Lazebnik, Y. (1998). Caspases: enemies within. Science *281*, 1312–1316.

Tirindelli, R., Dibattista, M., Pifferi, S., and Menini, A. (2009). From pheromones to behavior. Physiol. Rev. *89*, 921–956.

Umlauf, E., Mairhofer, M., and Prohaska, R. (2006). Characterization of the stomatin domain involved in homo-oligomerization and lipid raft association. J. Biol. Chem. *281*, 23349–23356.

Vassalli, A., Rothman, A., Feinstein, P., Zapotocky, M., and Mombaerts, P. (2002). Minigenes impart odorant receptor-specific axon guidance in the olfactory bulb. Neuron *35*, 681–696.

Wachowiak, M. (2011). All in a sniff: olfaction as a model for active sensing. Neuron *71*, 962–973.

Wang, Y., and Morrow, J.S. (2000). Identification and characterization of human SLP-2, a novel homologue of stomatin (band 7.2b) present in erythrocytes and other tissues. J. Biol. Chem. *275*, 8062–8071.

Wang, M.M., Tsai, R.Y., Schrader, K.A., and Reed, R.R. (1993). Genes encoding components of the olfactory signal transduction cascade contain a DNA binding site that may direct neuronal expression. Mol. Cell. Biol. *13*, 5805–5813.

Weiss, J., Pyrski, M., Jacobi, E., Bufe, B., Willnecker, V., Schick, B., Zizzari, P., Gossage, S.J., Greer, C.A., Leinders-Zufall, T., et al. (2011). Loss-of-function mutations in sodium channel Nav1.7 cause anosmia. Nature *472*, 186–190.

Wetzel, C., Hu, J., Riethmacher, D., Benckendorff, A., Harder, L., Eilers, A., Moshourab, R., Kozlenkov, A., Labuz, D., Caspani, O., et al. (2007). A stomatin-domain protein essential for touch sensation in the mouse. Nature *445*, 206–209.

Willmer, C., and Fricker, M. (1996). Stomata (Springer Science & Business Media).

Wong, S.T., Trinh, K., Hacker, B., Chan, G.C., Lowe, G., Gaggar, A., Xia, Z., Gold, G.H., and Storm, D.R. (2000). Disruption of the type III adenylyl cyclase gene leads to peripheral and behavioral anosmia in transgenic mice. Neuron *27*, 487–497.

Yan, C., Zhao, A.Z., Bentley, J.K., Loughney, K., Ferguson, K., and Beavo, J.A. (1995). Molecular cloning and characterization of a calmodulin-dependent phosphodiesterase enriched in olfactory sensory neurons. Proc. Natl. Acad. Sci. U. S. A. *92*, 9677–9681.

Yokoyama, H., Fujii, S., and Matsui, I. (2008). Crystal structure of a core domain of stomatin from Pyrococcus horikoshii Illustrates a novel trimeric and coiled-coil fold. J. Mol. Biol. *376*, 868–878.

Zhang, S., Arnadottir, J., Keller, C., Caldwell, G.A., Yao, C.A., and Chalfie, M. (2004). MEC-2 is recruited to the putative mechanosensory complex in C. elegans touch receptor neurons through its stomatin-like domain. Curr. Biol. CB *14*, 1888–1896.

Zhao, H., Ivic, L., Otaki, J.M., Hashimoto, M., Mikoshiba, K., and Firestein, S. (1998). Functional expression of a mammalian odorant receptor. Science *279*, 237–242.

Zheng, J., and Zagotta, W.N. (2004). Stoichiometry and assembly of olfactory cyclic nucleotide-gated channels. Neuron *42*, 411–421.

Zufall, F., and Leinders-Zufall, T. (2000). The cellular and molecular basis of odor adaptation. Chem. Senses *25*, 473–481.

Acknowledgments

Quisiera agradecer a mis padres y mi hermana, gracias por su apoyo, por escucharme, por animarme y por todos sus consejos, muchas gracias por todo su amor. Su vida ha sido dura y darles esta pequeña alegría me hace muy feliz.

Now I would like to express my gratitude to all people were part of my life during this time in Trieste…

I am very grateful with Professor Anna Menini for receiving me in her group and giving me the opportunity to come to Trieste and live this beautiful experience.

Thank you very much to Simone for being my scientific guide in these years, thank for your corrections, for the knowledge you shared with me and for your support.

Thanks, you Hasti!! Thanks a lot for being with me, all actions, achieves, dreams, failures, thoughts…all 'smell' better thanks to you ;)!

I would like to say thanks to all people have been part of my time in Trieste: Tiago, thanks for share with my many of your time. I would like to thanks Andres for his friendships and support from the even first moments I arrived to Italy. Many thanks to Xuan for share her time and her life with me, I enjoyed a lot the time with you and also, I could grow up a lot as person, thanks a lot. Abraham, Jaspreet, Sadaf, Mansh, Nora, Davide, Diletta, Ulisse, Mattia, Elena, Cesar, Carlos, Mandana, Thanh, Juanito, Negar, Phuong and Chris and all my friends in Trieste, thanks for the nice moments we shared.

Also, I want to acknowledge all the guys of the LAB: Stefano, Devendra, Chiara, Domenico, Nicole (Giorgia), Giorgia (Nicole), Emilio, Michele, many thanks for your kindness, for helping me many times, for discuss my project and make it better!

I would like to recognize the effort and work of Riccardo and Federica, you made us the life extremely easy without worries about paperwork and bureaucratic formalities

Elena, Jessica, Federica, Beatrice, Micaela, Elettra, Lorenzo, Angelo, Gianni… I am grateful with all of you for being so collaborative and help me in the lab so many times

Of course, now I want to express my gratitude to Lucia, Eleonora, Patricia, Silvia, Lucho and the other guys of the canteen, thanks for preparing our delicious food all these years and maintain us alive!

Enrico and Maria, I would like to specially thank both of you. You have a special place in my life, you are for me two extra second parents. Thanks to you I am here. Your passion and devotion to science have inspired many people and motivated to me to choose this pathway in my life. Thanks for support and for change the life of all your students, thanks for help us to pursuit our dreams. I had my first experience in the laboratory with you, I lived the most wonderful moments in Woods Hole, and thanks a lot for that gift.